Road Map for the Structural Assessment of Concrete Dams Suffering from AAR with Specific Application to [redacted] Dam

Cooperative Agreement No. R18AC00055

March 14, 2023

Victor E. Saouma
Mohammad Amin Hariri-Ardebili

University of Colorado, Boulder

This page intentionally left blank.

Preface

This report seeks to provide guidance to engineers assessing the static or dynamic safety of dams suffering from alkali aggregate reaction (AAR). Given the multitude of surrounding uncertainties, a probabilistic scheme is provided.

Its focus is on the various idiosyncrasies that make AAR particularly pernicious, unique, challenging and complex. However, since there is an evident need to contextualize the recommended approach, scant coverage is also given to some of the related pertinent issues. With over 150 references, the reader can readily find more detailed information when needed. On the other hand, given that AAR may cause structural cracks, particular attention is also given to the fracture mechanic of concrete.

This report is not a general manual of practice, nor does it seek to reinforce established State of the Practice. Instead it seeks to close the gap between the State of the Practice with the Reported State of the Art.

Hence, presents bold recommendations, written by two (academic) experts with over 50 years of cumulative experience in the field, and driven by their related expertise. Whereas some Engineers may be forced to step beyond their comfort level to pursue the proposed approaches, they will hopefully be reassured that a most rational approach is pursued with little room for unsupported "Engineering Judgment".

Victor E. Saouma — Boulder, CO

M. Amin Hariri-Ardebili — March, 2021

This page intentionally left blank.

Contents

List of Figures

List of Tables

1 Introduction

This introductory chapter will set the context of this report. What are the key questions to be addressed, and how is the report organized.

This report seeks to provide engineers with sufficient guidance to comprehensively and thoroughly assess the the structural integrity and safety of dams known to suffer from alkali aggregate reaction (AAR) using State of the Art techniques.

Key questions to be answered are:

Diagnosis: What is the current state of deterioration? what investigative steps must be undertaken to address this question.

Prognosis: What combination of field measurements and laboratory tests should be performed to determine the (approximate) rate of concrete expansion and deterioration, and how these results can be incorporated in an appropriate nonlinear transient analysis to assess the dam safety?

Safety How is AAR altering the serviceability (under normal operation load) and safety (under extreme loads) in the foreseeable future (5, 20, 20 40 years)?

Answers to those key questions must be science based (State of the Art and not Practice), quantitative (and not qualitative), and probabilistic.

Excellent reports have been written to address similar (but not identical problems. Most notably, (FHWA, 2006) (FHWA, 2010) (Gunn, Scrivener, and Leemann, 2017) (Leemann and Griffa, 2013) not to mention the most recent book edited by the Senior author under the auspices of RILEM (Saouma, 2020) for AAR.

This report will provide a road-map toward the safety assessment of a dam affected by AAR (such as [redacted] dam) through the following steps:

1. Review of existing documents.
2. Site investigation.
3. Laboratory investigation.
4. Understanding the fundamentals of Probabilistic Based Earthquake Engineering.
5. Finite element simulation.

Each one of them will be addressed in a separate chapter. The appendix will provided bench-

mark problems for finite element code validation to AAR analysis, as well as a fracture tests to determine concrete fracture energy.

Finally, the objective is not to necessarily copy/repeat what has already been published, but rather to identify the right "mixture" of field observations, laboratory tests, and finite element studies necessary to conduct the probabilistic based seismic safety assessment of a dam affected by AAR.

2 Review Existing Documents

Prior to any investigation, one should thoroughly review all available and relevant documents.

Identification, or location of such documents may not be evident as some of them may be quite old, not properly archived, or digitized.

This preliminary chapter will highlight key data to be collected.

2.1 Data Gathering

Whereas data gathering will naturally start with the "low hanging" documents in an institution, it may not be surprising that a thorough search in the archives would yield additional and critical ones (in particular some with construction details, actual mix designs, design revisions).

One may also have to interview retired engineers or on-site technicians who may have more vivid recollection of details not necessarily found in archived documents.

2.2 What to Collect

This initial data gathering phase should seek the following information[1]:

Analysis and Design files

- ‡ Construction drawings. Often those have been modified, altered in times.
- Analysis reports (trial-load and finite element analyses).

Pre-construction files

- ‡Mix designs.
- ‡Aggregate sourcing (quarry locations).
- Site investigation (foundation conditions).
- †Mix design test reports.
- Geological site records (location of faults)

Construction documents

- Foundation mapping.

[1] ‡ and † denote critical and important documents respectively.

- Actual mix design.
- Placement temperatures.
- QA test data.
- Issues during construction(e.g., shutdowns, submittals, changes).
- Construction photographs.

Field inspection reporting signs, locations, and time of occurrence of;

- †cracks
  - Surface (or hairline), noting depth and pattern (map-like or aligned).
  - Structural (larger than ≈ 0.25 inch., note depth.
- Desintegration (deterioration of concrete into small fragments).
- Efflorescences, formed by water seeping through cracks, then evaporation leaves behind some minerals that have been leached from the concrete or otherwise.
- Spalling and popouts.

Monitoring logs

- ‡Pendulum
- ‡Tiltmeters.
- Piezometric readings
- Seasonal (with the greates granularity possible) variation of temperature and pool elevations.
- Photogrammetry.
- Lidar.

Seismic Records which should include

- Dates, duration, magnitude and location of recorded seismic excitation.
- Local of faults.
- Geological records.

Laboratory Tests not all may be available

- †Mechanical properties: compressive strength f'_c, tensile strength $f't$, fracture energies G_F, Creep coefficients.
- ‡Petrographic reports.

2.3 Data Archive

Once retrieved, all documents should be digitized into searchable pdf files, and then logged in an spreadsheet with relevant keywords (tags) for ease of reference.

2.4 Data Analysis

To the extent possible selected data should be cross-correlated. Examples include:

- Plots of pendulum displacement with respect to temperature and pool elevation.

- Temporal and spatial variation of concrete properties (mechanical, cracks, damage).
- Correlation between numerically predicted displacements and recorded ones.

2.5 Summary Report

Once all the data has been collected, then an initial report could be written. The report should summarize the State of the dam up to the initiation of this study.

3 Site Investigation

No reasonable finite element analysis can be performed without a meaningful visit to the site, not only to "get a feel" for site/space/dimensions, but also to gather qualitative and quantitative information.

For the AAR study, one of the most critical information are record of (usually) crest displacements (in both radial and vertical directions).

3.1 Visual Observation

Bureau of Reclamation, (1995) provides an excellent, though outdated, first starting point to plan a field investigation of an existing dam.

Within the context of an investigation of a dam suffering from AAR (such as [redacted]), detailed visual inspection along all the galleries on on the downstream face (possibly with drone or through "rope access") is a must.

It should be emphasized that many of the following measurements are needed either to:

- Identify zones where AAR occurred in the dam. It is indeed very unlikely that the extent of damage is uniform throughout the dam, and it is most likely resent in particular "pockets".
- Provide material properties in the finite element modeling of AAR. For instance, there is a small chance to observe AAR in zones with low RH, unless these is continuous water transmission.
- Provide a "baseline" for the finite element
  - Calibration of the model through system identification. For instance, given the temporal variations of the pendulum displacements, one can calibrate the AAR properties to field a crest displacement very close to the one recorded.
  - Verification with respect to other locations not used for the calibration.

Site investigation should include (Fournier and Bérubé, 2000):

1. **Concrete surface features** indicative of alkali-aggregate reactivity
2. **Deformations and displacements:** The differential concrete swelling between adjacent members of a structure affected by AAR can cause misalignment, separation, or distortion of

adjacent structural units and associated mechanical equipment, excessive deflection, closure of joints, and ultimately spalling of concrete. Concrete deformation and movements may also be caused by mechanisms such as excessive loading, thermal or moisture movements, differential shrinkage, foundation effects, hydraulic pressure, creep, impact, and vibrations.

3. **Cracking:** The pattern of cracking due to AAR is influenced by the geometry of the concrete element, the environmental conditions, the presence and the arrangement of reinforcement, and the load or stress applied to the concrete. "Map-cracking" typically develops in AAR-affected concrete components free of major stress fields or poorly reinforced; drying shrinkage, freezing and thawing, and sulfate attack can also result in a similar pattern of cracking. In reinforced concrete members or under loading conditions, the cracking pattern will generally reflect the arrangement of the underlying steel or the direction of the major stress fields. Surfaces of concrete elements affected by AAR and exposed to sun, moisture, and frost action usually show more extensive cracking and deterioration. Surface macrocracking due to AAR rarely penetrates more than 25 to 50 mm of the exposed surface (in rare cases $>$ 100 mm). The width of surface macrocracks ranges from 0.1 to 10 mm in extreme cases.
4. **Surface discoloration:** Cracks caused by AAR are often bordered by a broad brownish zone, thus giving the appearance of permanent dampness.
5. **Gel exudation:** Surface gel exudation is a common and characteristic feature of AAR-affected concrete. It is usually associated with leaching of carbonated lime (efflorescence).
6. **Pop outs:** The expansion of unsound aggregate particles due to frost action is the main factor responsible for the development of pop outs in cold regions. Alkali-reactive aggregate particles undergoing expansion near the concrete surface may also induce pop outs, or open channels for the water to penetrate and freeze, thus promoting detachment of a conical portion of concrete.

3.2 In-situ monitoring

1. **Temperatures** Ambient (include solar exposure characteristics); water: upstream and downstream (if applicable) at various depth; thermocouples measurements inside the dam.
2. **Relative Humidity measurements:** with depth at various locations to establish the position of the internal equilibrium zone.
3. **Mapping of:** surface cracks, recording pattern, size, and width in various concrete elements, and with time.
4. **Measurements of:** movements, deflections, and deformations using Demec gauges and (or) metallic references, glass plates crossing surface macrocracks, invar wire extensometers, inclinometers, vibrating cords, overcoring, inverted pendulums, or levelling techniques.
5. **In situ stress measurements** in the dam (see below).

3.3 in-situ Stress Measurements

Traditionally dam monitoring has relied on "standard" instrumentation (FERC, 2019) (Batholomey, C. and Haverland, M., 1987) to measure displacements, inclinations, temperature, uplift, seapage, cracking.

Those will not be reviewed here, however the adoption of unconventional instruments that could more specifically be targeted for AAR expansion monitoring will be discussed.

As AAR causes concrete expansion (up to about 0.1%, and results in a build-up of stresses and uneven deformation, ideally those should be measured.

Unfortunately existing commonly used instruments are not ideal for such quantification, and as such one will have to examine for new ones typically used in other disciplines (such as mining).

Ideally, one should measure expansion or stresses at the same location through a bore-hole drilled deep into the dam.

The most commonly used instruments to record *in situ* stresses are the flat-discs (Fig. 3.1(a)), and over-coring or stress-meters, Fig. 3.1(b). However the former is limited to surface measurement, and over-coring may also be limited to a few feet from the surface.

An interesting addition would be a stress-meter, Fig. 3.1(c)that could output repeated readings of *in situ* elastic modulus and stresses through a probe. The author has worked with a stress-meter during a past project on a dam (Saouma, Broz, and Boggs, 1991) and would strongly recommend its adoption in monitoring AAR progress over time through repeated readings and measurement of (degrading) elastic properties, along with variations in the magnitude/direction of *in situ* stresses. However, it appears that the company manufacturing this devise (Serata Geomechanics) is no longer in business.

Rock over-coring for depths up to 250 m with boreholes of 46-76 mm are reported in Myrvang, A. and Beitnes, A. (2003).

Probes to measure either strains or stresses are now available. Those are manufactured by Geokon. Their Model A-4 Multiple Point Rod Extensometer has Snap-Ring Anchors (Geokon, 2002b) is quickly and easily installed in boreholes in hard or competent rock. Anchors are pushed to the required depth on the end of setting rods and then a cord is pulled to remove the locking pin which allows two retaining rings on each anchor to snap outward and grip the borehole, Fig. 3.2. Up to eight anchors can be installed, at various depths, in a 76 mm diameter borehole. Particularly useful in upward directed boreholes as described in the manual (Geokon, 2002a).

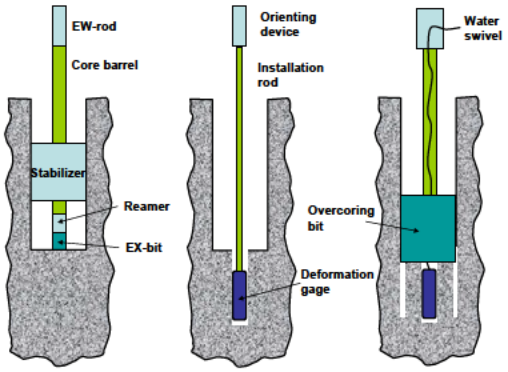

(a) Over core (Hydrofrac Inc., 2012)

(b) Flat-Jack (Matest Inc., 2012)

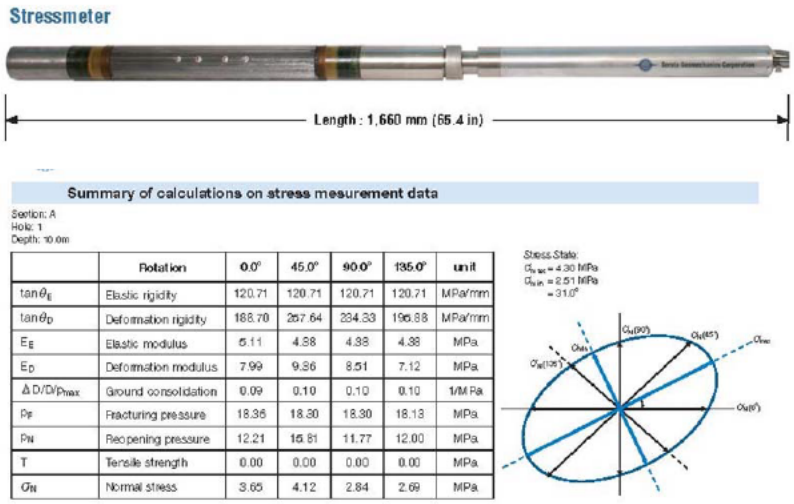

	Rotation	0.0°	45.0°	90.0°	135.0°	unit
$\tan\theta_E$	Elastic rigidity	120.71	120.71	120.71	120.71	MPa/mm
$\tan\theta_D$	Deformation rigidity	188.70	257.64	234.33	196.88	MPa/mm
E_E	Elastic modulus	5.11	4.38	4.38	4.38	MPa
E_D	Deformation modulus	7.99	9.36	8.51	7.12	MPa
$\Delta D/D/P_{max}$	Ground consolidation	0.09	0.10	0.10	0.10	1/MPa
P_F	Fracturing pressure	18.36	18.30	18.30	18.13	MPa
P_N	Reopening pressure	12.21	15.81	11.77	12.00	MPa
T	Tensile strength	0.00	0.00	0.00	0.00	MPa
σ_N	Normal stress	3.65	4.12	2.84	2.69	MPa

(c) Stress-Meter (Serata Geomechanics, 2005)

Figure 3.1: Existing Field stress measurements

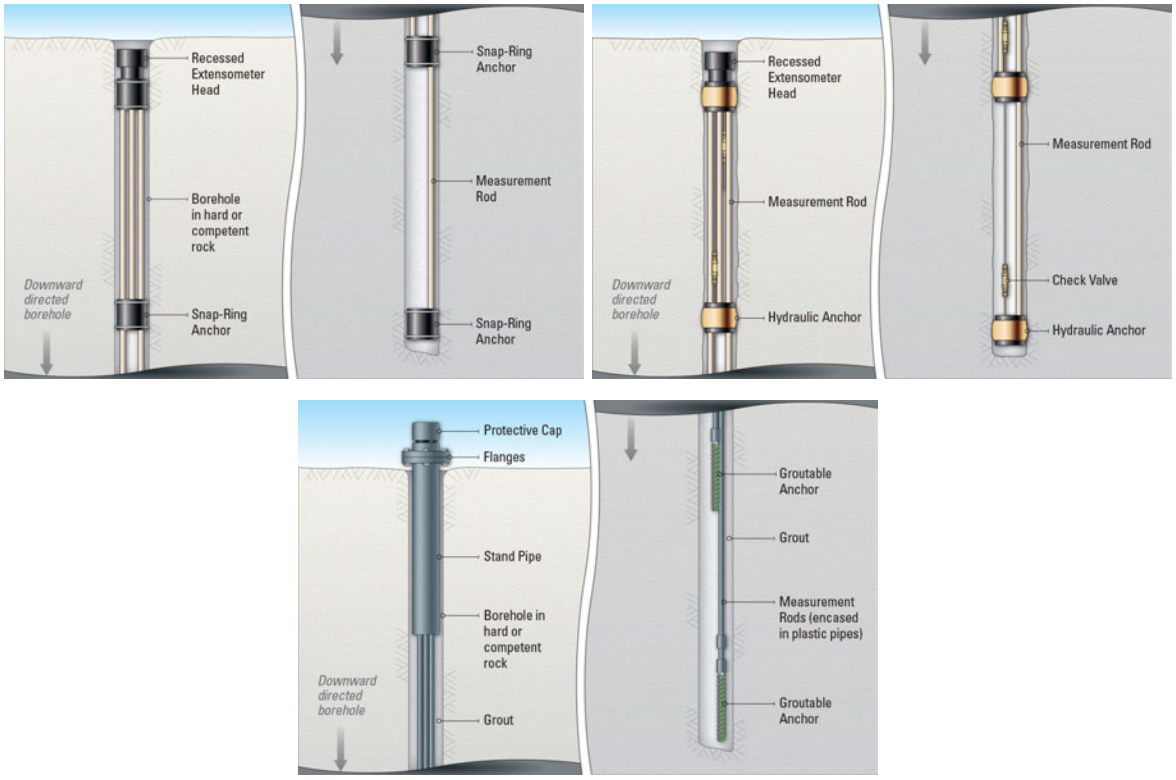

Figure 3.2: Borehole extensometers by Geokon

Finally, an excellent overview of the various applicable techniques is given by Ljunggren et al. (2003).

3.4 System Identification

As mentioned in the introduction, site measurements can be used for system (or parameter) identification of AAR properties.

It is therefore assumed that measurements (such as crest displacements) have been recorded, and AAR properties such as latency, characteristic times and maximum expansion (τ_L, τ_C and ε^∞) are unknown. The challenge is to "fine tune" those three variables in such a way that the historically recorded crest displacement is captured by the finite element analysis. This (least square error) procedure can be automated through a simple Matlab code (Saouma, 2013).

Mathematically, identification of the three parameters can be simply formulated as follows. The field-recorded displacements (e.g. crest displacement on a dam) are denoted by $\mathbf{u}(t)$, the target parameters by $\mathbf{x}$ (in our case $x(1) = \tau_c$, $x(2) = \tau_l$ and $(x(3) = \varepsilon(\infty))$, the finite element "operator" by $f(.)$, and computed results by $\mathbf{u}'(t)$. We thus have:

$$f(\mathbf{x}) = \mathbf{u}'(t) \neq \mathbf{u}(t) \tag{3.1}$$

and are seeking to minimize $(\mathbf{u}(t) - \mathbf{u}'(t))^2$, see Fig. 3.3. FloatBarrier

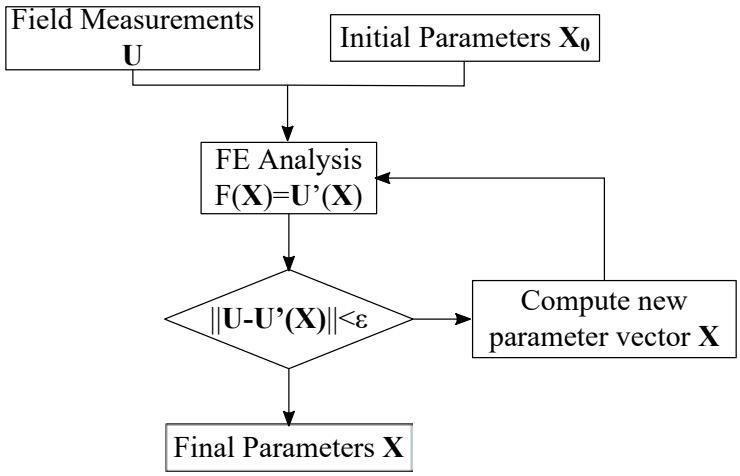

(a) Algorithm

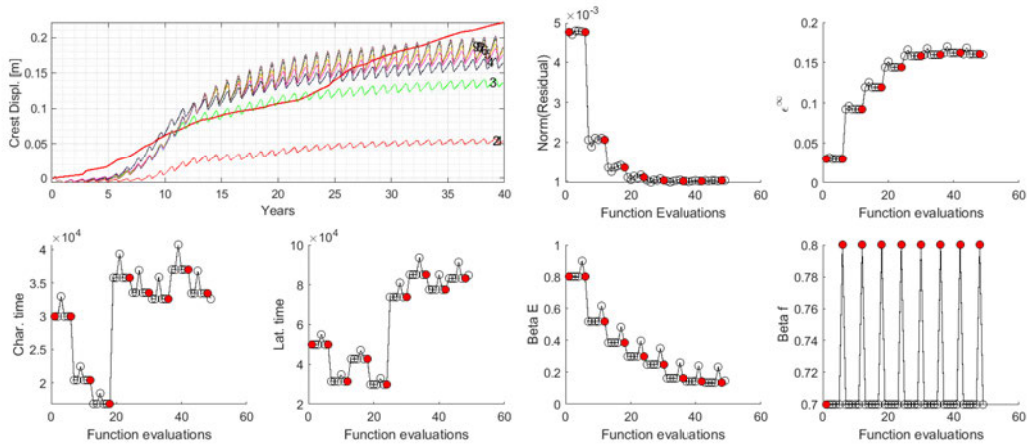

(b) Graphical displays during system identification procedure

Figure 3.3: System identification

3.5 Non Destructive Evaluation Techniques

Non Destructive Evaluation Techniques have been reported and summarized by (Courtois et al., 2021) and are shown in Table 3.1.

Table 3.1: Summary table of techniques for monitoring ASR-affected structures (Courtois et al., 2021)

Method	POC or PAT*	Accuracy for ASR diagnosis
Cracking/crack pattern		
Visual Inspection	POC	B
Cracking Index (CI) Method	POC	A
Crack-meters	POC	A
Infrared Thermography (IRT)	PAT	C
Structural Displacement		
Pendulum	POC	B
Surface Extensometer	POC	A
Expansion/deformation		
Vibrating Wire Strain Gauges	POC	A
Fiber-optic systems	POC	A/B/C (depending on the selected system or manufacturer)
Snap-Ring Borehole Extensometer	PAT	A
Temperature		
Temperature Probe (RTDs and Thermocouples)	POC	A
Distributed Fiber-Optics System	POC	A
Young modulus, local stiffness		
Ultrasonic Pulse Echo (UPE)	PAT	B
Ultrasonic Pulse Velocity (UPV)	POC	C
Impact-Echo (IE)	POC	C
Acoustic Emission (AE)	PAT	C
Promising techniques with high resolution and high sensitivity • Nonlinear acoustic • Diffusion • Surface waves	PAT	A (promising, high sensitivity)
Concrete moisture/ humidity/water content		
RH/Capacitance Probe	POC	C (specific care to avoid possible leaks)
Wood Stick	POC	B
Microwave Techniques: GPR	PAT	B (needs calibration on the tested concrete)
Microwave Techniques: TDR	POC	B (needs calibration on the tested concrete)
Microwave Techniques: Open-Ended Coaxial Probe	PAT	B (needs calibration on the tested concrete)

* POC: Proof-of-Concept for structural monitoring of ASR-relevant parameters on real structures.
PAT: Potentially Applicable Technique for monitoring ASR-relevant parameters, but not performed with success yet at the structural level in the field.

4 Concrete AAR & Fracture

Concrete is a very complex material. In the context of this report, of paramount importance is a basic understanding of AAR and of the ensuing fracture.

Focus will be on the modern aspects of AAR and fracture modeling, as well as on their interaction between laboratory testing and finite element analysis.

4.1 AAR

The theoretical underpinning of the first author model has been presented by the authors separately, (Saouma and Perotti, 2006) and (Saouma, 2013). It will be briefly summarized.

4.1.1 Volumetric Expansion

The AAR expansion is considered to be a volumetric one, which rate is given by the following function

$$\begin{aligned}\dot{\boldsymbol{\varepsilon}}_V^{AAR}(t,\theta,RH) = \Gamma_t(f_t'|w_c,\sigma_I|COD_{max})\ \Gamma_c(\overline{\sigma},f_c') \\ g(RH)\ \dot{\xi}(t,\theta)\ \ \varepsilon^{\infty}|_{\theta=\theta_0}\end{aligned} \tag{4.1}$$

where ε^{∞} is the final volumetric expansion as determined from laboratory tests at temperature θ_0. $0 \leq \Gamma_t \leq 1$ is a parameter which reduces the expansion in the presence of large tensile stresses (macro-cracks absorbing the gel), f_t' the tensile strength, and σ_I the major (tensile) principal stress. Similarly, $0 \leq \Gamma_c \leq 1$ is a parameter which accounts for the absorption of the gel due to compressive induced stresses, $\overline{\sigma}$ and f_c' are the hydrostatic stress, and the compressive strength of the concrete, respectively. $0 \leq g(RH) \leq 1$ is a function of the relative humidity (set to zero if the humidity is below 80%), $\dot{\xi}(t,\theta)$.

4.1.2 Reaction Kinetics

The kinetics law given by

$$\xi(t,\theta) = \frac{1-\exp(-\frac{t}{\tau_c(\theta)})}{1+\exp\left(-\frac{(t-\tau_l(\theta))}{\tau_c(\theta)}\right)} \tag{4.2}$$

where τ_l and τ_c are the latency and characteristic times, respectively. The former corresponds to the inflection point, and the latter is defined in terms of the intersection of the tangent at τ_l with the asymptotic unit value of ξ, figure 4.1(d). They are given by

$$\begin{aligned} \tau_l(\theta) &= \tau_l(\theta_0) \exp\left[U_l\left(\tfrac{1}{\theta} - \tfrac{1}{\theta_0}\right)\right] \\ \tau_c(\theta) &= \tau_c(\theta_0) \exp\left[U_c\left(\tfrac{1}{\theta} - \tfrac{1}{\theta_0}\right)\right] \end{aligned} \tag{4.3}$$

expressed in terms of the absolute temperature ($\theta^o K = 273 + T^o C$) and the corresponding activation energies. U_l and U_c are the activation energies, minimum energy required to trigger the reaction for the latency and characteristic times, respectively, Fig. 4.1(a).

4.1.3 Activation Energy

Like all chemical reactions, ASR is subject to Arrhenius Law (Arrhenius, 1889), which relates the dependence of the rate constant, k, of a chemical reaction on absolute temperature (T expressed in Kelvin, $T^o K = 273 + T^o C$) and activation energy, E_a.

$$k = Ae^{-\frac{E_a}{RT}} \tag{4.4}$$

Substituting k with τ_l and τ_c, Ulm et al. (2000) has shown that these values at temperature T can be expressed in terms of the corresponding values at temperature T_0. Activation energies can be easily determined by rewriting Equation 4.3 in its non-exponential form:

$$\ln k = \ln\left(Ae^{-\frac{E_a}{RT}}\right) = \ln A - \frac{E_a}{RT} \tag{4.5}$$

which is the equation of a straight line with slope $-E_a/RT$ (Figure 4.1(c)).

We can thus determine the activation energy from values of k observed at different temperatures by simply plotting k as a function of $1/T$.

4.1.4 Effect of Time and Temperature

The effect of time and temperature on the kinetics of the reaction is illustrated by Fig. 4.1(d) where the decrease in RH, results in a decrease of peak AAR while a in temperature will slow the reaction. Finally, the engineering significance of the (sigmoid) expansion is illustrated in Fig. 4.1(b) (Saouma et al., 2015).

Once the volumetric AAR strain is determined, it is decomposed into a tensorial strain in accordance to the three weight factors associated with the principal stresses, Fig. 4.1(e).

4.1.5 Degradation

Accompanying expansion is a degradation of the concrete mechanical properties. A simple model for this degradation of the tensile strength and elastic modulus, Fig. 4.1(f), is given by:

$$\begin{aligned} E(t,\theta) &= E_0\left[1-(1-\beta_E)\,\xi(t,\theta)\right] \\ f_t(t,\theta) &= f_{t,0}\left[1-(1-\beta_E)\,\xi(t,\theta)\right] \end{aligned} \tag{4.6}$$

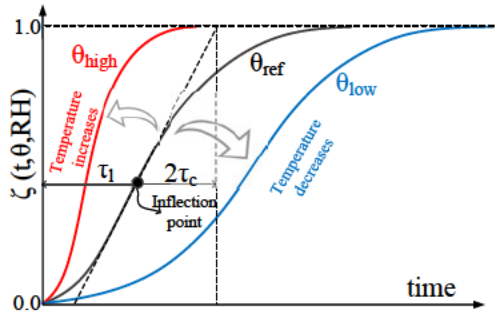

(a) Effect of temperature

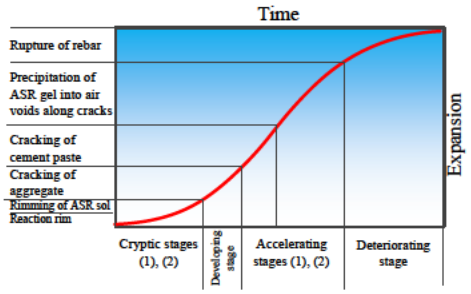

(b) Physical interpretation

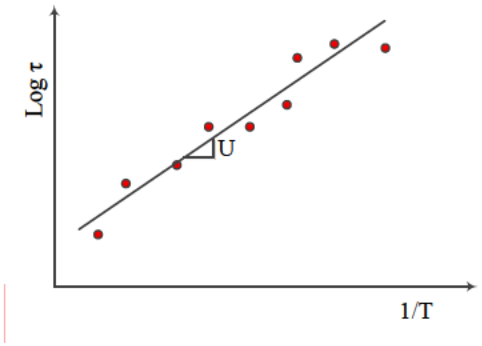

(c) Determination of Activation Energy

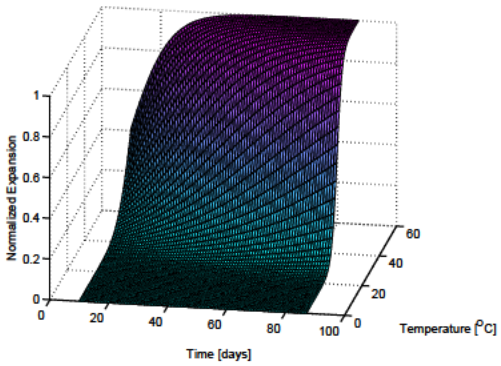

(d) Effect of time and temperature

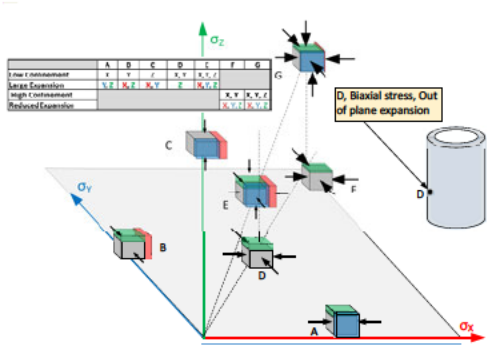

(e) Volumetric stress redistribution

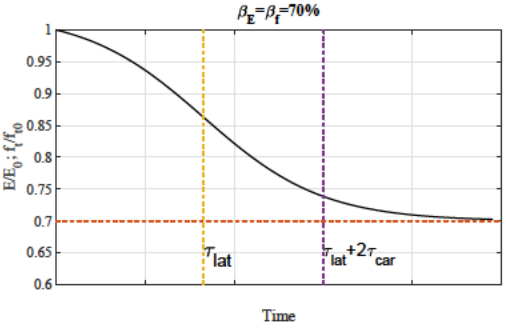

(f) Degradation of concrete with time

Figure 4.1: Illustrations of AAR model

4.1.6 Adoption

To the best of our knowledge, this is probably the most widely implemented model in other finite element codes:

1. Rodriguez et al. (2011) implemented the model in Abaqus and analysed an arch dam.
2. El Mohandes and Vecchio (2013) in the Vector3 program and the analysis of reactive shear walls.
3. Mirzabozorg (2013) in Iran for the analysis of Amir-Kabir arch dam in the NSA-DRI code.
4. Pan et al. (2013) from Tsinghua University for the analysis of Kariba dam.
5. (Huang and Spencer, 2016) Huang, Spencer, and Cai (2015) implemented in the fully coupled Grizzly/Moose program.
6. Ben-Ftima, Sadouki, and Bruhwiler (2016) Polytechnic of Montreal, and Swiss Federal Institute of Technology, Lausanne) as a model in Abaqus for the analysis of a hydraulic structure.
7. Roth (2021) at Hydro-Quebec's ANSYS model for AAR.
8. Thonstad et al. (2021) at NIST, implemented in LS-Dyna

4.2 Concrete Fracture

Finite element modeling of concrete structures remains a continuous challenges. Whereas the so-called "smeared crack" model is mostly used in reinforced concrete structures, the so-called "discrete crack" model is used for structural cracks, such as those likely to be caused by AAR in unreinforced ones.

In both cases, the so-called *quasi-brittle* nature of concrete is universally accepted. This model, is no longer based only on the tensile strength $f't$, but also on the concrete fracture energy G_F developed by Hillerborg (Hillerborg, Modéer, and Petersson, 1976).

4.2.1 σ-COD Diagram, Hillerborg's Model

Cementitious material softening is characterized by a stress-crack opening width curve (and not stress-strain). The exact characterization of the softening response should ideally be obtained from a uniaxial test of an uncracked specimen. This is extremely difficult, so the softening curve is often indirectly determined by testing notched specimens.

Hillerborg, Modéer, and Petersson (ibid.) presented a very simple and elegant model. In this *cohesive crack model*, the crack is composed of two parts, Figure 4.2:

True or physical crack across which no stresses can be transmitted. Along this zone we have both displacement and stress discontinuities.

Fictitious crack or Fracture Process Zone (FPZ) ahead of the previous one, characterized by:

- Peak stress at its tip equal to the tensile strength of cementitious material
- Decreasing stress distribution from f'_t at the tip of the fictitious crack to zero at the tip of the physical crack

Along FPZ, we have displacement discontinuity and stress continuity.

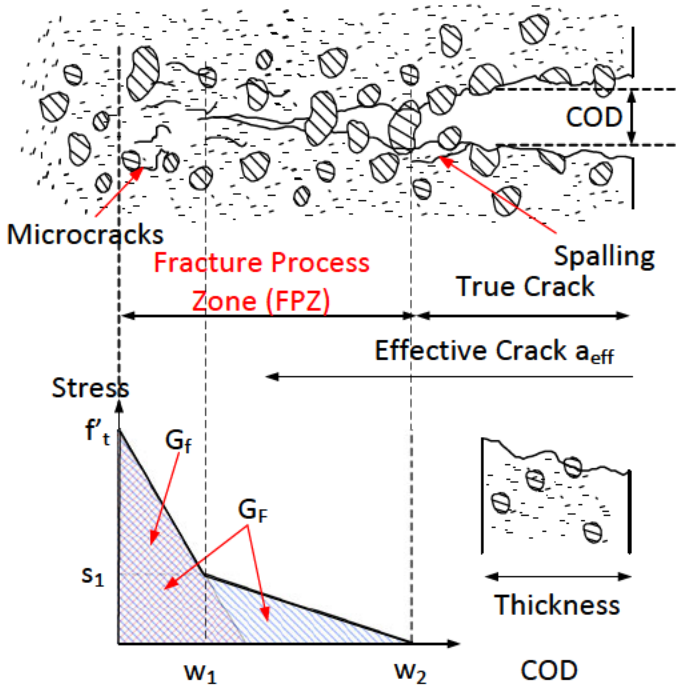

Figure 4.2: Hillerborg's model

It was observed frommany tests that there is an inflection point in the descending branch; the first part has been associated with (unconnected) microcracking ahead of the stress-free crack. The second part with bridging of the crack by aggregates.

The area under the curve is the *fracture energy,* G_F, (not to be confused with G_c or critical energy release rate) and is a measure of the energy that needs to be spent to generate a unit surface of crack.

The *characteristic length* in concrete is given by

$$l_{ch} = \frac{EG_F}{f_t'^2} \tag{4.7}$$

For the shape of the *softening diagram* ($\sigma - COD$), in general a bilinear model for the strain softening is used.

4.2.2 Fracture Energies

A key input value for the finite element analysis of dams with AAR induced structural cracks is the fracture energy. There are two such definition of this critical quantity, and those are described below.

Most importantly, a test to determine the fracture energy is described in Appendix A.

G_F The determination of the fracture energy G_F has been investigated by (Cedolin, Dei Poli, and Iori, 1987; Duda, 1990; Giuriani and Rosati, 1986; Gopalaratnam and Shah, 1985; Jeang and Hawkins, 1985; Petersson, 1981; Whitman et al., 1988). There are many models for concrete softening, and the two most commonly used ones are the one based on an exponential decay (Cornelissen, Hordijk, and Reinhardt, 1986) or bilinear (Whitman et al., 1988), Figure 4.2. This last model can be uniquely defined in terms of the tensile strength, f'_t, and the fracture energy, G_F. It was found that the optimal points for concrete with 1" maximum size aggregate are (Brühwiler and Whitman, 1990):

$$s_1 = 0.4 f'_t \tag{4.8}$$

$$w_1 = 0.8 \frac{G_F}{f'_t} \tag{4.9}$$

$$w_2 = 3 \frac{G_F}{f'_t} \tag{4.10}$$

whereas for structural concrete the corresponding values are (Whitman et al., 1988):

$$s_1 = \frac{f'_t}{4} \tag{4.11}$$

$$w_1 = 0.75 \frac{G_F}{f'_t} \tag{4.12}$$

$$w_2 = 5 \frac{G_F}{f'_t} \tag{4.13}$$

where f'_t is the uniaxial tensile strength.

As f'_t is seldom determined experimentally, it is assumed to be 9% of f'_c (Mindess and Young, 1981). In lieu of a direct tension test, a flexural test can be performed under strain control, and the fracture energy, G_F, could still be determined from the area under the load and corresponding displacement curve. For dynamic analysis, the fracture properties of dam concrete depend on both rate of loading and preloadings. Test results (Brühwiler and Whitman, 1990) show that the fracture properties generally increase with increasing loading rate. However, dynamic compressive preloading leads to a reduction of the fracture properties at both quasi-static and high loading rates.

G_f The maximum loads of structures depend mainly on the initial tangent of the softening stress-separation curve, which is fully characterized by G_f. They are almost independent of the tail of this curve, which depends mainly of G_F, Figure 4.2.

The prediction of the entire post-peak softening load-deflection curve of a structure, which is often of secondary interest for design, depends mainly on the tail of the stress-separation curve of the cohesive crack model, and thus on G_F.

G_f and G_F are two different material characteristics which are only partially correlated. G_F can be estimated from G_f and vice versa, but not accurately. Ideally, both G_f and G_F should be measured and used for calibrating the initial slope and the tail of the softening curve of

the cohesive crack model (or crack band model), which are both needed for fracture analysis of structures. A rough approximation

$$G_F \approx 2.5 G_f \tag{4.14}$$

is reported by Planas and Elices (1992) and further verified by Bažant and Becq-Giraudon (2001).

Bažant and Becq-Giraudon (ibid.) analyzed 238 tests reported in the literature, conducted extensive nonlinear optimization studies based on the Levenberg-Marquardt algorithm, and obtained two simple approximate formulae for the means of G_f and G_F as functions of the compressive strength f'_c, maximum aggregate size d_a, water-cement ratio w/c, and shape of aggregate (crushed or river):

$$\begin{aligned} G_f &= \alpha_0 \left(\tfrac{f'_c}{0.051}\right)^{0.46} \left(1+\tfrac{d_a}{11.27}\right)^{0.22} \left(\tfrac{w}{c}\right)^{-0.30} && \omega_{G_f} = 17.8\% \\ G_F &= 2.5\alpha_0 \left(\tfrac{f'_c}{0.051}\right)^{0.46} \left(1+\tfrac{d_a}{11.27}\right)^{0.22} \left(\tfrac{w}{c}\right)^{-0.30} && \omega_{G_F} = 29.9\% \\ c_f &= \exp\left[\gamma_0 \left(\tfrac{f'_c}{0.022}\right)^{-0.019} \left(1+\tfrac{d_a}{15.05}\right)^{0.72} \left(\tfrac{w}{c}\right)^{0.2}\right] && \omega_{c_f} = 47.6\% \end{aligned} \tag{4.15}$$

where $\alpha_0 = \gamma_0 = 1$ for rounded aggregates, while $\alpha_0 = 1.44$ and $\gamma_0 = 1.12$ for crushed or angular aggregates; ω_{G_f} and ω_{G_F} are the coefficients of variation of the ratios G_f^{test}/G_f and G_F^{test}/G_F for which a normal distribution may be assumed. ω_{c_f} is the coefficient of variation of c_f^{test}/c_f for which a lognormal distribution should be assumed (ω_{c_f} is approximately equal to the standard deviation of $\ln c_f$).

5 Laboratory Investigation

Modern (nonlinear) finite element codes rely on a plethora of input variables. Some, but usually not all, can be determined from proper laboratory tests. Those are typically governed by ASTM standards. AAR results in first swelling (or expansion) of the concrete, followed by cracking. Unfortunately, there is not yet standards to either perform laboratory accelerated expansion tests, or fracture tests. Hence, this chapter will begin with recommendations for the extraction of cores from the dam to the laboratory, then address a number of tests that should be performed.

5.1 From Dam to Laboratory

`Adapted from (Saouma, 2020)`

5.1.1 Samples extraction

The location and the number of specimens to be taken is based on the objectives, scope, and budget of the study, access (downstream, galleries, or even upstream) and the extent of deterioration. It should be recalled that it is extremely unlikely that the entire dam is suffering from AAR to the same extent, whereas more likely is the presence of "pockets" of AAR randomly present.

Ideally, one would need three repetitive tests to get a meaningful value. However, this is not always possible due to both technical and financial considerations.

AAR is known to occur if the internal relative humidity is above 85%, hence cores too close to the surface should be avoided (specially if AAR damage may be compounded by freeze/thaw), (Stark and De Puy, 1987).

AAR causes a volumetric expansion, thus if confined in one direction, expansion in the other two increases. Thus as depth of the core increases, one should take horizontally (as opposed to vertically) oriented cores.

While the extraction and transportation of concrete cores, ASTM C 42 requires that cores be tested "in the same moisture condition than that they were in the field". However, a moisture gradient is often observed within concrete elements in contact or not with an external source of moisture, which very likely increases the variations in the test results. In order to minimize changes

in moisture conditions, it is recommended to wrap the cores in plastic film (or suitable materials - see section below) and store them for at least five days before testing ASTM (1999).

5.1.2 Conditioning

Once a core has been extracted from a dam, special attention must be given to conditioning.

Conditioning is what occurs after the core was extracted and before it is tested so as to keep the sample in as much as possible in its field conditions. This is essential because:

- Moisture condition (i.e. conditioning history) of the specimens prior to testing can largely influence mechanical properties of concrete such as compressive and tensile strength, modulus of elasticity, viscous behaviour, etc. Drying of the cores/test specimens is normally found to increase their stiffness and compressive strength Sanchez (2014) Sanchez et al. (2015). It is therefore desirable that the moisture state reflects the field conditions.
- Drying and re-wetting the samples can have dramatic effects on the subsequent expansion, making prognosis unreliable Merz (2015).
- Drying effect is also verified to affect specimens that are well wrapped (sealed) in plastic sheets, but to a much lower degree. However, a 48-hour rewetting period was found to contribute at reducing the deleterious effect of drying of the test specimens, restoring their initial conditions and thus enabling reliable condition assessment. However, re-wetting procedures increase significantly the variability (i.e. standard deviation) among companion samples;
- AAR depends on the concrete pore solution features. Careful wrapping of the samples is required so that pore solution extraction be possible, if desired.
- Re-saturation of concrete samples can have dramatic effects on the subsequent expansion, making prognosis unreliable Merz (ibid.). Otherwise, interesting results were found in the works from Larive (1998b) and Sanchez (2014) who verified that re-saturating procedures are able to re-set somehow the initial condition of AAR affected samples.

5.1.3 Samples sealing and conditioning prior to testing

The materials which are typically used for sample conditioning are:

- Polyurethane sheets: these plastic sheets allow a tight binding of the sample, however, they are slightly porous and when used exclusively, a sample needs to be wrapped with 20 layers of the material for good isolation. A better method is to use sturdier sheets of plastic and vacuum seal the sample.
- Adhesive aluminum sheets: such sheets are used to control the humidity of samples in creep experiments, they are the most effective means to produce a seal. However, this cover can be easily damaged, and it is recommended that a plastic wrapping be added to protect the aluminium. Further, removing the aluminium is difficult if it is applied directly on the sample.
- Damp cotton cloth: damp cotton cloth can be used to avoid desiccation in conjunction with plastic wrapping. It is placed between the samples and a polyurethane wrap. This keeps the sample for drying, but provides a significant source of water and can therefore induce

leaching. As aluminum is known to play a role in the kinetics of AAR (Chappex, 2012), it may be undesirable to have the aluminum for in direct contact with the sample, beyond considerations on the ease of unwrapping. It is however the most reliable method to preserve the humidity of the sample over long periods of time. Vacuum sealing samples in plastic provide good isolation for typical transportation times and may be easier to apply when on-site. In any case, using damp cloth to provide a source of moisture is not recommended as it can lead to leaching, does not preserve the sample in its pristine state, and is delicate to do correctly.

The procedure of samples conditioning before testing is still largely debatable. Although re-saturation was verified to be convenient, re-setting somehow the initial condition of AAR affected samples in a number of works (Larive, 1998b) (Sanchez, 2014), some researchers found that this procedure might cause dramatic effects on AAR prognosis, making its further development unreliable (Merz, 2015). Otherwise, drying effect is one of the main parameters affecting the reliability of AAR diagnosis and prognosis test procedures and thus it should be avoided. Moreover, it has been found that drying effects happen even in well-wrapped concrete specimens sealed in plastic sheets, but with a much lower degree compared to unsealed samples. Therefore, a maximum of a 48-hour rewetting period as by CSA23.2-14C (48 hours "re-saturation" in the moist curing room (protected from running water) at 23 $\pm$ 2^{o}C and 100% R.H.) was found largely suitable to contribute at reducing the deleterious effect of drying of AAR test specimens, restoring their initial conditions and thus enabling reliable condition assessment. Finally, it should be noted that re-wetting procedures tend to increase the variability of results of companion samples.

5.1.4 Procedure

In order to minimize the transportation and storage effects on reliability of AAR diagnosis and prognosis test procedures, 6 very important steps are needed to mitigate further problems due to transportation and/or storage of AAR specimens:

1. After casting or extraction, the samples should be weighted and well-wrapped.
2. In the case of testing drilled cores, the specimens should be stored in the laboratory for at least five days prior to testing, in order to homogenize their moisture degree;
3. Once wrapped, in the case of mechanical testing, the ends of the samples should be prepared (e.g. grinding or capping). The length to diameter ratio of the samples should be selected as a function of the test to be performed but shall not be lower than 2.
4. In the case of mid/long-term transportation and or storage, a temperature equal or slightly lower to 12°C should be selected. This low temperature was found to be able to avoid AAR further development, (Saouma, 2020).
5. After transportation and/or period of storage, the samples should be weighted again to assess potential drying. Then, in the case of significant difference from their original weight, samples shall be placed in the moisture curing room (CSA23.2-14C, 2009) at 23 $\pm$ 2^{o}C and 100% R.H. (protected from running water) until either the samples reach their initial measured weight

or for a maximum of 48 hours. The period of re-saturation shall not exceed 48 hours;

6. Samples are ready for testing.

5.1.5 Shipment

During transportation and shipment, cores must be placed in a temperature-controlled box to ensure $T \leq 12°C$. It was found that

FedEx has temperature range that vary between 2° and 8°C for up to 96 hours (4 days), (FedEx, 2017).

5.2 laboratory Testing

Diagnosis and prognosis of the AAR in the dam is a multilevel endeavor, Fig. 5.1 and should

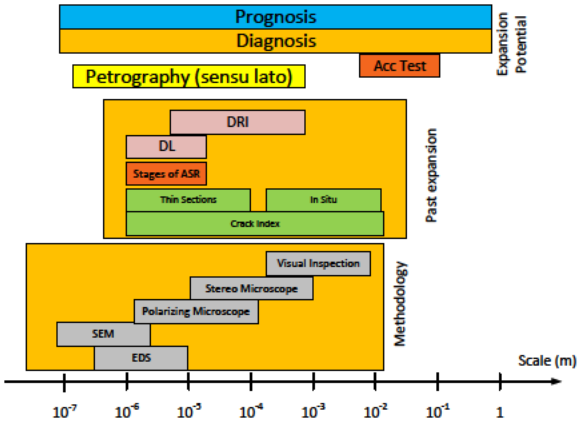

Figure 5.1: Overview of Methodology (Saouma, 2020)

include at a minimum (Fournier and Bérubé, 2000):

Laboratory investigation

petrographic examination

Qunatitative petrographics assessment of internal damage.

water-soluble alkali content of concrete

Expansion tests of concrete cores.

Mechanical testing of specimens.

5.2.1 Petrographic examination

Core samples are examined using tools such as the petrographic, stereobinocular, and scanning electron microscopes to identify the presence and distribution of typical petrographic signs of AAR. This is an essential test to diagnose AAR in concrete.

Microcracking develops wherever the tensile stress generated by swelling of aggregate particles undergoing AAR exceeds the tensile strength of the particles and of the surrounding cement paste.

Microcracks, first limited to the aggregate particles, will extend into the cement paste and typically between aggregate-to-aggregate particles with increasing expansion. The proportion of cracked aggregate particles increases with the progression of AAR.

Loss of the cement paste - aggregate bond was reported as a consequence, but not necessarily indicative of AAR. Aggregate shrinkage, plastic shrinkage of cement paste, AAR, and internal sulphate attack can generate cracks around the edges of aggregate particles and debonding at the interface.

Qualitative Alkali-silica reaction typically produces secondary reaction products containing silica, alkalies, and calcium as typical constituents. On polished sections of concrete affected by AAR, gel can be found lining or filling pores and cracks within the aggregate particles and the cement paste. Broken surfaces of such concrete cores often show deposits of reaction products covering more or less extensive areas of the cement paste along with a typical arrangement of reaction products through the reactive particles, i.e., a layer of massive gel forming a dark rim and surrounding powdery white deposits corresponding to microcrystalline reaction products. Alkali-silica reactive aggregates are often bordered by a dark reaction rim on polished sections of concrete affected by AAR. These rims must not be mixed up with "alteration" rim often found in the outer portion of weathered gravel particles.

Quantitative A quantitative petrographic assessment of internal damage consists of counting the number of petrographic features of AAR on 15-mm squares of a grid drawn on polished concrete sections using a stereobinocular (16x) microscope. The total number of each type of defects is counted, normalized to a surface of 100 cm^2, and then multiplied by weighing factors. The sum of the factored totals of each defect gives the Damage Rating Index (DRI).

5.2.2 Water-soluble alkali content of concrete

A simple technique involving the hot-water extraction of alkalies from concrete was proposed and investigated in detail by Berube et al. (2000a). A 2-kg sample of concrete is first crushed to pass the 75-μm (no. 200) sieve. A 10-g subsample is then immersed in 100 mL of distilled water, boiled for 10 min, and allowed to stand in the solution overnight at room temperature. The suspension is then filtered, the volume of solution adjusted at 100 mL with distilled water, and the alkali (Kand Na) content in the solution determined by flame photometry. For example, tests performed on samples cored from concrete structures affected by AAR in New Brunswick gave water soluble alkali contents ranging from 1.2 to 5.0 kg/m^3 Na_2O eq. Data from this test can be used both for diagnosis and prognosis purposes.

5.2.3 Expansion tests

This is one of the most important test that can be performed for prognosis purpose.

Description of this test being beyond the scope of this report, the reader is referred to the state of the art report that has recently been published in (Saouma, 2020) by researchers worldwide. It is the author's opinion that the best approach is the one of Katayama (2017).

5.3 Mechanical Testing

`Section adapted from (Saouma, 2013)`

5.3.1 Randomness of Properties

The selection of material properties should take into account their inherent spatial variability within a structure (where concrete, possibly from various sources, is likely to have been cast over an extended period of time with less than perfect quality control).

A variation in test results is expected due to multiple factors, including the method for placing and aging concrete under field conditions. As a case in point, Figure 5.2 illustrates typical compressive stress-strain curves, as measured on 15 core samples taken from a single Reclamation dam and then tested at Reclamation laboratories according to ASTM standards, (Mills-Bria et al., 2006). In

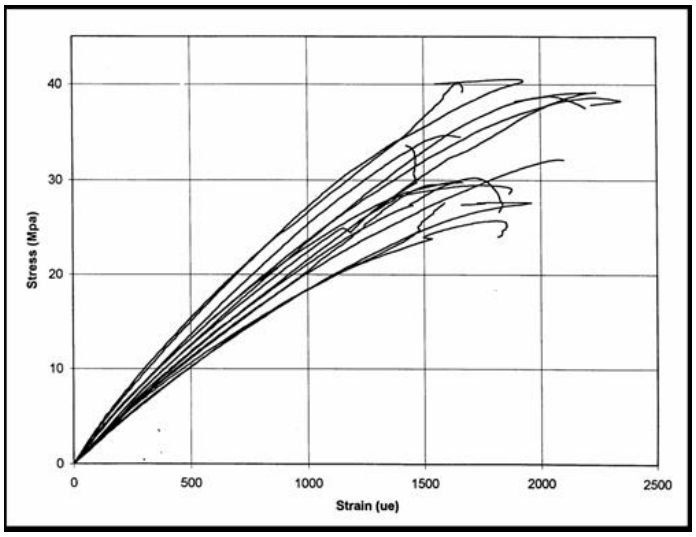

Figure 5.2: Variation in 15 compressive stress-strain tests conducted at the same dam (Mills-Bria et al., 2006)

another related study, the Reclamation facility tested 6-inch diameter cores (i.e. with a maximum aggregate size of approx. 6 inches) drilled perpendicular to the top surface dams and sealed in plastic to preserve the in situ moisture content during shipping. Table lists the average, maximum and minimum values for eleven dams. The ratio of the maximum average to the minimum average is observed to be approximately 7:1 for compressive strength, 10:1 for the modulus of elasticity and 4:1 for compressive strain at failure. If examined project-by-project, the maximum range would be 3.5 times for compressive strength, 8 times for modulus of elasticity and 2 times for compressive strain at failure.

It thus appears obvious that the properties for a given structure should be based on multiple tests on cores retrieved from the altered structure.

Moreover, due to uncertainly regarding project-specific materials, the properties selected for

Project	Average			Maximum			Minimum		
	Strength MPa	E GPa	Strain $\times 10^{-6}$	Strength MPA	E GPa	Strain $\times 10^{-6}$	Strength MPa	E GPa	Strain $\times 10^{-6}$
Deadwood	32.4	24.1	1,785	41.5	29.7	2,240	22.1	20.7	1,103
Elephant Butte	17.4	19.1	1,450	31.1	30.3	2,055	8.8	10.3	
Englebright	45.0	32.4		45.0	32.4				
Folsom	29.3	14.5		29.3	14.5				
Hoover	47.5	38.6		63.6	51.7	29.3	14.5		
Monticello	30.5	35.6	1,183	40.1	49.6	1,400	41.9	26.9	
Pine Flat	26.8	26.9		26.8	26.9				
Roosevelt	37.3	37.9	1,175	48.8	55,2	1,625	28.2	18.6	
Seminoe	24.1	11.7	951	36.4	22,4	2,880	15.6	6.9	
Stewart Mountain	34.8	26.9		46.0	40.0	24.8	14.5		
Warm Springs	20.2	23.4		46.0	46.2		10.2	5.5	
All projects	31.4	26.2		63.6	55.1		8.8	5.5	

Table 5.1: Summary of static compression tests performed on 11 dams (Mills-Bria et al., 2006)

input should include a bandwidth of $\pm\sigma\%$ of expected values, where σ depends on the number of tests performed. If no more than one test data point were available, then σ should equal 15-20%.

5.3.2 Elastic properties

Elastic properties are the most basic mechanical properties needed to conduct a finite element analysis; this section will individually address each of the most essential elastic properties. We will omit compressive strength since it is the unanimously tested property and most often serves to derive the other quantities (similar to the physical quantities expressed in terms of L, T and M for length, time and mass, respectively).

It should be noted that the following tests were written for small aggregate sizes by ACI or ASTM standards. Those will not be applicable for concrete dams where the MSA can be as high as 3 inches if not higher. However, those same tests are referenced in Reclamation report (Harris et al., 2006) and by FERC (FERC, 1999) and hence they are kept with a word of caution.

5.3.2.1 Elastic modulus

Based on a large number of tests conducted, ACI 318.2-14 (2014) has established the following empirical relationship between compressive strength f'_c MPa (lb/in^2) and the unit weight of the concrete kg/m^3 (lb/ft^3):

$$E_c = \begin{cases} 0.043 w_c^{1.5} \sqrt{f'_c} & \text{MPa} \\ 33 w_c^{1.5} \sqrt{f'_c} & \text{lb/in}^2 \end{cases} \tag{5.1}$$

Assuming a density of normal weight concrete equal to 2,320 kg/m^3 (145 lb/ft^3), this expression can be reduced to:

$$E_c = \begin{cases} 4,730 \sqrt{f'_c} & \text{MPa} \\ 57,000 \sqrt{f'_c} & \text{lb/in}^2 \end{cases} \tag{5.2}$$

It is commonly assumed that the modulus of elasticity remains the same whether in tension or compression.

5.3.2.2 Tensile strength

As with the compressive strength, one must differentiate between two types of tensile strength:

- Load-controlled
- Strain controlled.

In the former, one could use a standard testing machine, and if the specimen is properly attached, the peak tensile strength can be obtained. It should be noted that results can vary greatly with the slightest misalignment of the specimen. Hence, it is recommended that at least three tests be performed.

On the other hand, modern computational codes require the fracture energy G_F of the concrete. This should, ideally, be determined from a *servo-controlled* hydraulic testing machine to capture the post-peak response.

For small specimen setups, the set-up shown in Figure 5.3. Should laboratory tests be unavail-

(a) Experimental set-up (b) Ruptured specimen

Figure 5.3: Experimental set-up for a direct tension test (Delft University)

able, empirical equations can be used to estimate concrete tensile strength values.

Empirical relations for tensile strength are given by:

$$f_t' = \begin{cases} 3 - 5\sqrt{f_c'} & \text{psi} \quad \text{ACI-318} \\ 1.4\left(\frac{f_{ck}}{f_{ck0}}\right)^{2/3} & \text{MPa} \quad \text{CEB-FIP} \end{cases} \tag{5.3}$$

where: f_{ck} is the cylinder compression strength and f_{ck0} equals 10 MPa.

Finally, splitting tensile tests can be determined from the procedure described by (Salamon, 2018).

For mass concrete, Raphael (1984) studied concrete tensile strength from nearly 12,000 concrete specimens and showed the limited basis for assuming a linear relationship between tensile and compressive strength. The author compared: 1) the relationship between direct tensile strength, splitting tensile strength and modulus of rupture; 2) the relationship between linear and nonlinear assumptions applicable to concrete strength; and 3) the relationship between the static and dynamic strength of concrete. It was found that the direct tensile strength is typically about half the splitting tensile strength. It was also demonstrated that the drying of cylinders affects their strength.

In the absence of test results, Raphael suggested a method for estimating splitting strength from the compressive strength of concrete, namely:

$$f_{st} = \frac{2P}{\pi LD} = \alpha f_c^{2/3} \tag{5.4}$$

where:

α	1.7 for static loading
	2.3 for static loading, though this accounts for concrete nonlinearity
	2.6 for seismic loading
f_{st}	Splitting tensile strength
P	Compressive force applied to the specimen
L	Specimen length
D	Specimen diameter
f_c	Uniaxial static compressive strength of the concrete

Raphael also recommended using α =2.3 for static finite element analysis and:

$$f_{st} = \frac{2P}{\pi LD} = 3.4 f_c^{3/2} \tag{5.5}$$

for linear finite element analysis under seismic loading.

The modulus of rupture can then be estimated from:

$$f_{mr} = \frac{PL}{bd^2} = 1.33 f_{st} = 2.3 f_c^{2/3} \tag{5.6}$$

where:

f_{mr}	Tensile strength obtained from a modulus of rupture test
P	Force applied to the specimen
L	Specimen length
b	Specimen width
d	Specimen depth

f_c Uniaxial static compressive strength of the concrete

5.3.2.3 Poisson's ratio

The Poisson's ratio for concrete typically lies between 0.2 and 0.25. Results from the structural analysis are relatively insensitive to the assumed value. As a consequence, Poisson's ratio is typically set to 0.2 (unless data are available).

5.4 Thermal properties

AAR expansion is very sensitive to temperature (and relative humidity). Hence, a proper AAR assessment of a structure must begin with a finite element thermal analysis.

This section is intended to simply provide assistance in assigning (air) temperature and physical property values as part of a thermal analysis.

5.4.1 Temperatures

5.4.1.1 Air temperature

The daily variation in air temperature obviously depends on the geographic location. The National Oceanographic and Atmospheric Agency (NOAA) has set up a National Climatic Data Center http://www.ncdc.noaa.gov/oa/climate/climatedata.html#surface containing thousands of locations worldwide that can be accessed for thermal analyses.

On the other hand, should data be limited, the transient variation of temperature can be estimated based on T_{mean}, T_{min} and T_{max}, which denote the mean, minimum and maximum temperatures respectively:

$$T_a(t) = A \sin\left(\frac{2\pi(t-\xi)}{365}\right) + T_{mean} \tag{5.7}$$

where $A = 0.5\,(|T_{max} - T_{mean}| + |T_{min} - T_{mean}|)$, t is the time in days, and ξ the time in days when $T_a = T_{mean}$. To avoid having to use the highly nonlinear equation for temperature exchange through radiation, a common approach is to increase ambient temperature by 0.5 to 1.0 deg C (i.e. 1 to 2 deg F). USACE (1994) and ACI-207 (2005) provided charts to allow approximating the estimates of solar radiation effects.

5.4.1.2 Pool temperature

An empirical equation for the reservoir temperature in terms of depth has been given by Anon. (1985):

$$T_w(y) = c + (T_{surf} - c)\, e^{-0.04y} \tag{5.8}$$

where:

$$c = \frac{T_{bot} - e^{-0/.04H} T_{surf}}{1 - e^{-0.04H}} \tag{5.9}$$

and T_{bot} T_{surf}, H and y are respectively the annual mean water temperatures at the bottom and surface, the reservoir depth (in meters), and the water depth in meters.

5.4.2 Concrete thermal properties

The material properties required to conduct a thermal analysis are summarized in Table 5.2. Ther-

Table 5.2: Material parameters required for a thermal analysis

	Steady-state	Transient
Material properties		
Mass density		ρ
Specific heat		c
Conductivity	k	k
Boundary conditions		
Temperature	T	T
Film	h	h
Flux	q	q

mal diffusivity h is a measure of the rate at which temperature change can occur in a material; its value is derived by dividing the thermal conductivity by the product of specific heat and unit weight. For mass concrete, typical thermal diffusivity values range from 0.003 to 0.006 m^2/hr.

For mass concrete, the thermal conductivity k equals approx. 2.7 J/sec.m.K., and the specific heat varies between 0.75 and 1.17 kJ/kg-K.

The film coefficients for heat transfer by convection are on the order of $h_{air} = 34 \text{W/m}^2 \ ^{oC}$ and $h_{water} = 100 \text{W/m}^2 \ ^{oC}$.

It should be noted that in a stress analysis, results are very sensitive to the selected coefficient of thermal expansion α, which depends on the type of aggregate and can be assumed equal to 1 $\times 10^{-5}$ m/m/^{o}C. Finally, it should be noted that in general the thermal analysis of the concrete dam assumes adiabatic conditions, (Malm, Hassanzadeh, and Hellgren, 2017) and thus the rock temperature can be ignored.

6 Analyses Procedures

This final chapter will procedurally describe the methodology to perform a modern safety assessment of a dam suffering from AAR. It will begin with general considerations regarding analysis, and then address the AAR analysis of dams. In this context, clear distinction will be made between the State of the Practice, and the State of the Art process advocated in this report.

6.1 Science and Art of Modeling

6.1.1 Introduction

This chapter provides the reader with basic recommendations prior to *any* finite element study. More specifically, how to understand and articulate and then mathematically define the problem, how to gather the required data from multiple sources and synthetize them, how to define the mathematical (finite element) model, how to identify the computer codes and assess the quality of the results, and finally how to prepare a report. Modeling is the science and art of addressing all of the above.

Coverage (albeit condensed) of the finite element method is left to any of the multiple references on the method (Zienkiewicz, Taylor, and Zhu, 2005) (Zienkiewicz, Taylor, and Nithiarasu, 2005) (Hughes, 1987) (Belytschko, Liu, and Moran, 2000).

This chapter will focus on a topic seldom addressed in the literature, that is the science and art of modeling. Cautionary note: modeling existing structure is very different from modeling new structures. In the later, one is confined (typically) with linear elastic analyses for service loads, and known material physical properties and loads (based on design specifications). In the former, typically one seeks to assess the safety margin (or factor) based on the ultimate loads. Hence, material properties must be the actual ones (may require coring), loads to be considered are different (may not simply rely on factored loads of the LRFD method). For existing structures (more so than for new ones), great caution should be exercised in addressing aging factors such as: creep, relaxation, chloride diffusion-carbonation and possible ensuing corrosion of rebars, alakli-aggrgate reactions, and other factors.

Broadly speaking, the finite element analysis of a dam can be summarized by Fig. 6.1. each of

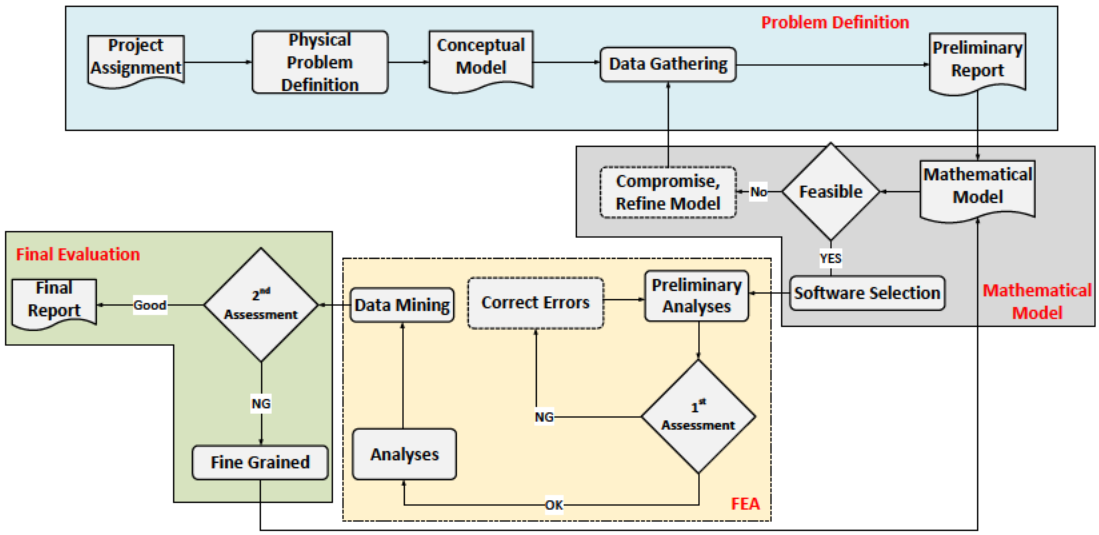

Figure 6.1: Finite Element Process (inspired by Bathe (1996))

the major blocks will be separately addressed below.

6.1.2 Tasks

6.1.2.1 Problem Definition

The first step consists in simply defining the problem in terms of the following:

Project Assignment is typically a document written with input from regulators, site and safety engineers and others interested in assessing the structural safety of the dam. It is typically driven by safety and regulatory requirements, and should not be unduly influenced by potential task complexity, lack of data, expertise or resources. In other words it is a "wish list".

Physical Problem Definition is a translation of the previous document to specific requirements of the analyses to be undertaken. It should include the specifically desired numerical results in a manner easily understood by the finite element analyst.

Conceptual Model is based on the "wish list" of the project manager for the task. It is coarse grained, does not dwell in actual details, and summarizes all assumptions, algorithms, relationships, and data that describe the reality of interest from which the mathematical model and validation experiment can be later constructed. It will also spell out the expectation, break down the project in clearly identifiable tasks, and translate what may be a partially legalistic document into an engineering one (see Sect. 6.1.4). This document should never be modified. If possible, prior to any analysis, it should include anticipated orders of magnitudes of the desired response bracketed between *minima* and *maxima* and anticipated failure modes. This will be important for subsequent "reality/sanity checks" in the first assessment.

Data Gathering is the first attempt by the analysis to translate the previous assignment into

specific tasks such as:

- Are all necessary material properties available? Where could one get them (archives, site engineer, literature, others), how reliable are they?
- Is there a need to perform laboratory tests, are the financial resources available, can one easily obtain regulatory authorization to extract cores?
- Software requirements should be spelled out before identifying the one to be used. It may very well be that the "commonly used one" does not have the required features. Eventual discrepancies should be duly noted.
- Is there in-house the expertise to
  1. Perform the numerical simulation.
  2. Supervise/review the simulation performed by others.
- Identify third party independent reviewers for the project.

Preliminary Report Report on data gatherings, and repeat the anticipated results (failure modes, order of magnitudes of results).

6.1.2.2 Mathematical Model

A mathematical model is the link between the problem statement and the actual finite element simulation. It is a fine-grained document which details of the following

Mathematical Model Based on the "marhing orders" defined previously in the Conceptual Model, and involves identifying material properties Sect. 6.1.3.3; loads and boundary conditions, Sect. 6.1.3.2 below; type of analysis (linear, nonlinear, implicit, explicit).

Assess Feasibility This is a "reality check" on whether the *desiderata* can indeed be fulfilled realistically.

Compromise If the model can not fully respond to the needs articulated in the second report, then compromises must be made, recorded, and the process of data gathering is repeated.

Software Selection is a critical step which affect the overall performance.

6.1.2.3 Finite Element Analyses

Preliminary Analysis usually, linear elastic to test definition of material properties, boundary conditions, and loads.

Preliminary Assessment Perform a "reality check" on the results. Are they out of bound (different orders of magnitude) of those anticipated in the preliminary report? are there blatant erroneous data entries, mixed units? are the displacements consistent with loads or boundary conditions? Is the load path realistic? are there zone of the mesh which should be refined? Should one use different number of increments, integration scheme? are the convergence criteria too tight?

Correct Errors that may have resulted in unacceptable preliminary results.

Analyses of the structure going incrementally from the simplest to the most complex.

Data Mining Is the process of extracting all relevant results from piles of output. Some software allow specific data to be dumped on disk files, others not. Data may have to be extracted wither from the graphical post-processor or from the ascii-output, and stored. It is best to store all retrieved data in an Excel sheet, and then use programs such as Matlab or Python to read the data and plot them as is best suited for the demand.

6.1.2.4 Final Evaluation

Finally a final evaluation of the series of analyses must be performed.

2^{nd} Assessment Is a "fine grained" assessment of results to determine if they are truly meaningful and reflect a solution to the problem. If not, then the mathematical model itself must be revisited.

Final Report Should have a short executive summary, the body of the report, and typically many appendices with plots and graphs.

6.1.3 Key Considerations

6.1.3.1 Modeling

Prior to modeling a complex structure, important questions must first be addressed, as they will subsequently guide the analyst in the model.

- Can the structure be modeled as 2D or 3D? In the former should it be plane strain. Given available computational powers, a 3D model should be used when possible albeit mesh preparation time is a major consideration.
- Are we interested only in the limit state, that is only the failure load, or in the full nonlinear response. Limit states loads are either upper or lower bound solutions.
- Transient analysis is increasingly favored over response spectrum or modal analyses. The later were *in-vogue* when computational power was in limited supply and are not suitable for nonlinear response. Hence, the nonlinear dynamic response of a structure can be obtained wither through the full power of a nonlinear transient analysis, or a simplified pushover one.
- Response can be highly dependent on damping. Rayleigh damping is essentially an artificial scheme to implicitly account for energy dissipation due to nonlinear response. It is both mass and stiffness proportional. Hence, analyst should exercise great care in selecting damping coefficients (if any) in the context of a nonlinear analysis where energy dissipation is implicitly factored in the algorithm.
- Extent of nonlinear analysis must be ascertained. Are we only interested in the peak load for safety or are we also interested din the post-peak response (softening) for ductility assessment?
- How certain are we with the loads, material properties? Should one be limited to a single deterministic analysis, or should a probabilistic investigation be conducted through multiple analyses (Monte-Carlo)?

The final model is ultimately not only a compromise between requirements and time/cost constraints, but also a function of understanding of the problem, the available tools/expertise and type of results expected (very precise deterministic, or more approximate probabilistic

How should one perform an analysis where interest is in a localized zone. At a time when computational power was limited, substructuring was *in vogue* modern approach tends to focus on an "intelligent" mesh, that is one properly graded in terms of density, and assignment of material properties (linear *vs.* nonlinear).

Modeling attention to details must be uniformly distributed over the entire process, Fig. 6.2. On the one hand, one may inadvertently underestimate the importance of a modeling aspect, and this weakest link may then trigger failure. For instance bond failure may be overlooked, yet for seismic loads it is critical at the base of the container. Similarly, disproportionate effort may be spent in modeling an aspect of the structure which is unlikely to play a critical role. For instance, modeling the stiffness of the liner or of the sleeves inside which the post-tensioning cables are housed may require much effort, increase the complexity of the model and is ultimately un-necesary.

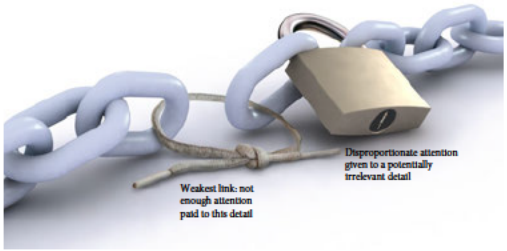

Figure 6.2: Uniformly distributed model complexity

Contrarily to linear elastic solutions, there is a multitude of acceptable nonlinear solutions. Different software, models and analysts will get different results and this does not imply that they are all "wrong" (but some may be) It should be kept in mind that, often, large scale failure driven by small overlooked details which in retrospect could and should have been considered in the model while major effort may have been spent on modeling irrelevant other details. Hence, great care should be exercised in identifying what must be modeled, what is relevant, and what is not. In the end, the finite element analysis is just a tool to confirm or quantify a response anticipated through proper solid engineering judgment.

6.1.3.2 Loads and Boundary Conditions

Loads should receive special attention specially in the context of a nonlinear (incremental analysis). Point loads should be completely discarded as they will induce a localized stress concentration which may slow down the analysis. Point loads should be replaced by distributed traction over a narrow strip.

Initial loads should be carefully applied initially through one or more increments even though they are unlikely to induce any nonlinearity. This is mostly for the gravity loads and initial

displacements. In all cases, too large of an increment will result in a slow convergence (assuming an implicit analysis), too small will result in increased computational time.

In a dynamic analysis time steps should be a function of the type of analysis. In an implicit one (where equilibrium is nearly enforced through iterations within an increment), the "usual" time step is 0.02 sec. Whereas in an explicit analysis, the time step should be much smaller to make ensure that a stress wave does not cross an entire element during a time step (thus computation time is in this case conditioned on the smallest element size in the mesh), (Courant, Friedrichs, and Lewy, 1967).

Whereas *a priori* boundary conditions may not be perceived as loads, they are. Indeed a non zero fixed support will induce loads. Careful in not drastically changing the boundary conditions on an analysis without the "buffer" of a few increments to allow equilibrium to be properly recovered.

Specially in an incremental nonlinear analysis, loading of each increment should be referenced, Table 6.1.

Table 6.1: Sample of Excel file storing load information

Increments		**Description**	multirow2[4]***Comments**
From	**To**		
1	end	B.C.: Lateral support	*on patch 231*
1	3	Initial gravity load	*this is a total and not an increment load*
4	8	Initial thermal load	
9	50	Incremental load	
51	52	Detention cable 21	
53	300	Incremental AAR load	*Careful about the time increment here*
Save and restart with removed BC			
301	20000	Seismic excitation	*uniform ground excitation hor. and ver.*

6.1.3.3 Material Properties

Material properties for a nonlinear analysis go well beyond the traditional compressive strength f'_c. Though each plant may be governed by different codes of construction (not to be confused with codes for safety assessment), in order of importance, the following data should be gathered for multiple site locations and prevalent standards recommended:

Compressive strength per ACI 349 (2006) or ASTM, C39 (2016).

Elastic Modulus per ACI 349 (2006) or ASTM C469 (2016). Ideally, the full stress-strain curve should be measured and reported. If possible, test should be conducted under strain control.

Tensile strength per ACI 349 (2006) or ASTM C496 (2016).

Fracture Energy is a most important parameter for modern nonlinear analysis.

Creep Coefficients per ASTM C512 (2016).

One should keep in mind that in a nonlinear analysis there are two types of material properties to be specified: the basic ones (typically tensile and compressive strength, elastic modulus, and

Poisson's ratio), and others specific to the nonlinear constitutive model. For the first set, and specially in the context of a safety assessment investigation, one can not rely on the construction specified values, but must be determined either from cores (preferably) or from non destructive evaluations (NDE). Furthermore, material properties are likely to vary spatially within a dam more specifically across vertical lifts. Hence, either probabilistic analyses should be conducted after selection of the distribution (normal, log-normal are the most common), the corresponding mean, standard deviation of key variable. Alternatively a homogenization technique must be adopted (this methodology is still in its infancy). Finally, selection of constitutive model specific input data should be preceded by a sensitivity analysis as those are nearly never obtainable from laboratory tests.

A major tenet in the scientific and engineering community is that a paper or report should contain sufficient detail (data, figures, and others) and references to permit others to replicate the work. Hence, all input data should be clearly identified: value, symbol, value, reference and properly tabulated in an excel spreadsheet.

6.1.4 Verification and Validation *vs.* Calibration

When conducting a nonlinear analysis, it is essential that the finite element code be validated and verified if possible.

Verification, validation and calibration are only three of multiple issues the analysis should consider. Thacker et al. (2004) breaks them down as follows

Verification deals with the mathematics of the problem and is the process of determining that a model implementation accurately represents the developer's conceptual description of the model and the solution to the model by comparing numerical solutions to analytical or highly accurate benchmark solutions.

Validation on the other hand deals with the physics of the problem and is the process of determining the degree to which a model is an accurate representation of the real world from the perspective of the intended uses of the model. It compares numerical solutions to experimental data.

Calibration is the process of adjusting numerical or physical modeling parameters in the computational model for the purpose of improving agreement with experimental data.

Calibration Experiment Experiment performed for the purpose of fitting (calibrating) model parameters.

Code Verification Process of determining that the computer code is correct and functioning as intended.

Computer Model Numerical implementation of the mathematical model, usually in the form of numerical discretization, solution algorithms, and convergence criteria.

Conceptual Model Collection of assumptions, algorithms, relationships, and data that describe the reality of interest from which the mathematical model and validation experiment can be constructed.

Confidence Probability that a numerical estimate will lie within a specified range.

Error is a recognizable deficiency in any phase or activity of modeling and simulation that is not due to lack of knowledge.

Experiment Observation and measurement of a physical system to improve fundamental understanding of physical behavior, improve mathematical models, estimate values of model parameters, and assess component or system performance.

Experimental Data Raw or processed observations (measurements) obtained from performing an experiment.

Experimental Outcomes Measured observations that reflect both random variability and systematic error.

Experiment Revision The process of changing experimental test design, procedures, or measurements to improve agreement with simulation outcomes.

Fidelity The difference between simulation and experimental outcomes.

Field Experiment Observation of system performance under fielded service conditions.

Inference Drawing conclusions about a population based on knowledge of a sample.

Irreducible Uncertainty Inherent variation associated with the physical system being modeled.

Laboratory Experiment Observation of physical system performance under controlled conditions.

Mathematical Model The mathematical equations, boundary values, initial conditions, and modeling data needed to describe the conceptual model.

Model Conceptual/mathematical/numerical description of a specific physical scenario, including geometrical, material, initial, and boundary data.

Model Revision The process of changing the basic assumptions, structure, parameter estimates, boundary values, or initial conditions of a model to improve agreement with experimental outcomes.

Nondeterministic Method An analysis method that quantifies the effect of uncertainties on the simulation outcomes (also known as probabilistic method).

Performance Model A computational representation of a model's performance (or failure), based usually on one or more model responses.

Prediction Use of a model to foretell the state of a physical system under conditions for which the model has not been validated.

Pretest Calculations Use of simulation outcomes to help design the validation experiment.

Reality of Interest The particular aspect of the world (unit problem, component problem, subsystem or complete system) to be measured and simulated.

Reducible Uncertainty Potential deficiency that is due to lack of knowledge, e.g., incomplete information, poor understanding of physical process, imprecisely defined or nonspecific description of failure modes, etc.

Risk The probability of failure combined with the consequence of failure.

Risk Tolerance The consequence of failure that one is willing to accept.

Simulation The ensemble of models—deterministic, load, boundary, material, performance, and uncertainty—that are exercised to produce a simulation outcome.

Simulation Outcome Output generated by the computer model that reflect both the deterministic and nondeterministic response of the model.

Uncertainty A potential deficiency in any phase or activity of the modeling or experimentation process that is due to inherent variability (irreducible uncertainty) or lack of knowledge (reducible uncertainty).

Uncertainty Quantification The process of characterizing all uncertainties in the model and experiment, and quantifying their effect on the simulation and experimental outcomes.

Validation Experiment Experiments that are performed to generate high-quality data for the purpose of validating a model.

Validation Metric A measure that defines the level of accuracy and precision of a simulation.

Warning: Too often nonlinear finite element code are presumed as "validated" by merely capturing the experimentally observed data (displacements typically). Often times, this is accompanied with very colorful figures, and juxtapositions. It should be kept in mind that nonlinear models have sufficient variables to "tune" many of them and then obtain what is perceived as an acceptable model.

Such model should scrutinized to make sure that all assumptions are sound and reasonable, that material properties adopted are realistic. In other words a mere superficial pictorial comparison is not sufficient.

6.2 Finite Element Modeling of AAR

Prognosis of hydraulic structures suffering from AAR is notoriously difficult and for some impossible.

For the most part, current approach relies on one or more investigative tools, Fig. 6.3. Unfortunately those methodologies tend to be disjointed and difficult to directly relate to others. For example a petrographer may find the DRI (or other measure microscopically determined) too elevated, and hence consider the structure unfit. Expansion tests may be performed, but results are seldom fed into the finite element study. Finite element studies themselves may be conducted with unvalidated codes.

There are essentially two possible approaches to model AAR, Fig. 6.4. The first is representative of thee State of the Practice, while the second captures the State of the Art in AAR.

A brief summary of the two methods is shown below.

Methods	State of the Practice (e.g. Hatch)	State of the Art (e.g. Merlin)
# of Analyses	Multiple, one for each year we are interested in	Single analysis that starts at time 0 (dam construction) up till desired year

What do we need for input data

Parameters	Topological distribution of damaged concrete properties over the dam at the time of analysis	Characteristics of the concrete expansion to capture its kinetics (3 parameters)
How do we obtain them	Subdivide the dam in multiple regions; Extract sufficient representative cores from each one of them; perform tests (E and f_c primarily)	1. Perform expansion and appropriate petrographic tests (Katayama), determine the 3 parameters that characterize the concrete since time of construction 2. Same as above, without petrographic tests, characterization since date of core extraction 3. Perform a parameter identification based on the historical record of crest deflections
	Analysis	
Advantage	Easier to perform the analysis if one does not have a finite element code that can track the expansion with time.	Single analysis that capture the entire response (displacements and internal deterioration of concrete); Requires only three parameters that capture the cause of the expansion (as opposed to multiple tests that reflect the consequences of the reaction); Truly captures the complex response of a structure subjected to AAR (listed as disadvantage for Method 1 below).
Disadvantage	Approximate as we have to assign material properties over large zones, many input data coming from tests. May not be representative enough as it does not capture: 1) interaction of temperature with expansion; 2) effect of confinement on the anisotropic expansion;	Some numerical instability may occur in a nonlinear time history analysis
	Analysis Output	

Dislacements stresses	Yes, a snapshot at time t (of analysis), i.e. one single scalar quantity at time t	Yes, a "movie" that captures the evolution of the dam response, i.e. a vector for each response in terms of time)
Concrete deterioration	No, that was part of the input	Yes as computed by the AAR model
	Future Prediction	
Possible	Will have to be based on the time dependent concrete deterioration	By just letting the analysis go beyond present date.
Reliability	Low would rely on the extrapolation of concrete damage measured in the laboratory and inputted in the mesh	High, embedded in the analysis are the expansion characteristics measured in the lab (or extracted from a parameter identification based on historical record of crest displacement)

6.2.1 State of the practice

The simplest approach, and one which does not require any specialized finite element code, is based on a mapping of the field determined concrete deterioration on the ensuing finite element mesh. The analysis, is then calibrated with some of the field measurements. Thus, a separate analysis will be conducted for each year of recorded mechanical properties.

6.2.1.1 AAR Modeling

One would start with testing cores (E, f_c and f_t, but not necessarily all three of them all the times) recovered from the dam at time t_i. Then, one would, semi-arbitrarily but certainly approximately, assign a representative region to each one of the cores. Within that region, elements of the mesh will be assigned the same mechanical properties.

Separately, at time t_i one would estimate the AAR expansion $\varepsilon^{\infty}(t_i)$, and its spatial distribution $\varepsilon^{AAR}(t_i, x, y)$.

Finally, combining those two, a finite element analysis is performed. However, this is very likely to yield good correlation with recorded field displacements. Hence, correction are made with *some* of the recorded data, and verification is made with the others. This is repeated until adequate comparison at time t_i is achieved. Adjustments are for a given time t_i and are very unlikely to be the same for time t_j.

The outcome of such a calibration (for $E|f_t|f_c$) is a spatial and temporal partitioning shown

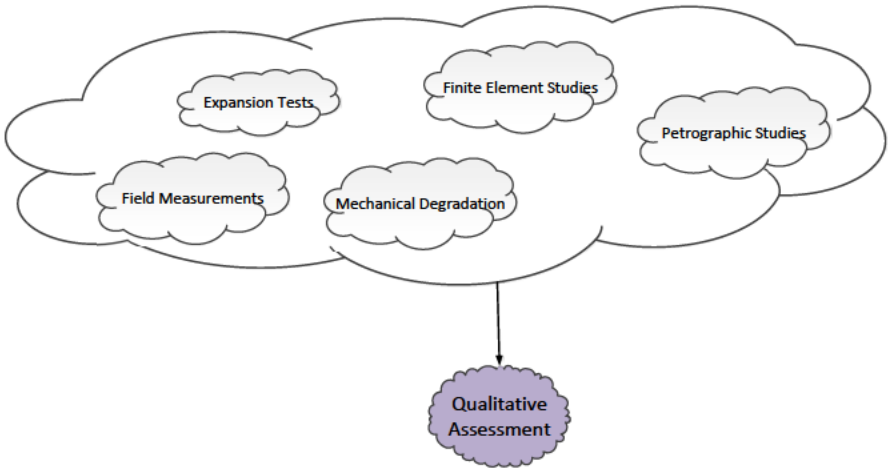

Figure 6.3: A clouded approach

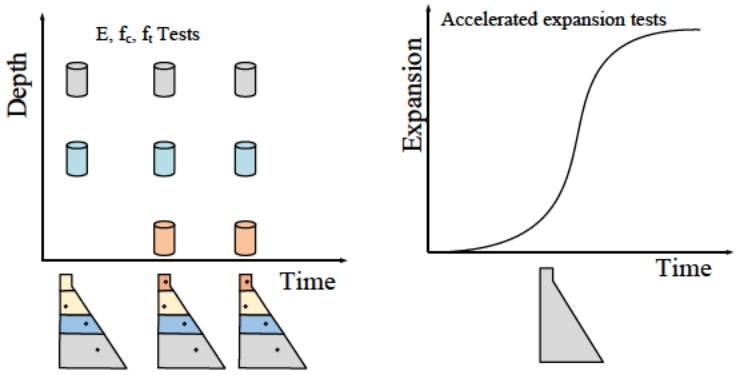

Figure 6.4: AAR FEA models

below, Fig. 6.5

$$
\begin{aligned}
[E|f_t|f_c](h,t) &= \begin{cases}
a_1 f_1(h) \times f_2(t) & yr_1 \le t \le yr_2 \quad \& \quad h \ge h_1 \quad ① \\
a_2 f_2(t) & yr_1 \le t \le yr_2 \quad \& \quad h < h_1 \quad ② \\
a_3 f_1(h) & t < yr_1 \quad \& \quad h \ge h_1 \quad ③ \\
a_4 f_1(h) & t > yr_2 \quad \& \quad h \ge h_1 \quad ④ \\
a_5 & t < yr_1 \quad \& \quad h < h_1 \quad ⑤ \\
a_6 & t > yr_2 \quad \& \quad h < h_1 \quad ⑥
\end{cases} \\
f_1(h) &= b_1 + b_2 h + b_3 h^2 \\
f_2(t) &= c_1 + c_2 t + c_3 t^2
\end{aligned}
\tag{6.1}
$$

The major (but not only) concern with this method, is that typically one would have not only very limited measurements but those are also widely spaced in times. This is further exacerbated by the seldom performance of tensile strength. This handicap is best illustrated by Fig. 6.6. One

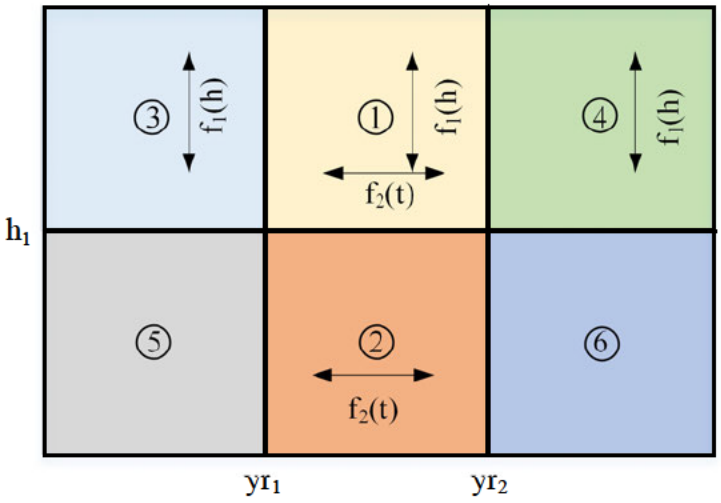

Figure 6.5: Spatial and temporal partitioning

can readily note the very gross approximation one has to resort to in such an analysis[1].

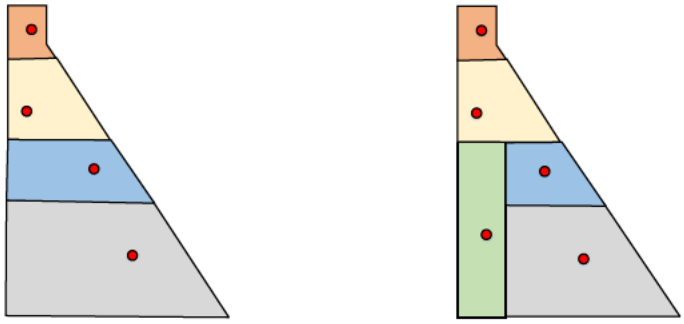

(a) Time t_1 (b) Time t_2

Figure 6.6: Mapping of recovered core test results (E, f_c, f_t) measurement into finite element mesh

Typically, only few cores are drilled and tested during the life of the dam. Hence, mapping deterioration over the dam is at best approximate. Furthermore, the idiosyncrasies of the AAR (Saouma, V.E., 2014) are not captured.

This approach has been primarily used by consulting engineers.

6.2.1.2 Failure Criterion

Typically, the failure criterion is a post-processing of an otherwise linear elastic analysis (with possible exception for the contact elements). Those would include:

[1]Though an idealization, these curves are based on an actual study espousing this method.

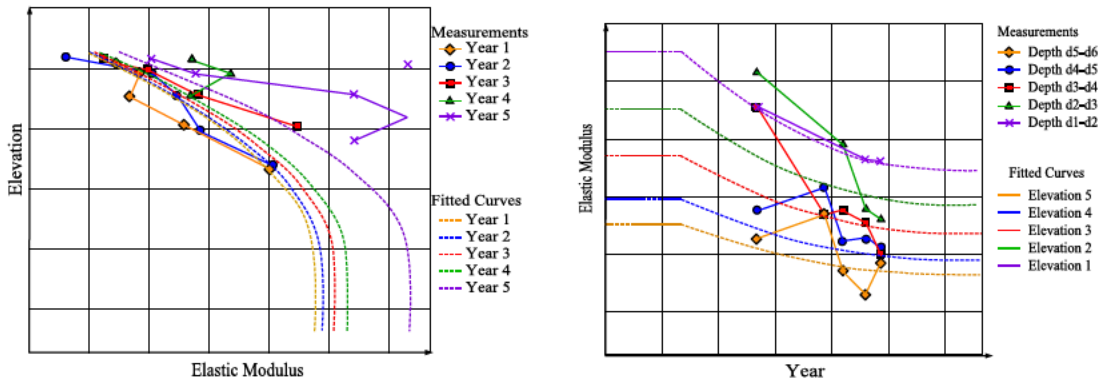

(a) Elastic modulus

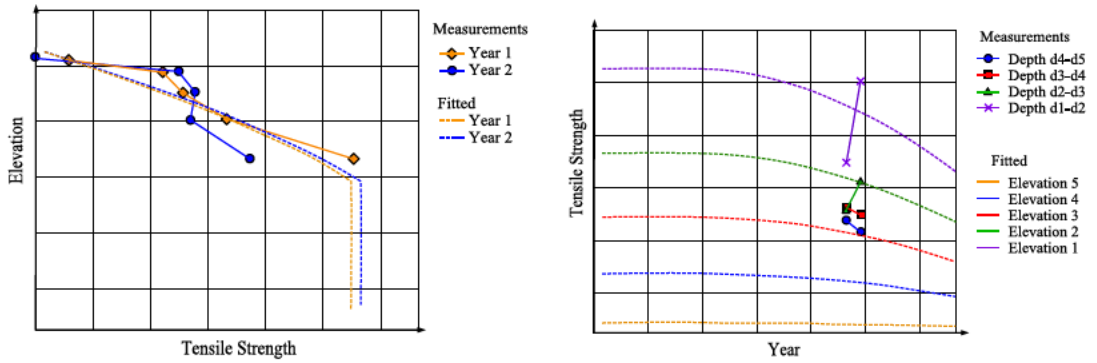

(b) Tensile strength

Figure 6.7: Spatial and temporal fitting for concrete mechanical properties based on limited cores and observations (courtesy Y. Gakuhari)

1. Uniaxial compression failure criterion
2. Uniaxial tension failure criterion
3. Triaxial failure criterion

Also, a final '*concrete cracking analysis* may be performed using the so-called *smeared crack model*. This will inherently allow for internal stress redistribution and a corresponding increase in compressive stresses.

6.2.2 State of the Art

In this second approach, one that is rooted in the State of the Art, one would take into account apparent (or not so apparent) synergy between investigative tools, Fig. 6.8.

It should be noted that the approach about to be presented has been used by some researchers already, (Saouma, Perotti, and Shimpo, 2007) (Comi, Fedele, and Perego, 2009) (Sellier et al., 2009a) (Huang and Spencer, 2016) to name a few. The most recent, and comprehensive, study was recently presented by Joshi et al. (2021).

This approach consists of three major stages, each one will be described separately in the next

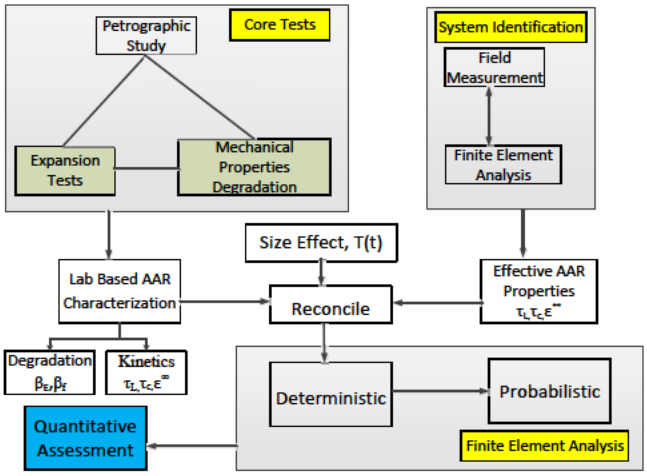

Figure 6.8: Assessment paradigms for AAR affected structures

section.

6.2.2.1 AAR Modeling

It should be emphasized that, in this approach, any quantitative assessment will have to rely on a mathematical model for the concrete expansion. The model usually adopted is based on the one of Ulm et al. (2000) which is nearly universally accepted. The model, along with its extension by the author, is described in Appendix §4.

6.2.2.2 Core Tests

Historically, and for good reasons, once external signs of AAR manifested themselves (irreversible displacement, map cracking) engineers have testes core samples extracted from the dam.

Tests have been handled by two different professions:

Petrographers who identify the type of reactive aggregate, the presence of micro-cracks, and who ultimately come up with a either a qualitative assessment (such as "severely damaged") or a quantitiave one (such as a Damage Rating Index). Neither one of those two assessment can be taken at face value. One then perform a spatial and temporal analysis of the damage.

Engineers: instead are more likely to perform both mechanical tests (E, f_c and occasionally f_t), and expansion tests. However we do not have a universally accepted testing and assessment method (Saouma, 2020). Furthermore, results of those expansion tests are seldom used in an ensuing finite element analysis.

Questions that can be answered from core tests (not to be confused with dam response) are, Figure 6.9:

1. What was the past expansion, ε_1 when cores were recovered?
2. At what time t_2 will the reaction stop[2]?

[2]Some argue that the reaction may go indefinitely, however this would violate the fundamental law of conservation

3. What would be the corresponding future expansion, ε_2 (note that the total expansion will be then $\varepsilon_1 + \varepsilon_2$)?

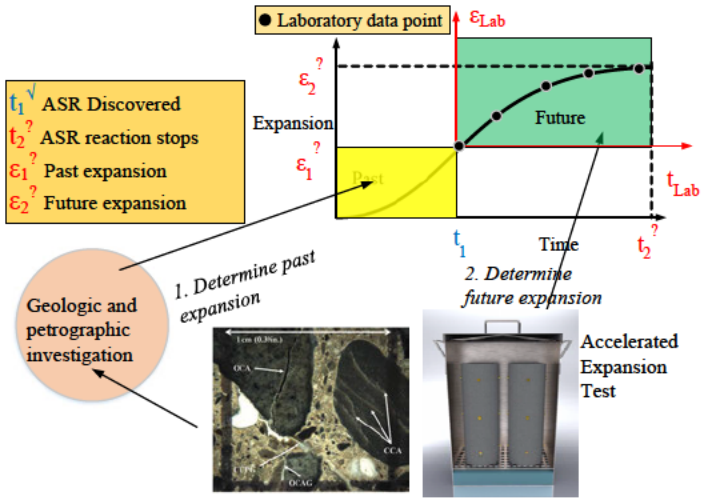

Figure 6.9: Estimate of past and future ASR expansions

6.2.2.3 Past Expansion

Having a grasp of past expansion is important to capture the entire kinetics of the expansion and its accompanying concrete degradation. Though not essential, knowledge of the past expansion reinforces the reliability of the reaction kinetics, and thus makes extrapolation more reliable.

There are two approaches to estimate past approaches.

6.2.2.3.1 Petrographic study pioneered by Katayama (Saouma, 2020, Appendix B).

A unique feature of the method, is that through petrographic analysis, Katayama can estimate τ_c, τ_L ε^{AAR} that mathematically characterize concrete expansion (Eq. 4.2 ??) since construction.

It should be emphasized that the type of petrographic study needed, and its interpretation is quite different than what is likely to have been performed for Mactaquac by Laval University.

The method is described in appendix B.

6.2.2.3.2 Young's Modulus Degradation As discussed in (Esposito, Hendriks, and Çopuroğlu, 2016) and (Gowripalan et al., 2019), there is an apparent correlation between past expansion and degradation of mechanical properties. Though not yet fully understood, the method is being used in the assessment of a nuclear containment building (NextEra-ML16216A240, 2016). However, one should be cautioned that there may be a wide margin of error in the method, Fig. 6.10.

of mass (Saouma et al., 2015).

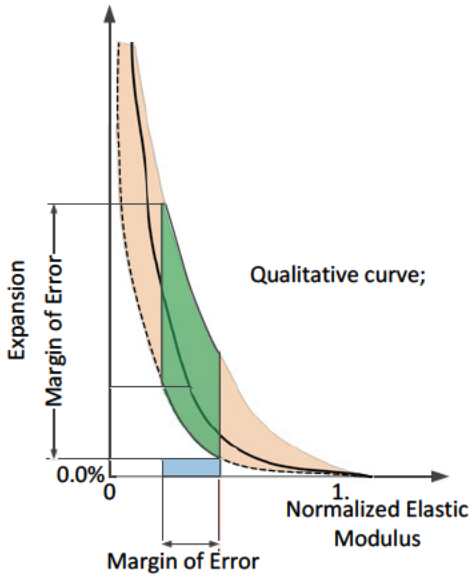

Figure 6.10: Estimate of past expansion based on reduction of Elastic Modulus

6.2.2.4 Future Expansion

Answers to the second and third questions can be addressed through careful examination of accelerated expansion tests.

6.2.2.4.1 Deterministic Presently, there is no universally accepted test procedure, and the major ones are reported in (Saouma, 2020). Laboratory expansion is accelerated by storing samples at high temperatures (typically 38°C.).

In this context, the term future expansion can be misleading, and we need to distinguish between the following:

1. End of time corresponding to core accelerated expansion tests.
2. Exhaustion of the reaction (i.e. reached a plateau).

The (complex) interaction is illustrated by Fig. 6.11.

1. The laboratory accelerated expansion curve provides us with curve ① (in the $\varepsilon_{\text{lab}} - t_{\text{lab}}$ coordinates).
2. Determination of the characteristic and latency times (τ_l and τ_c) require the knowledge of the corresponding activation energies (U_l, U_c.), Eq. ??. Though presumably those are "universal" values, they were found to be concrete dependent, and can be determined if identical tests were conducted at different temperatures, Fig. 4.1(c) through Eq. 4.5.
3. Following the determination of the activation energies, the laboratory data is fitted to Eq. 4.2, and the set of $[\tau_l, \tau_c, \varepsilon^\infty]$ are determined.
4. Knowledge (albeit approximate) of the past expansion, enables us to extend the first curve into curve ② (in the $\varepsilon_{\text{field/lab}} - t_{\text{lab}}$ coord.).

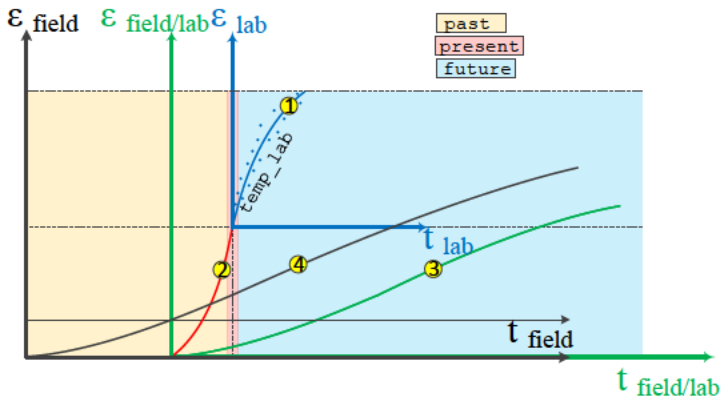

Figure 6.11: Schematic representation of the proposed algorithm

5. ① ∪ ② ($\varepsilon_{\text{field/lab}} - t_{\text{lab}}$ coord.) now constitutes the full expansion in laboratory time.
6. One can determine the updated set of $[\tau_l, \tau_c, \varepsilon^{\infty}]$
7. The previous combined curve is now expanded to real time, and the total expansion is reduced because the actual structure may have a RH lower than the one in the laboratory, ③ ($\varepsilon_{\text{field/lab}} - t_{\text{field}}$ coord.) For a dam, this reduction may be minimal.
8. ④ ($\varepsilon_{\text{field}} - t_{\text{field}}$ coord.) The curve is now shifted back to the construction time.

6.2.2.4.2 Probabilistic Though rigorous in nature, the previously described methodology is prone to uncertainties associated with the nature of the data (i.e. we are confronted with aleatoric uncertainties, but not epistemic ones). It was described with the assumption of the existence of a single curve, Figure 6.11.

When multiple curve data is available (i.e., curves ① in Figure 6.12), then for each one we will generate corresponding curves, then we could evaluate for each of the three final sets $[\tau_{l,field}, \tau_{c,field}, \varepsilon^{\infty}_{\text{field}}]$ a mean, and standard deviation.

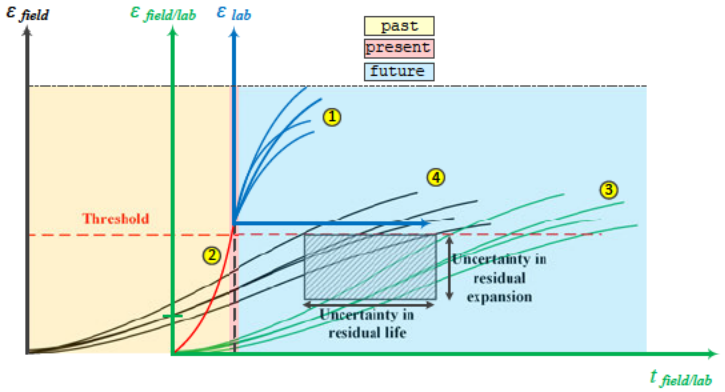

Figure 6.12: Incorporating multiple curves towards uncertainty quantification of residual life and expansion

6.2.2.5 Reconciliation

At this point AAR characteristics have been obtained from laboratory tests, and possibly through system identification. In all likelihood, they are quite different.

The laboratory tests, were obtained on small specimen in controlled environment. Specimens were likely to be immersed in NaOH solution to prevent leaching. Hence a major question is how to correct laboratory values in such a way that they can be used in a full 3D analysis of a massive structure.

This question was partially addressed by (Lothenbach and A., 2020) and would require further attention to account for size effects, variation in storage conditions (Fournier et al., 2009). In this context a full report of the exposure tests undertaken by RILEM TC-258 (Prof. Berube sub-committee?), to a lesser extent (Lindgård et al., 2013) and others should be studied.

6.2.2.6 Finite Element Simulation

6.2.2.6.1 Requirements A finite element code seeking to perform AAR simulation, using this proposed State of the Art approach, should have the following features:

- Role of temperature, relative humidity in the expansion.
- Volumetric nature of the expansion.
- Induced anisotropy whereas high confinement would inhibit AAR expansion in that direction.
- Time dependent degradation of mechanical properties.
- Joint elements to properly model: a) vertical joints in a dam; b) concrete rock interfaces; and c) closure of cut slot.

Ideally a finite element code should be validated to the extent possible. Saouma (2020) has published a battery of problems for validation, and a number of analysts have submitted results of their analysis.

The finite element code Merlin (Saouma, Červenka, and Reich, 2010) seems to have addressed the largest number of problems. It is indeed the code that my group has developed over the years.

Further details for the finite element analysis can be found in Saouma and Hariri-Ardebili (2021).

6.2.2.6.2 Procedure By now, the analyst has available key AAR characteristics to perform a detailed finite element simulation. The following steps should be undertaken:

- The seasonal pool elevation variation (for both the thermal and stress analyses) must first be identified, Figure 6.13(b).
- The stress-free temperature, T_{ref} (typically either the grouting temperature or the average annual temperature) needs to be identified, along with the external temperature, Figs. 6.13(d).
- The pool elevation will affect the internal state of stress, which in turn will alter AAR expansion. This situation is more relevant for high Alpine dams (where the annual pool variation is greater than for low-head, low-altitude dams).

- This variation will then be replicated over n years for the duration of the analysis, Fig. 6.13(c).
- External air and water temperatures will be considered next, Fig. 6.13(d). In the absence of precise field data, the air temperature may be obtained from NOAA (2013).

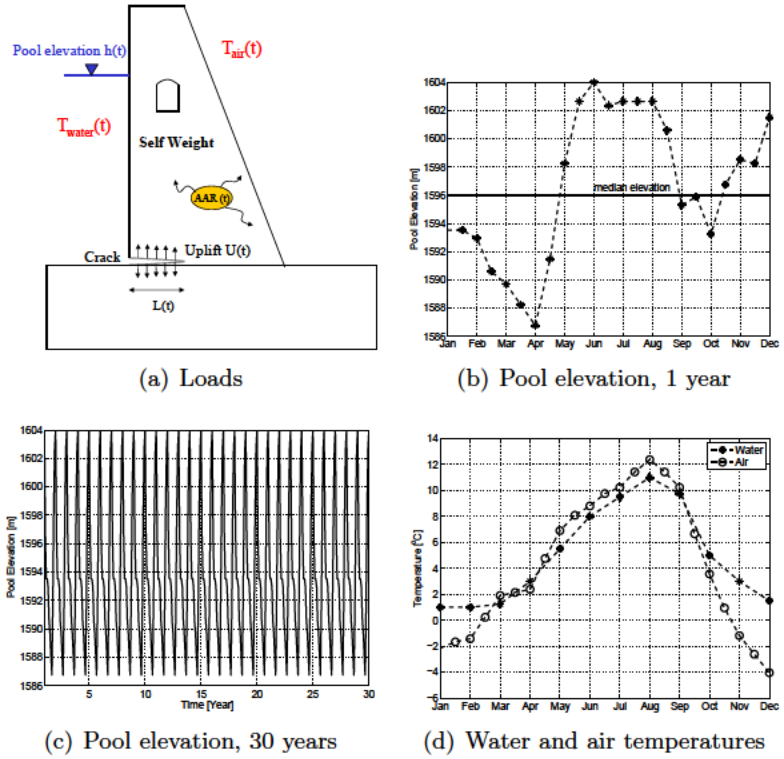

(a) Loads

(b) Pool elevation, 1 year

(c) Pool elevation, 30 years

(d) Water and air temperatures

Figure 6.13: Preliminary load data to be collected for the AAR analysis of a dam

- For time, the ATU (Analysis Time Unit) has been adopted, which can be in the order of week or a month.
- The next step calls for conducting a transient thermal analysis since the reaction is thermodynamically activated. Consequently, the total temperature is included as part of the constitutive model. Heat transfer by both conduction and convection are taken into account, whereas radiation is implicitly incorporated, Fig. 6.14(a).
- Radiation is implicitly included by means of a simplified procedure, whereby ambient air temperature is modified (Malla and Wieland, 1999):

$$\begin{aligned} T_{us} &= 0.905 T_{air} - 0.4^{o}\mathrm{C} \quad \text{Upstream} \\ T_{us} &= 0.937 T_{air} + 7.2^{o}\mathrm{C} \quad \text{Downstream} \end{aligned} \tag{6.2}$$

resulting in the temperature distribution shown in Fig. 6.14(c).
- Even though the external boundary conditions can be readily determined, the condition associated with the gallery is of primary importance for potential internal cracking (Fig.

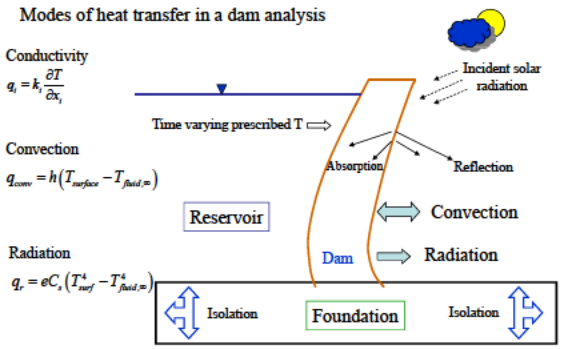

(a) Governing equations for the thermal analysis

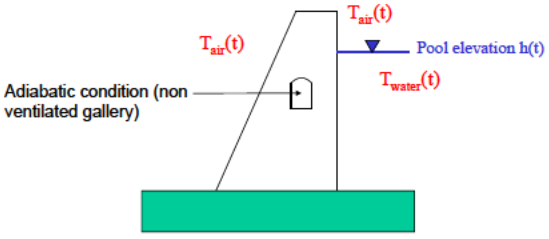

(b) Thermal boundary conditions

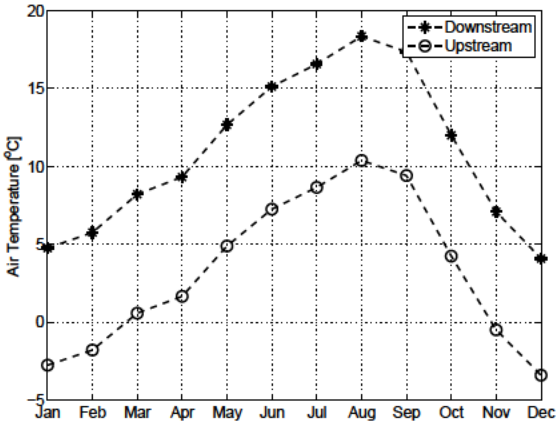

(c) Upstream and downstream air temperatures with inclusion of radiation

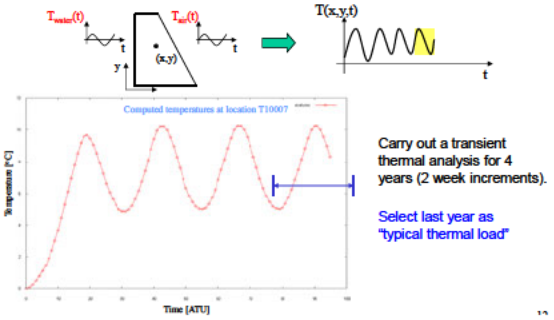

(d) Preliminary transient analysis

Figure 6.14: Data preparation for thermal analysis of a dam subjected to AAR

6.14(b)). More specifically, it is important to know whether during construction the gallery is closed or open to the outside air. The precise thermal analysis should be performed in accordance with Figure 6.14(a).

- Next, the transient thermal analysis is to be performed for at least 3-5 years, until the annual variation appears to converge (Fig. 6.14(d)). These analyses enable deriving, among other things, the spatial and temporal variations of temperature ($T(x, y, z, t)$).
- The dam however must first be discretized. As is the case with most dams, a set of analytical parametric curves defining the arches (in general, circular segments in the US, while parabolic or elliptical segments elsewhere) is (typically) given.
- Joint elements are placed at both the joints and the rock-concrete interface.
- Let's point out that a different mesh is (usually) required for the thermal analysis, since the interface elements needed to be removed.
- After N years of thermal analysis, the temperature field will be harmonic with a one-year frequency. At this point, the analysis is interrupted and $T_{thermal}(x, y, z, t)$ recorded. A sample computed temperature distribution is shown in Figure 6.15. Note that these temperatures

are to be used to evaluate the thermal strains, given that for the AAR analysis the total (i.e. absolute) temperature is needed.

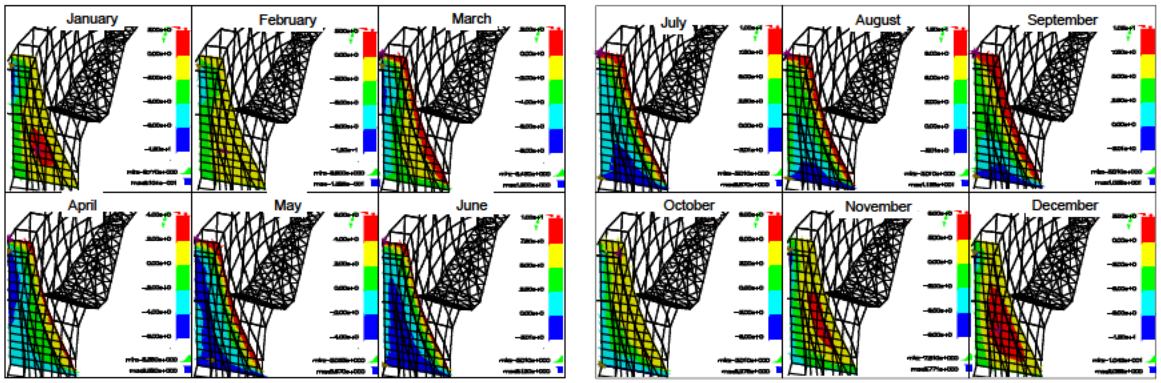

(a) January-June (b) July-December

Figure 6.15: Computed internal temperature distribution variation

- Subsequent to the thermal analysis, $T_{thermal}(x, y, t)$ must be transferred to $T_{stress}x, y, t$ since, in general, the same finite element mesh is not available (the foundations, joints and cracks are not typically modeled as part of the thermal analysis).
- Lastly, a comprehensive input data file must be prepared for the stress analysis; this file includes:
  1. Gravity load (first increment only).
  2. $\Delta\dot{T}(x, y, t) = \dot{T}_{stress}(x, y, t) - T_{ref}$ in an incremental format. This is a subtle step that must not be overlooked. The stress analysis is in fact based on the difference between the actual and stress-free temperatures. In addition, an incremental analysis requires this set of data to be provided in an incremental format.
  3. Stress-free referenced temperature, which is to be added to the temperature data in order to determine the total absolute temperature needed for AAR.
  4. Cantilever and dam/foundation joint characteristics. The former must be included in any arch dam, since expansion may lead to an upstream joint opening, while the latter must be taken into account given that AAR-induced swelling may result in a separation of the dam from the foundation in the central portion of the foundation.
  5. Uplift load characteristics (typically matching the upstream hydrostatic load).
  6. AAR data, which has been described above.
- Moreover, the compiled set of data must be looped over at least 50 years in order to provide a complete and correct set of natural and essential boundary conditions, Fig. 6.16.
- The dead load is applied during the first increment. Following this step, displacements are reset to zero, while maintaining the internal strains/stresses. During increments two through five, the hydrostatic (and uplift) load is applied, and the AAR expansion only initiates at increment six.
- Following completion of the transient thermal analysis, the stress analysis may be performed.

		January		February		March		April		May		June	
Incr.		**6.00**	**7.00**	**7.00**	**8.00**	**9.00**	**10.00**	**11.00**	**12.00**	**13.00**	**14.00**	**15.00**	**16.00**
Body force		dam											
Hydrostatic	**Pool Elevation**	1596.47	1593.53	1593.53	1592.94	1590.59	1589.71	1588.24	1586.76	1591.47	1598.24	1602.65	1604.00
	Incremental Elevation	-5.03	-2.94	0.00	-0.59	-2.35	-0.88	-1.47	-1.47	4.71	6.76	4.41	1.35
Uplift	**Pool Elevation**	1596.47	1593.53	1593.53	1592.94	1590.59	1589.71	1588.24	1586.76	1591.47	1598.24	1602.65	1604.00
	Incremental Elevation	-5.03	-2.94	0.00	-0.59	-2.35	-0.88	-1.47	-1.47	4.71	6.76	4.41	1.35
Temperature [^{o}C]	**Air**	-3.10	-2.14	-1.67	-1.43	0.24	1.90	2.14	2.38	4.76	6.90	8.10	8.81
	Water	1.00	1.00	1.00	1.00	1.00	1.50	3.00	3.00	5.00	6.00	8.00	8.00

		July		August		September		October		November		December	
Incr.		**17.00**	**18.00**	**19.00**	**20.00**	**21.00**	**22.00**	**23.00**	**24.00**	**25.00**	**26.00**	**27.00**	**28.00**
Body force		dam											
Hydrostatic	**Pool Elevation**	1602.35	1602.65	1602.65	1602.65	1600.59	1595.29	1595.88	1593.24	1596.76	1598.53	1598.24	1601.50
	Incremental Elevation	-1.65	0.29	0.00	0.00	-2.06	-5.29	0.59	-2.65	3.53	1.76	-0.29	3.26
Uplift	**Pool Elevation**	1602.35	1602.65	1602.65	1602.65	1600.59	1595.29	1595.88	1593.24	1596.76	1598.53	1598.24	1601.50
	Incremental Elevation	-1.65	0.29	0.00	0.00	-2.06	-5.29	0.59	-2.65	3.53	1.76	-0.29	3.26
Temperature [oC]	**Air**	9.76	10.24	11.43	12.38	11.43	10.24	6.67	3.57	0.95	-1.19	-2.62	-4.05
	Water	9.00	10.00	11.00	11.00	11.00	8.50	6.00	4.00	3.00	3.00	2.00	1.00
AAR	**AAR**	**Activated**											

Figure 6.16: Data preparation, cyclic load

It should be noted however that the finite element mesh for the stress analysis of a dam affected by AAR must differ from the mesh used for the thermal analysis and moreover includes joints, the interface between dam and rock foundation, and the rock foundation. These components are not required in the thermal analysis but are very important to capturing the real behavior of a dam affected by AAR (and thus capturing the real crest displacements on which parameter identification is based, as will be explained in the following section).

- AAR expansion can indeed result in: 1) opening of the downstream vertical joints and closure of the upstream vertical joints in an arch dam; 2) possible movement of the various buttresses on a gravity dam along the joints; and 3) sliding of the dam when subjected to a compressive state of stress on the foundation joint.
- With regard to the temporal and spatial variations of temperature, it should be kept in mind that the stress analysis requires a temperature difference with respect to the stress-free temperature (namely the grouting temperature $T(x, y, z) - T_{grout}$), whereas AAR evolution depends on the total absolute temperature inside the dam $T(x, y, z)$.

6.2.2.7 Earthquake load

Should the dam be possibly subjected to seismic load, then a two step approach should be followed:

1. Perform a multi-year simulation of the AAR swelling. Save the state variables (to retain the concrete mechanical degradation).
2. Restart the analysis by subjecting the dam to seismic load.

6.2.2.8 Failure Criterion

In most cases, the concrete and rocks can be assumed to remain linear elastic. Hence, in this case nonlinearity is only caused by joint responses. Then, one would have to post-process the results to

check for

1. Uniaxial compression failure criterion
2. Uniaxial tension failure criterion
3. Triaxial failure criterion

Those are very unlikely to be governing. However, of greater concern would be joint opening caused by the swelling of the concrete. This may cause at a minimum excessive leak, and worst case scenario unacceptable sliding of the dam.

If need be, a nonlinear model for the concrete could be envisioned, but this would place a heavy computational burden on the analysis.

6.2.2.9 Summary

Fig. 6.17 provides a simple pictorial description of the various tasks that would be performed in a detailed assessment of a structure affected by AAR.

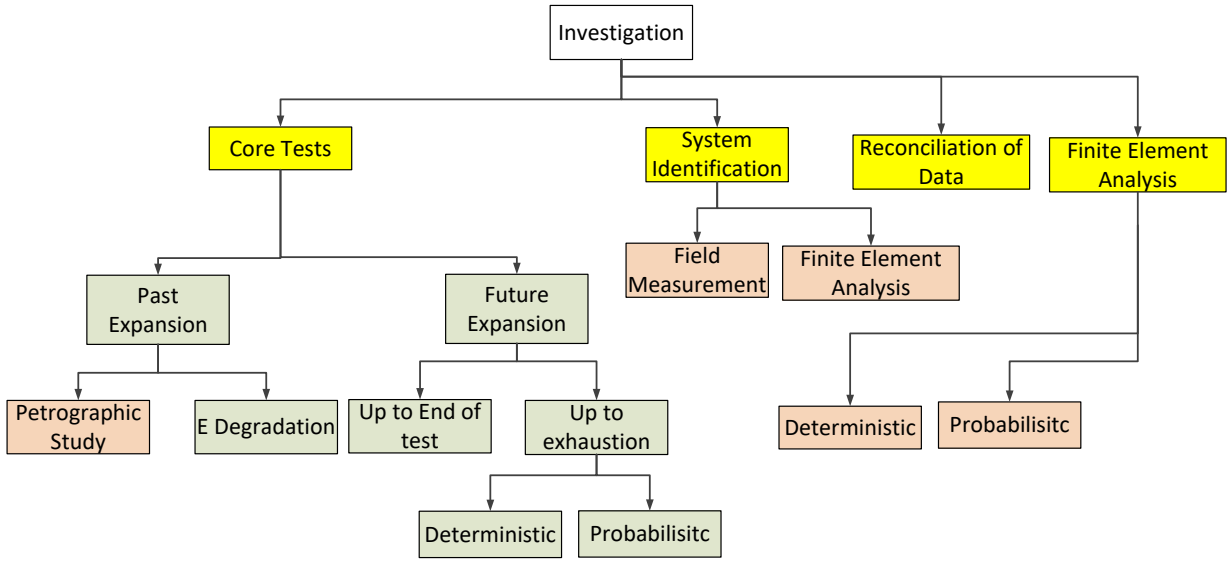

Figure 6.17: Schematic of complete tasks for a structural assessment

6.3 Step By Step Probabilistic Analysis

Once a deterministic finite element model is prepared for the dam (or any other concrete infrastructure), the response is further investigated accounted for all the potential uncertainties in the system. For this purpose, a series of Matlab-based algorithms are developed. It includes many Matlab scripts and functions facilitates the probabilistic assessment of structures. Figure 6.18 shows the general algorithm of this program and interaction among different programs. This algorithm is applicable for any types of structures and any probabilistic model (load, material, time). This algorithm is explained step by step.

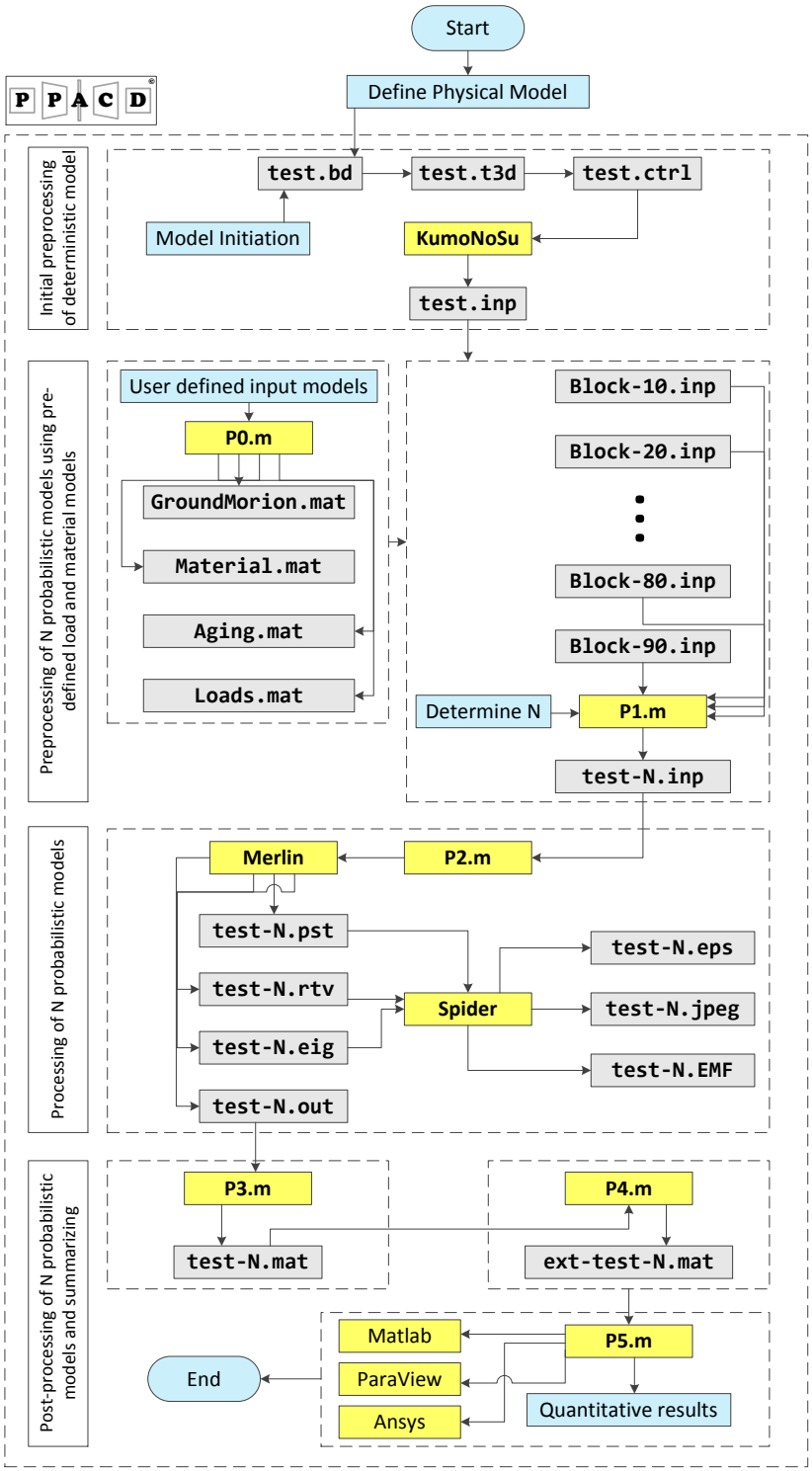

Figure 6.18: Interaction among different programs in Matlab-based code

- First the pre-processor (in our case KumoNoSu) is used to build a initial finite element model

based on information from physical model. Hypothetical material property or load magnitude may be used in this step to develop a deterministic `test.inp`.

- The generated `test.inp` file is then broken to different sub-blocks, i.e. `Block-10.inp`, `Block-20.inp`, ...; each one includes a specific information about the FE model (e.g. analysis type, nodes, elements, material, loads, boundary condition).
- `P0.m` is used to determine the user-defined input parameters for FE model. This includes information about ground motions, material properties, hydraulic loads, or any time-dependent, spatial variable properties. This step is, in fact, the heart of the algorithm and controls all the subsequent steps/results:
  - `P0-Seismo.m`: The scripts in this module provide a set of appropriate ground motions to be used in dynamic analyses, Figure 6.19. The general steps and feature are:
    - Select the type of the performance assessment: 1) intensity-based performance assessment (IBPA) assuming that the dam is subjected to a specific intensity of shaking (e.g. specific target response spectrum), 2) scenario-based performance assessment (SBPA) assuming that the dam is subjected to a specific $< R_{rup}, M_w >$ scenario (earthquake intensity is uncertain parameter), and 3) time-based performance assessment (TBPA) assuming the uncertainty in R_{rup}, M_w and the intensity of motion.
    - Select between the real (recorded) ground motions and the synthetic one (which is suitable for dam sites that there is no enough recorded signals).
    - In the case of real ground motions, either use the direct ground motion selection through PEER online tool, or use a set of Matlab codes developed by Baker research group. In both cases, the selected ground motions are saved in the form of `GMList.xlsx`. The same procedure should be performed for synthetic ground motions.
    - The selected ground motions can be truncated (e.g. $[5\%, 95\%]$ A_I using `GM_Truncat.m`.
  - `P0-Temp.m`: They provide all the required information for thermal transient analysis of structure.
    - Seasonal pool variation,
    - Determination of seasonal temperatures for air, water, stress-free
    - Thermal properties of the material
    - Solar radiation (if possible)
    - Hydration temperature (for a newly built dams)
  - `P0-Hydro.m`: They provide information about the potential flooding hazard at the dam site
    - Hydrological hazard analysis
    - Uncertainty in pool elevation for different return period
- `P1.m` uses all input blocks (i.e. `Block-10.inp`, ...) and input data from `P0.m` (`Material.mat`, `GroundMotion.mat`, ...) to generate N new input files, `test-N.inp` which have the desired probabilistic model.

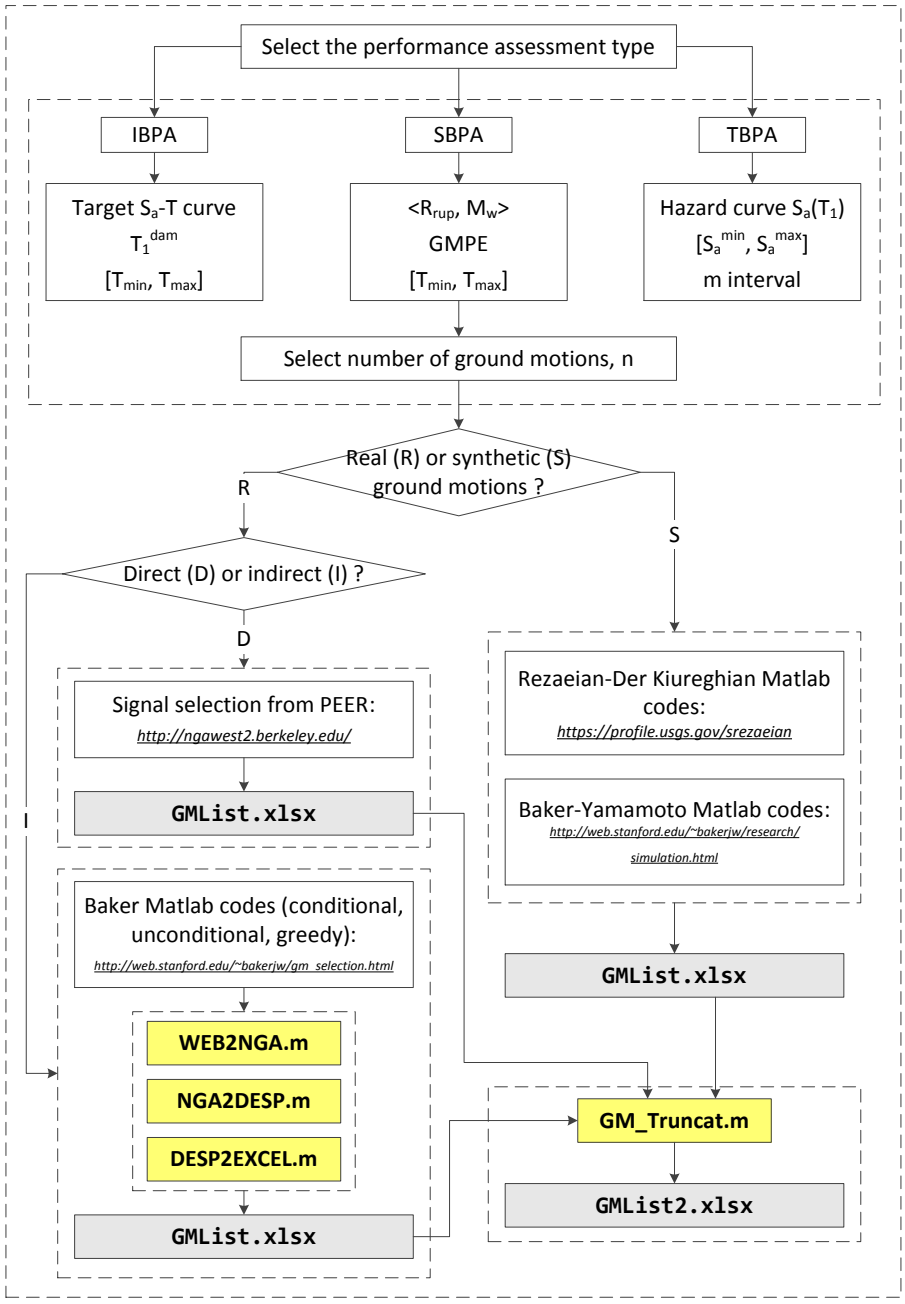

Figure 6.19: General algorithm in `P0-Seismo.m`

– Seismic analysis is performed in two steps: 1) static analysis with all the body forces and hydrostatic one, and 2) through a "restart", a dynamic analysis is initiated form the preceding static one. Thus, two set of `.inp` and `.out` files will generate for each analysis. Hereafter, the static input file corresponds to N^{th} analysis refers to `test-N_dyn1.inp` and the dynamic one refers to `test-N_dyn2.inp`.

– Figure 6.20 shows the general algorithm to generate input files for static analysis. The

initially generated input file should break into different sub-blocks as:

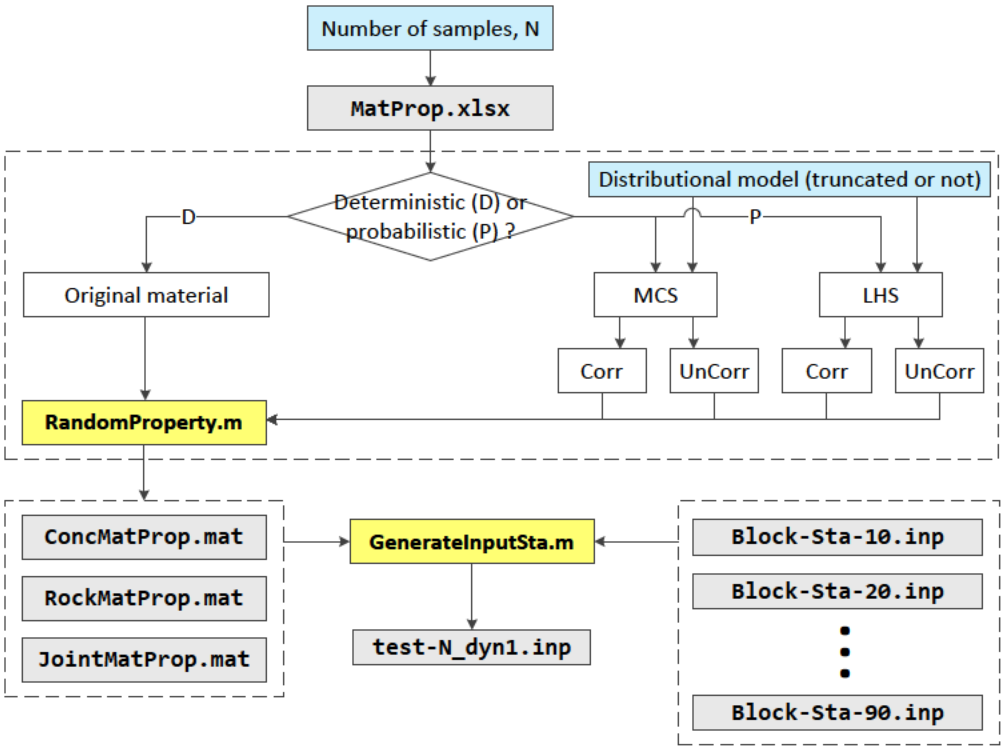

Figure 6.20: General algorithm in `P1Sta.m`

  - `Block-Sta-10.inp`: title and definition
  - `Block-Sta-20.inp`: control block, includes number of increments, ...
  - `Block-Sta-30.inp`: element group, includes element types and material property
  - `Block-Sta-40.inp`: mesh group, includes nodal mass and damping, master/slave crack
  - `Block-Sta-50.inp`: analysis control, includes iterations, error, ...
  - `Block-Sta-60.inp`: body forces
  - `Block-Sta-70.inp`: uplift model (if any)
  - `Block-Sta-80.inp`: displacement boundary condition
  - `Block-Sta-90.inp`: hydrostatic pressure (if any)
- In figure 6.20, `RandomProperty.m` reads a user defined Excel file storing relevant data for the probabilistic based simulation and then generates N samples based on either crude Monte Carlo Simulation (MCS) or Latin Hypercube Sampling (LHS), Figure 6.21.
- In both cases the correlated or uncorrelated modes are possible, Figure 6.22. Sampling is based on predefined distributional model (e.g. normal, lognormal, ...) by user for each RV. Moreover the upper and lower bounds can be defined to truncate the distributional model.

ID	RandType	Mean	COV	Activation	STD	BoundLimit	LowerB	UpperB	Property	Unit
1	Normal	1	0.2	0	0	0.5	0	0	Model No.	-
2	LogNormal	0.005	0.2	1	0.001	0.5	0.0025	0.0075	Maximum volumetric strain	-
3	Normal	10.966	0.2	1	2.1932	0.5	5.483	16.449	Characteristic time	ATU
4	Normal	87.164	0.2	1	17.4328	0.5	43.582	130.746	Latency time	ATU
5	Normal	5400	0.2	0	0	0.5	0	0	Activation energy for char	^{o}K
6	Normal	9400	0.2	0	0	0.5	0	0	Activation energy for lat	^{o}k
7	Normal	0.1	0.2	0	0	0.5	0	0	Residual red. Factor tension	-
8	Normal	0.8	0.2	0	0	0.5	0	0	Fraction of tension pre-AAR	-
9	LogNormal	-58.7	0.2	1	-11.74	0.5	-29.35	-88.05	Compressive strength	MPa
10	LogNormal	5.9	0.2	1	1.18	0.5	2.95	8.85	Tensile strength	MPa
11	Normal	-2	0.2	0	0	0.5	0	0	Shape factor for Gamma_c	-
12	Normal	10.1	0.2	1	2.02	0.5	5.05	15.15	Reference temperature test	^{o}C
13	Normal	-8	0.2	0	0	0.5	0	0	Upper comp. stress limit	MPa
14	Normal	0.69	0.2	1	0.138	0.5	0.345	1.035	Reduction factor Young	-
15	Normal	0.48	0.2	1	0.096	0.5	0.24	0.72	Reduction factor tensile	-

(a) Concrete properties

ID	1	2	3	4	5	6	7	8	9	10	11	12	13	14	15
1	1														
2	0	1													
3	0	0	1												
4	0	0	0.5	1											
5	0	0	0	0	1										
6	0	0	0	0	0	1									
7	0	0	0	0	0	0	1								
8	0	0	0	0	0	0	0	1							
9	0	0	0	0	0	0	0	0	1						
10	0	0	0	0	0	0	0	0	0.8	1					
11	0	0	0	0	0	0	0	0	0	0	1				
12	0	0	0	0	0	0	0	0	0	0	0	1			
13	0	0	0	0	0	0	0	0	0	0	0	0	1		
14	0	0	0	0	0	0	0	0	0	0	0	0	0	1	
15	0	0	0	0	0	0	0	0	0	0	0	0	0	0.7	1

(b) AAR properties

Figure 6.21: User defined Excel file with distribution models, mean, standard deviation and L/U bounds.

NRV	1	2	3	4	5	6	7	8	9	10	11	12	13	14	15
1	1														
2	0	1													
3	0	0	1												
4	0.2	0	0.5	1											
5	0	0	0	0	1										
6	0	0	0	0	0	1									
7	0	0	0	0	0	0	1								
8	0	0	0	0	0	0	0	1							
9	0.8	0	0	0.5	0	0	0	0	1						
10	0	0	0	0	0	0	0	0	0.8	1					
11	0	0.5	0	0	0	0	0	0	0	0	1				
12	0	0	0	0	0	0	0	0.1	0	0	0	1			
13	0.4	0	0	0	0.7	0	0	0	0	0	0	0	1		
14	0	0	0	0	0	0	0	0	0	0	0	0.4	0	1	
15	0	0	0	0	0	0	0	0	0	0.3	0	0	0	0.7	1

Figure 6.22: User defined Excel file with possible correlation coefficients.

– Figure 6.23(a) shows 500 samples for each of three RVs based on LHS. There is a weak correlation between Mat_1 and Mat_2 and also Mat_1 and Mat_3; however, the correlation is strong between Mat_2 and Mat_3. On the other hand, figure 6.23(b) shows an un-symmetry truncation of a normal distribution in the range [18, 38] GPa.

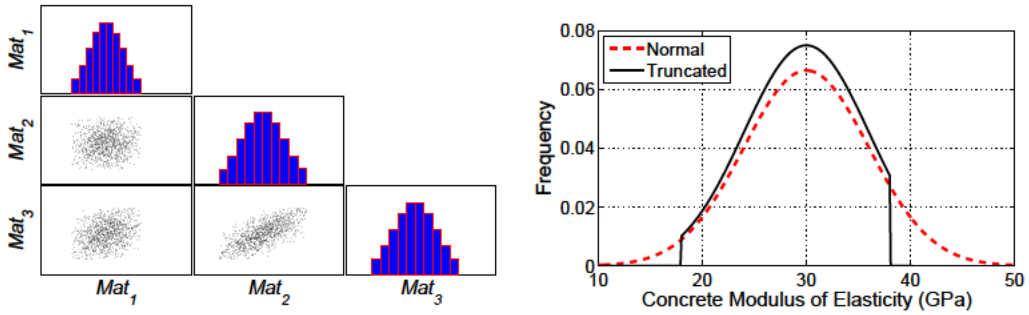

(a) Correlation among RVs

(b) Unsymmetry truncation of normal distribution

Figure 6.23: Sampling the material properties based on algorithm in figure 6.20

– Figure 6.24 shows the general algorithm to generate input files for dynamic analysis. Similar to static analysis, figure 6.24, there are nine blocks define the `test-N_dyn2.inp`; however, some of them are empty in dynamic analysis (e.g. material, mesh) because they already defined though the static input file. User selects the type of dynamic analysis and a `Groundmotion.mat` file is generated includes all the required seismic input with their specifications. Five types of analysis are:

  * Single ground motion (SGM): only a single ground motion is used for the all N samples. If $N = 1$, this results to single deterministic analysis, and if $N =$ "large number" this is either sensitivity or material uncertainty assessment.
  * Cloud analysis (CLA): N (un-scaled) ground motions are applied to N samples. If all the samples have same characteristics, this method only shows the record-to-record variability. However, if samples are different, it accounts for epistemic uncertainty also.
  * Endurance time analysis (ETA): Only three samples are required for three acceleration functions.
  * Multiple stripe analysis (MSA): N ground motions are applied in m level (n=N/m for each level).
  * Incremental dynamic analysis (IDA): N ground motions are incrementally scaled in N/n levels and applied to dam.

- `P2.m` runs the Merlin $2N$ times (pre-dynamic + dynamic) and generates N `test-N.pst` and `test-N.out` (if requested `test-N.rtv` and `test-N.eig` also) files. Each of the N `test-N.pst` can be separately read by Spider and provide required graphical output.
  – If the objective is to perform sensitivity analysis, then $2N + 1$ distinct analyses are required.

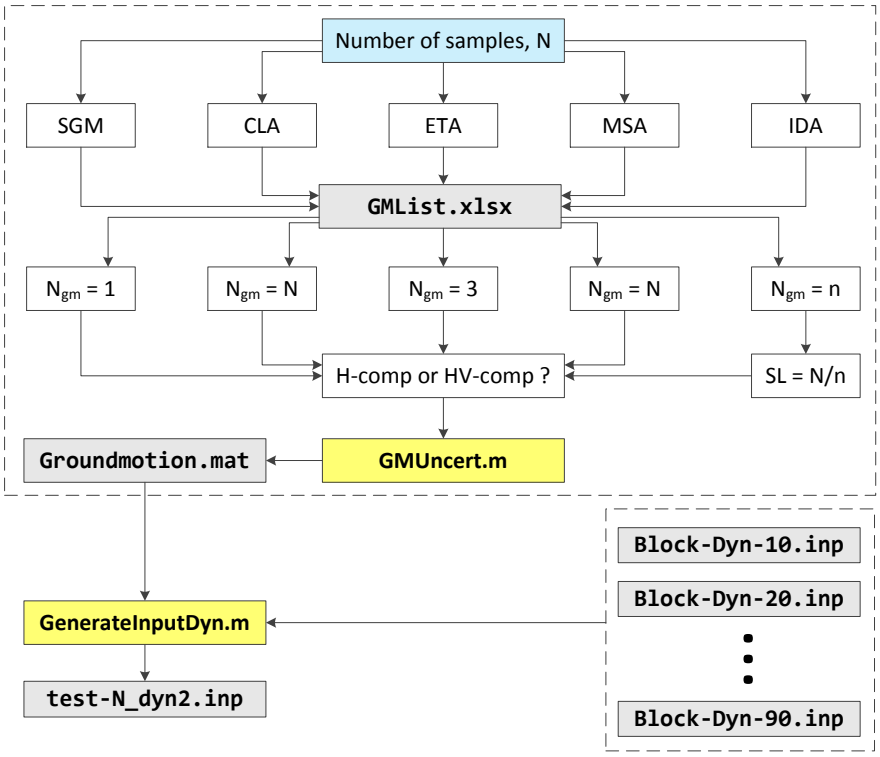

Figure 6.24: General algorithm in `P1Dyn.m`

  - If the objective is to develop a response surface meta-model, Then, N_{RSM} simulations should be analyzed based on according to the specific design of experiment (DOE) protocol.

- `P3.m` uses N `test-N.out` files (in the form of ASCII) and coverts them to `test-N.mat` files (in the form of Binary). `P3Dyn.m` is computationally expensive especially for long duration ground motions with small time step. It can be run on both PC and supercomputer (CU's 184-teraflop Dell supercomputer called Janus is used for some of the analyses; it is currently ranked 164 among the world's top-500 supercomputer sites).
- `P4.m` further process the N `test-N.mat` files and generates N `ext-test-N.mat` files. This step includes process of the results for a specific structure, define the limit states and etc.
  - In the context of AAR analysis, extraction of expansion, strains, rebar stress, damage pattern are of interests.
  - In the context of PBEE, two major set of post-processing are required:
    * Processing the ground motion intensity measures (IM), and
    * Processing the engineering demand parameters (EDP).
- `P5.m` uses the N `ext-test-N.mat` files, unifies them, and post-process them.
  - Apply the probabilistic operations on them (e.g. different fractile, regression, probability of exceedance, ...).

- Use machine learning is needed.
- The final results can be either represented quantitatively (tabulated or central values) or graphically.
- For seismic analyses:
  - CLA:
    - Determination of histograms and best fit to IM parameters
    - Determination of optimal IM in terms of efficiency, sufficiency, proficiency, and practicality
    - Determination of optimal vector IM
    - Determination of fragility curves and surfaces
  - IDA:
    - Determination of capacity curves
    - Summary of capacity curve into central values and fractiles
    - Determination of optimal IM parameter
    - Determination of fragility curves

Bibliography

ACI-207 (2005). *Guide to Mass Concrete (ACI 207.1R-05)*. American Concrete Institute.

ACI 318.2-14 (2014). *Building code requirements for sConcrete Thin Shells (ACI 318.2-14) and commentary*. Tech. rep. American Concrete Institute.

ACI 349 (2006). *Code Requirements for Nuclear Safety-Related Concrete Structures (ACI 349 M-06) and Commentary*. Tech. rep. American Concrete Institute, Farmington Hills.

Anon. (1985). *Design specifications of concrete arch dams*. Tech. rep. Ministry of Water Conservancy and Electric Power of the People's Republic of China.

Arrhenius, S. (1889). "On the Reaction Velocity of the Inversion of Cane Sugar by Acids". In: *Zeitschrift für physikalische Chemie* 4, p. 226.

ASTM, C (1999). "42/C 42M–99 Standard Test Method for Obtaining and Testing Drilled Cores and Sawed Beams of Concrete". In: *West Conshohocken, PA*.

ASTM C192 (2016). "Standard Practice for Making and Curing Concrete Test Specimens in the Laboratory". In: *Annual book of ASTM standards* 04.02.

ASTM C31 (2016). "Standard Practice for Making and Curing Concrete Test Specimens in the Field". In: *Annual book of ASTM standards* 04.02.

ASTM, C39 (2016). "39, Standard test method for compressive strength of cylindrical concrete specimens". In: *Annual book of ASTM standards* 04.02.

ASTM C42 (2016). "Standard Test Method for Obtaining and Testing Drilled Cores and Sawed Beams of Concrete". In: *Annual book of ASTM standards* C09.61.

ASTM C469 (2016). "469, Standard test method for static modulus of elasticity and Poisson's ratio of concrete in compression". In: *Annual book of ASTM standards* 04.02.

ASTM C496 (2016). "496, Standard test method for splitting tensile strength of cylindrical concrete specimens". In: *Annual book of ASTM standards* 04.02.

ASTM C512 (2016). "469, Standard Test Method for Creep of Concrete in Compression". In: *Annual book of ASTM standards* 04.02.

ASTM E4 (2016). "Standard Practices for Force Verification of Testing Machines". In: *Annual book of ASTM standards* 03.01.

Bathe, K.J. (1996). *Finite Element Procedures*. Prentice-Hall Inc.

Batholomey, C. and Haverland, M. (1987). *Concrete Dam Instrumentation Manual*. Tech. rep. United States Department of the Interior, Bureau of Reclamation.

Bažant, Ž. and E. Becq-Giraudon (2001). "Estimation of fracture energy from basic characteristics of concrete". In: *Fracture Mechanics of Concrete Structures (Proc., FraMCoS-4 Int. Conf., Paris)*. Ed. by R. de Borst et al. Balkema, pp. 491–495.

Belytschko, T., W.K. Liu, and B. Moran (2000). *Nonlinear Finite Elements for Continua and Structures*. Wiley & Sons, Ltd.

Ben-Ftima, M., H. Sadouki, and E. Bruhwiler (2016). "Development of a computational multi-physical framework for the use of nonlinear explicit approach in the assessment of concrete structures affected by alklai-aggregate reaction". In: *9th International Conference on Fracture Mechanics of Concrete and Concrete Structures; FraMCoS-9*. Ed. by V.E. Saouma, J. Bolander, and E. Landis. Berkeley, CA.

Brühwiler, E. and F.H. Whitman (1990). "Failure of Dam Concrete Subjected to Seismic Loading Conditions". In: *Engineering Fracture Mechanics* 35.3, pp. 565–572.

Brühwiler, E. (1992). "The Wedge Splitting Test for the determination of fracture properties". In: *Numerical Models in Fracture Mechanics of Concrete, Proceedings of the 1st Bolomey Workshop on Numerical Models in Fracture Mechanics of Concrete*. Ed. by F.H. Whitman. Zurich, Switzerland: Balkema, pp. 19–27.

Bureau of Reclamation, (1995). *Safety Evaluation of Existing Dams*. Tech. rep. U.S. Department of the Interior, Bureau of Reclamation.

Capra, B. and A. Sellier (2003). "Orthotropic modeling of Alkali-Aggregate Reaction in Concrete Structures: Numerical Simulations". In: *Mechanics of Materials* 35, pp. 817–830.

Caron, P et al. (2003). "Slot cutting of concrete dams: Field observations and complementary experimental studies". In: *Structural Journal* 100.4, pp. 430–439.

Cedolin, L., S. Dei Poli, and I. Iori (1987). "Tensile Behavior of Concrete". In: *J. of Engineering Mechanics, ASCE* 113.3.

Chappex, Théodore (2012). "The role of aluminium from supplementary cementitious materials in controlling alkali-silica reaction". PhD thesis. École Polytechnique Fédérale de Lausanne.

Charlwood, R. G. et al. (1992). "A Review of Alkali Aggregate Reactions in Hydroelectric Plants and Dams". In: *Proceedings of the International Conference of Alkali-Aggregate Reactions in Hydroelectric Plants and Dams*. Ed. by CEA and CANCOLD. Fredericton, Canada, pp. 1–29.

Comi, C., R. Fedele, and U. Perego (2009). "A chemo-thermo-damage model for the analysis of concrete dams affected by alkali-silica reaction". In: *Mechanics of Materials* 41.3, pp. 210 –230.

Cornelissen, H., D. Hordijk, and H. Reinhardt (1986). "Experimental determination of crack softening characteristics of normalweight and lightweight". In: *Heron* 31.2, p. 45.

Courant, R., K. Friedrichs, and H. Lewy (1967). "On the partial difference equations of mathematical physics". In: *IBM Journal of Research and Development* 11.2, pp. 215–234.

Courtois, A. et al. (2021). "Field Assessment of ASR-Affected Structures". In: *Diagnosis & Prognosis of AAR Affected Structures*. Ed. by V.E. Saouma. Springer, pp. 41–93.

CSA23.2-14C (2009). "Obtaining and Testing Drilled Cores For Compressive Strength Testing". In: *Canadian Standards Association*.

Denarié, E. and Saouma, V.E. and Iocco, A. and Varelas, D. (1999). "Concrete Fracture Process Zone Characterization; Part I Experimentallly with Internal Fiber Bragg Grating Sensors". In: *Journal of Engineering Mechanics* 127.5, pp. 494–502.

Duda, H. (1990). "Stress-Crack-Opening Relation and Size Effect in High-Strength Concrete". In: *Darmastad Concrete* 5, pp. 35–46.

El Mohandes, F. and F.J. Vecchio (2013). *VecTor3: A. User's Manual; B. Sample Coupled Thermal and Structural Analysis*. Dept. of Civil Engineering, University of Toronto. Toronto, Canada.

Esposito, R., M. Hendriks, and O. Çopuroğlu (2016). "Influence of the alkali-silica reaction on the mechanical degradation of concrete". In: *Journal of Materials in Civil Engineering* 28.6, p. 04016007.

Fasseu, P. andMahut B. (1997). *Aide à la gestion des ouvrages atteints de réactions de gonflement interne*. Tech. rep. 66 pages. Paris, France: Laboratoire Central des Ponts et Chaussées. URL: \url{http://www.ifsttar.fr/fileadmin/user_upload/editions/lcpc/GuideTechnique/GuideTechnique-LCPC-GONFLIN.pdf}.

FedEx (2017). *Temperature Controlled Shipping Boxes*.

FERC (1999). *Engineering guidelines for the evaluation of hydropower projects: Chapter 11: Arch dams*. Tech. rep. Washington, DC, USA: Federal Energy Regulatory Commission.

FERC (2019). "Instrumentation Concrete Dams". In: *Engineering Guidelines for the Evaluation of Hydropower Projects*. Last Accessed Feb. 2019.

FHWA (2006). *Petrographic Methods of Examining Hardened Concrete: A Petrographic Manual*. Tech. rep. FHWA-HRT-04-150. Federal Highway Administration.

— (2010). *Report on the Diagnostis, Prognosis, and Mitigation of Alkali-Silica Reaction (ASR) in Transportation Structures*. Tech. rep. FHWA-HIF-09-004. Federal Highway Administration.

Fournier, B. et al. (2009). "Effect of environmental conditions on expansion in concrete due to alkali–silica reaction (ASR)". In: *Materials Characterization* 60.7, pp. 669–679.

Fournier, Benoit and Marc-André Bérubé (2000). "Alkali-aggregate reaction in concrete: a review of basic concepts and engineering implications". In: *Canadian Journal of Civil Engineering* 27.2, pp. 167–191.

Geokon (2002a). *Model 1200 (Model A4) Borehole Extensometer; Instruction Manual*. Tech. rep. Geokon.

— (2002b). *Model 1200 (Model A4) Borehole Extensometer; Specification*. Tech. rep. Geokon.

Gilks, P. and D. Curtis (2003). "Dealing with the Effects of AAR on the Water Retaining Structures at Mactaquac GS". In: *Proceedings of the 21st Congress on Large Dams*. Montreal, Canada, pp. 681–703.

Giuriani, E. and G. P. Rosati (1986). "Behaviour of Concrete Elements under Tension After Cracking". In: *Studi e Ricerche, Corso di Perfezionamento per le Costruzioni in Cemento Armato* 8. (in Italian), pp. 65–82.

Gopalaratnam, V. S. and S.P. Shah (1985). "Softening Response of Plain Concrete in Direct Tension". In: *ACI Journal* 82, pp. 310–323.

Gowripalan, N et al. (2019). "Evaluation of elastic modulus reduction due to ASR". In: *Concrete in Australia*.

Gunn, R., K. Scrivener, and A. Leemann (2017). "The Identification, Extent and Prognosis of Alkali-Aggregate Reaction Related to Existing Dams in Switzerland". In: *Swelling Concrete in Dams and Hydraulic Structures: DSC 2017*. Ed. by Alain Sellier et al. John Wiley & Sons.

Harris, D. et al. (2006). *State of the Practice for the Nonlinear Structural Analysis of Dams at the Bureau of Reclamation*. Tech. rep. PB2006108499. Washington, D.C.: Department of the Interior, US Bureau of Reclamation.

Hillerborg, A., M. Modéer, and P.E. Petersson (1976). "Analysis of Crack Formation and Crack Growth in Concrete by Means of Fracture Mechanics and Finite Elements". In: *Cement and Concrete Research* 6.6, pp. 773–782.

Huang, H. and B. Spencer (2016). "Grizzly model for fully coupled heat transfer, moisture, diffusion, alkali-silica reaction and fractureing process in concrete". In: *9th International Conference on Fracture Mechanics of Concrete and Concrete Structures; FraMCoS-9*. Ed. by V.E. Saouma, J. Bolander, and E. Landis. Berkeley, CA.

Huang, H., B. Spencer, and G. Cai (2015). *Grizzly Model of Multi-Species Reactive Diffusion, Moisture/Heat Transfer, and Alkali-Silica Reaction in Concrete*. Tech. rep. INL/EXT-15-36425. Idaho Falls, Idaho 83415: Idaho National Laboratory.

Hughes, T.R. (1987). *The Finite Element Method*. Prentice-Hall.

Hydrofrac Inc. (2012). Date retrieved, Nov. 1, 2012. URL: \url{http://www.hydrofrac.com/deformation_gage.pdf}.

Institution of Structural Engineers (1992). *Structural effects of alkali-silica reaction. Technical guidance on the appraisal of existing structures*. Tech. rep. Report of an ISE task group.

Jeang, F. L. and N. M. Hawkins (1985). *Nonlinear Analysis of Concrete Fracture*. Structures and Mechanics Report. Seattle, WA: Department of Civil Engineering, University of Washington.

Jenq, Yeoushang and S.P. Shah (1985). "Two parameter fracture model for concrete". In: *Journal of engineering mechanics* 111.10, pp. 1227–1241.

Joshi, Nirmal R et al. (2021). "Time-Dependent Deformation of a Concrete Arch Dam in Thailand-Numerical Study on Effect of Alkali Silica Reaction on Deflection of Arch". In: *Journal of Advanced Concrete Technology* 19.3, pp. 181–195.

Katayama, T. (2017). "Estimation of Residual Expansion". In: *RILEM TC 259-ISR report: Diagnostic & Prognosis of AAR in Existing Structures*. In Preparation.

Larive, C. (1998a). *Apports combinés de l'expérimentation et de la modélisation à la compréhension de l'alcali-réaction et de ses effets mécaniques*. Tech. rep. OA28. 404 pages. Laboratoire Central des Ponts et Chaussées.

— (1998b). *Apports Combinés de l'Experimentation et de la Modélisation à la Comprehension del'Alcali-Réaction et de ses Effets Mécaniques*. Tech. rep. *In French*. Paris: *Ecole Normale des Ponts et Chaussées*.

Leemann, Andreas and Michele Griffa (2013). "Diagnosis of alkali-aggregate reaction in dams". In: *EMPA, Materials Science & Technology*.

Léger, P., P. Côte, and R. Tinawi (1996). "Finite Element Analysis of Concrete Swelling Due to Alkali-Aggregate Reactions in Dams". In: *Computers & Structures* 60.4, pp. 601–611.

Lindgård, J. et al. (2013). "Alkali–silica reaction (ASR) performance testing: influence of specimen pre-treatment, exposure conditions and prism size on alkali leaching and prism expansion". In: *Cement and Concrete Research* 53, pp. 68–90.

Ljunggren, C et al. (2003). "An overview of rock stress measurement methods". In: *International Journal of Rock Mechanics and Mining Sciences* 40.7-8, pp. 975–989.

Lothenbach, B. and Leemann A. (2020). "From Laboratory to Field". In: *Diagnosis & Prognosis of AAR Affected Structures; State-of-the-Art Report of the RILEM Technical Committee 259-ISR*. Ed. by V.E. Saouma. Springer Nature.

Malla, S. and M. Wieland (1999). "Analysis of an arch-gravity dam with a horizontal crack". In: *Computers & Structures* 72.1, pp. 267–278.

Malm, Richard, Manouchehr Hassanzadeh, and Rikard Hellgren (2017). "Proceedings of the 14th ICOLD International Benchmark Workshop on Numerical Analysis of Dams". In: *14th ICOLD International Benchmark Workshop on Numerical Analysis of Dams*. KTH Royal Institute of Technology.

Matest Inc. (2012). Retrieved: Oct. 2012. URL: \url{http://www.matest.com/products/concrete/flat-jacks-tests-on-brickworks-0.aspx}.

Merz, C. (2015). Personal communication to Sanchez, L.

Metalssi, O. et al. (2014). "Modeling the cracks opening–closing and possible remedial sawing operation of AAR-affected dams". In: *Engineering Failure Analysis* 36, pp. 199–214.

Mills-Bria, B. et al. (2006). *State-Of-Practice For The Nonlinear Structural Analysis Of Dams At The Bureau Of Reclamation*. Tech. rep. U.S. Dept. of the Interior, Bureau of Reclamation.

Mindess, S. and F. Young (1981). *Concrete*. Prentice-Hall, Inc.

Mirzabozorg, H. (2013). Personal Communication.

Multon, S. (2004). *Evaluation expérimentale et théorique des effets mécaniques de l'alcali-réaction sur des structures modèles*. Tech. rep. Etudes et recherches des Laboratoires des ponts et chaussées, Série Ouvrages d'art OA46.

Multon, S., J.F. Seignol, and F. Toutlemonde (2005). "Structural behavior of concrete beams affected by alkali-silica reaction". In: *ACI Materials Journal* 102.2, p. 67.

Multon, S. and F. Toutlemonde (2006). "Effect of Applied Stresses on Alkali-Silica Reaction Induced Expansions". In: *Cement and Concrete Research* 36.5, pp. 912–920.

Myrvang, A. and Beitnes, A. (2003). *In Situ Rock Stress Measurements; Brief description of methods applied by SINTEF*. Tech. rep. Trondheim, Norway: SINTEF, Civil and Environmental Engineering Rock and Soil Mechanics.

Newell, V. and C. Wagner (1999). "Fontana dam: a crack in the curve". In: *Waterpower'99: Hydro's Future: Technology, Markets, and Policy*, pp. 1–10.

NextEra-ML16216A240 (2016). *Seabrook, License Amendment Request 16-03 - Revise Current Licensing Basis to Adopt a Methodology for the Analysis of Seismic Category I Structures with Concrete Affected by Alkali-Silica Reaction. Attachment 1 Markup of UFSAR Pages Enclosed. (73 page(s), 8/1/2016)*.

NOAA (2013). *Satellite and Information Servis (NESDIS)*.

Pan, J. et al. (2013). "Numerical prediction of swelling in concrete arch dams affected by alkaliaggregate reaction". In: *European Journal of Environmental and Civil Engineering* 17.4, pp. 231–247.

Petersson, P.E. (1981). *Crack Growth and Development of Fracture Zones in Plain Concrete and similar Materials*. Tech. rep. TVBM 1006. Lund, Sweden: Lund Institute of Technology.

Planas, J. and M. Elices (1992). "Asymptotic Analysis of a Cohesive Crack: 1. Theoretical background". In: *International Journal of Fracture* 55, pp. 153–177.

Poole, A.B. (1992). "Introduction to Alkali-Aggregate Reaction in Concrete". In: *The Alkali-silica Reaction in Concrete*. Ed. by R.N. Swamy. Van Nostrand Reinhold, New York, pp. 1–28.

Raphael, J. (1984). "Tensile Strength of Concrete". In: *ACI Journal*, pp. 158–165.

Rodriguez, J. et al. (2011). "Contribution to Theme A of the Benchmark Workshop: Effect of Concrete Swelling on the Equilibrium and Displacements of an Arch Dam". In: *Proceedings of the XI ICOLD Benchmark Workshop on Numerical Analysis of Dams*. Valencia, Spain.

Roth, Simon-Nicolas (2021). "Benchmark Study Results: Hydro-Québec". In: *Diagnosis & Prognosis of AAR Affected Structures*. Ed. by V.E. Saouma. Springer, pp. 439–459.

Salamon, J. (2018). *Developments for the Concrete Tensile Split Test*. Tech. rep. DSO-2018-11. Washington, D.C.: Department of the Interior, US Bureau of Reclamation.

Sanchez, L. (2014). "Contribution to the assessment of damage in aging concrete infrastructures affected by alkali-aggregate reaction". PhD thesis. Laval University, Department of Geology and Geological engineering.

Sanchez, L. et al. (2015). "Evaluation of the Stiffness Damage Test (SDT) as a tool for assessing damage in concrete due to ASR: input parameters and variability of the test responses". In: *Construction and Building Materials* 77, pp. 20–32.

Saouma, V.E. (2013). *Numerical Modeling of Alkali Aggregate Reaction*. 320 pages. CRC Press.

— ed. (2020). *Diagnosis & Prognosis of AAR Affected Structures; State-of-the-Art Report of the RILEM Technical Committee 259-ISR*. Springer Nature.

Saouma, V.E., J.J. Broz, and H.L. Boggs (1991). "In-situ Field Testing for Fracture Properties of Dam Concrete". In: *ASCE, Journal of Materials in Civil Engineering* 3.3, pp. 219–234.

Saouma, V.E. and M.A. Hariri-Ardebili (2019). "Seismic capacity and fragility analysis of an ASR-affected nuclear containment vessel structure". In: *Nuclear Engineering and Design* 346, pp. 140–156.

Saouma, V.E. and M.Z. Hariri-Ardebili (2021). *Aging, Shaking and Cracking of Infrastructures; From Mechanics to Concrete Dams and Nuclear Structures*. Springer-Nature.

Saouma, V.E. and L. Perotti (2006). "Constitutive Model for Alkali Aggregate Reactions". In: *ACI Materials Journal* 103.3, pp. 194–202.

Saouma, V.E., L. Perotti, and T. Shimpo (2007). "Stress Analysis of Concrete Structures Subjected to Alkali-Aggregate Reactions". In: *ACI Materials Journal* 104.5, pp. 532–541.

Saouma, V.E., J. Červenka, and R.W. Reich (2010). *Merlin Finite Element User's Manual*.

Saouma, V.E. et al. (1991). "Effect of aggregate and specimen size on fracture properties of dam concrete". In: *ASCE, Journal of Materials in Civil Engineering* 3.3, pp. 204–218.

Saouma, V.E. et al. (2015). "A Mathematical Model for the Kinetics of the Alkali-Silica Chemical Reaction". In: *Cement and Concrete Research* 68, pp. 184–195.

Saouma, V.E. (2014). *Numerical Modeling of AAR*. 324 pages. CRC Press.

Sellier, A. et al. (2009a). "Combination of structural monitoring and laboratory tests for assessment of alkali aggregate reaction swelling: application to gate structure dam". In: *ACI Material Journal*, pp. 281–290.

— (2009b). "Combination of structural monitoring and laboratory tests for assessment of alkali-aggregate reaction swelling: application to gate structure dam". In: *ACI materials journal* 106.3, pp. 281–290.

Serata Geomechanics (2005). *In-Situ Stress/Property Measurements for Quantitative Design and Construction*. Tech. rep. Serata Geomechanics, Inc.

Stark, D. and G.W. De Puy (1987). "Alkali-silica reaction in five dams in southwestern United States". In: *Special Publication* 100, pp. 1759–1786.

Thacker, B.H. et al. (2004). *Concepts of Model Verification and Validation*. Tech. rep. LA-14167. Los Alamos National Laboratory.

Thonstad, Travis E et al. (2021). *Structural Performance of Nuclear Power Plant Concrete Structures Affected by Alkali-Silica Reaction (ASR)-Task 2: Assessing Bond and Anchorage of Reinforcing Bars in ASR-Affected Concrete*. Tech. rep. Technical Note 2127. NIST.

Trunk, B. (2000). *Einfluss der Bauteilgrösse auf die Bruchenergie von Beton (Effect of specimen size on the fracture energy of concrete)*. Tech. rep. In German. Freiburg, Germany: Building Materials Report N 11, Aedificatio Verlag.

Ulm, F. et al. (2000). "Thermo-Chemo-Mechanics of ASR Expansion in Concrete Structures". In: *ASCE J. of Engineering Mechanics* 126.3, pp. 233–242.

USACE (1994). *Arch Dam Design*. URL: \url{http://www.usace.army.mil/publications/eng-manuals/em1110-2-2201/entire.pdf}.

Whitman, F.H. et al. (1988). "Fracture Energy and Strain Softening of Concrete as Determined by Means of Compact Tension Specimens". In: *Materials and Structures* 21, pp. 21–32.

Zienkiewicz, O.C., R. L. Taylor, and P. Nithiarasu (2005). *The Finite Element Method for Fluid Dynamics*. 6th. Elsevier Butterworth-Heinemann.

Zienkiewicz, O.C., R. L. Taylor, and J.Z. Zhu (2005). *The Finite Element Method for Solid and Structural Mechanics*. 6th. Elsevier Butterworth-Heinemann.

This page intentionally left blank.

Acronyms

AAR	Alkali Aggregate Reaction
ACI	American Concrete Institute
ACII	American Standard Code for Information Interchange
ASR	Alkali Silica Reaction
ASTM	American Society for Testing and Materials
ATU	Analysis Time Unit
CCDF	Complementary Cumulative Distribution Function
CDF	Cumulative Distribution Function
CEB	European Concrete Committee
CLA	Cloud Analysis
CMS	Conditional Mean Spectra
COD	Crack Opening Displacement
CS	Conditional Spectra
DI	Damage Index
DM	Damage Measure
DOE	Design of Experiment
DSA	Double Stripe Analysis
DSHA	Deterministic Seismic Hazard Analysis
DV	Damage Variable
DV	Decision Variable
EDP	Engineering Demand Parameter
ETA	Endurance Time Analysis
ETAF	Endurance Time Acceleration Functions
FEA	Finite Element Analysis
FEM	Finite Element Model
FEMA	Federal Emergency Management Agency
IBPA	Intensity Based Performance Assessment
IDA	Incremental Dynamic Analysis
IM	Intensity Measure
LHS	Latin Hypercube Sampling
LRFD	Load And Resistance Factor Design
LVDT	Linear Variable Displacement Transducer
MCE	Maximum Credible Earthquake
MCS	Monte Carlo Simulation
MDE	Maximum Design Earthquake
MSA	Multiple Stripe Analysis
NOAA	National Oceanographic and Atmospheric Agency

OBE	Operating Base Earthquake
PAT	Potentially Applicable Technology
PBEE	Performance Based Earthquake Engineering
PDF	Probability Density Functions
PEER	Pacific Earthquake Enngineering Research
PFM	Potential Failure Mode
PFMA	Potential Failure Mode Analysis
PGA	Peak Ground Acceleration
PGV	Peak Ground Velocity
POA	Pushover Analysis
POC	Proof of Concept
PSDA	Probabilistic Seismic Demand Analysis
PSHA	Probabilistic Seismic Hazard Analysis
RH	Relative Humidity
RILEM	International Union of Laboratories and Experts in Construction Materials, Systems and Structures
RP	Return Period
RV	Random Variable
SBPA	Scenario Based Performance Assessment
SEE	Safety Evaluation Earthquake
SEED	Safety Evaluation of Existing Structure
SIL	Seismic Intensity Levels
SSA	Single Stripe Analysis
TBPA	Time Based Performance Assessment
UHS	Uniform Hazard Spectra
WST	Wedge Splitting Test

A— Fracture Tests for Nonlinear Finite Element Analysis

A critical material property for most modern nonlinear analysis of concrete structures (such as the one needed to analyse a dam cracked by AAR) is their fracture energy G_f. Yet, and surprisingly, there is not yet a "standards" to test concrete fracture energy. This chapter describes a test method being finalized by ACI/ASCE Committee 446 (Fracture Mechanics of Concrete).

A.1 Wedge Splitting Test

Based on the (first) author experience, a testing method, Wedge Splitting Test method (WST) is hereby proposed. The basic principle behind it is the controlled opening of a crack by a controlled movement of a wedge. It is a closed loop servo-controlled test Fig. A.1.

This method introduces, through a wedge, a controlled lateral opening displacement to induce stable crack growth in a prismatic or cylindrical specimen Fig. A.2. From the splitting force-average crack opening displacement response of the specimen, the specific fracture energy is determined.

The major advantages of the proposed WST method are:

1. Easiest method to perform tests on concrete cores recovered from sites.
2. Can be performed on specimens, prismatic or cylindrical, cast in place or on cores recovered from existing structures.
3. Has a substantially longer ligament length per unit weight of concrete as compared to other tests (and in particular compared to the three point bending beam test).
4. Self-weight effect can be neglected for usual sizes (20 x 20 x 10 cm prismatic specimen) (Denarié, E. and Saouma, V.E. and Iocco, A. and Varelas, D., 1999).
5. Test set-up and specimen geometry can be easily adapted for larger or smaller specimen sizes, (Trunk, 2000).
6. Has been used for over 25 years by researchers, and practitioners in the US, Europe and Japan with specimens ranging from 5 cm up to 3.2 m in size, on various types of concretes, mortars, advanced cementitious materials and rock.

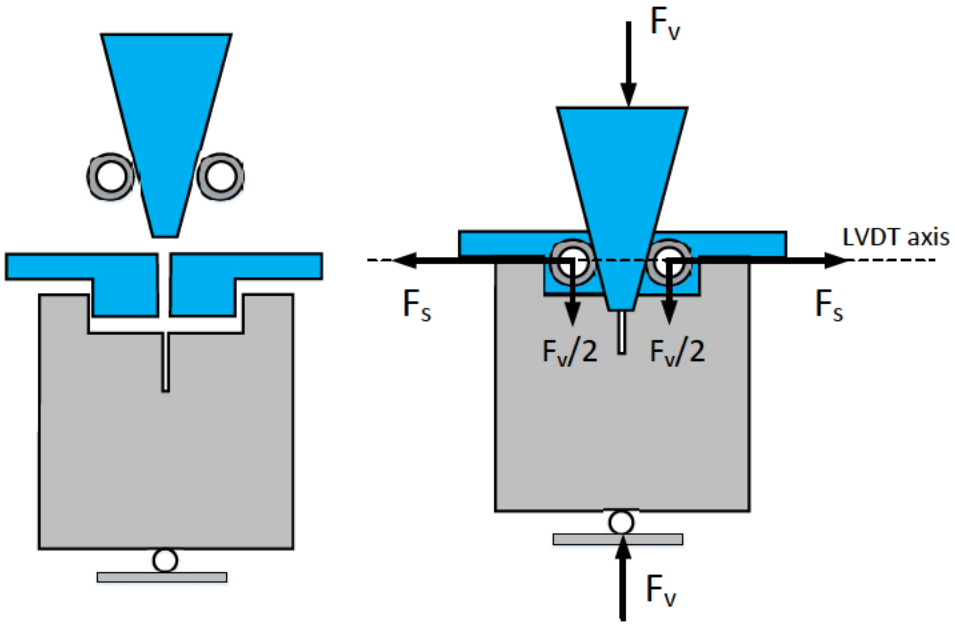

Figure A.1: Test set-up and acting forces, for a prismatic specimen

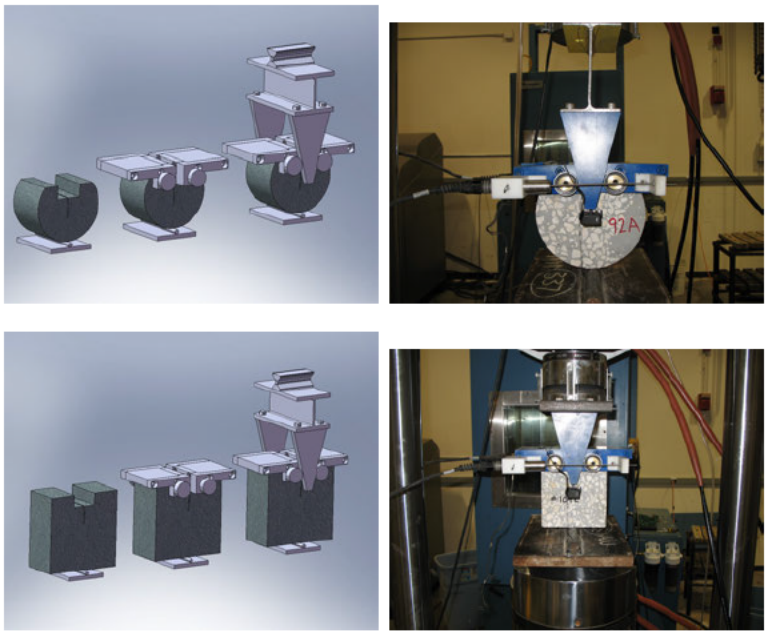

Figure A.2: Principle of the Wedge Splitting Test Set-up

7. The interpretation of the tests results for the determination of G_F as well as the tensile softening diagram is straightforward and requires only very simple calculations.
8. Can be used to measure most fracture properties of concrete: G_F, G_f, K_{Ic}, K_{IC}^S-CTOC$_c$ (Jenq and Shah, 1985).

In a first approximation, the derivation of the tensile softening diagram can be based on the regressions performed on extensive data sets, for different types of concretes, at quasi-static imposed displacement rates (Brühwiler, E., 1992).

The uniaxial tensile strength f_t should be preferably determined experimentally by means of a uniaxial tensile test. If adequate software modules are available, f_t and the tensile softening diagram can also be indirectly determined by means of an inverse analysis using a FEM simulation of the experimental specimen response.

A.1.1 Symbols

D_{max}	Maximum aggregate size of the concrete.
α	Wedge angle: 15^o.
δ_V	Vertical displacement.
A_{lig}	Ligament area.
F_s	Splitting force.
F_V	Vertical force.
G_F	Specific fracture energy
W_F	Work of fracture
f_t	Uniaxial tensile strength

A.2 Apparatus

The testing apparatus is described next:

Testing System: The testing system consists of frame, actuator, force cell, controller, and data acquisition equipment as a minimum. Whereas it is preferable to have a closed-loop servo-controlled machine, this is not essential.

Force Cell: The force measuring device shall have sufficient capacity and shall be accurate to within 1.0 % of the peak force measured in the test. The device shall be calibrated in accordance with ASTM E4 (2016).

Displacement Measurement Devices: Two displacement measuring devices shall be used for measuring the displacements in the axis of the horizontal splitting force, one on each side of the specimen (COD1 on side 1, COD2 on side 2). The displacement measurement devices shall be of a type having sufficient capacity to enable the complete splitting of the specimen in two halves, and shall be accurate to within 1.0 % of the displacement measured while the specimen is at peak force.

Test Setup: The principle of the wedge splitting test set-up is shown in Fig. A.1, with the successive steps, from 1 to 3, of mounting of the test for a prismatic specimen. The test set-up between the actuator or force cell and the specimen consists of a beam with wedges, plates equipped with roller bearings, and a rounded support.

A.2.1 Test Specimens

A.2.1.1 Specimen Configuration and Dimensions

The wedge splitting test specimen can be either prismatic or cylindrical, cast in molds or taken as cores from the structure. Dimensions are shown in Fig. A.3 where h_1 is 130 and 85 mm for closed loop control of COD nad stroke control respectively.

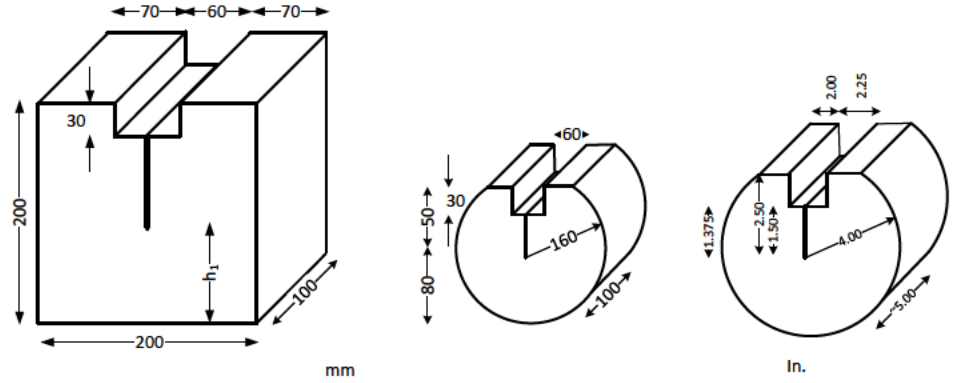

Figure A.3: Dimensions of the specimens for the wedge splitting test (all dimensions in mm)

A.2.1.2 Specimen Preparation

The specimens shall be prepared and cured in accordance with Practices ASTM C31 (2016) ASTM C42 (2016) and ASTM C192 (2016). The groove and notch shall be cast or cut into the specimen.

In order to force a straight path of the crack propagation, a 5 mm deep groove can be cut on both sides of the specimen, on the surface following the plane of the ligament, Fig. A.4(a). Instrumentation should be carefully installed through a temporary support Fig. A.4(b).

A.3 Procedure

Procedure for the test is as follows:

1. Moist-cured specimens shall be tested as soon as possible after removal from moist storage.
2. Test specimens shall be kept moist by any convenient method during the period between removals from moist storage and testing.
3. Place displacement measuring systems on both sides of the specimen.
4. Place specimen on the rounded support Fig. A.4(a)
5. Carefully insert the wedge between the roller bearings.
6. Bring the wedges in contact with the roller bearings until faire and perform the test, in either one of two test control modes:

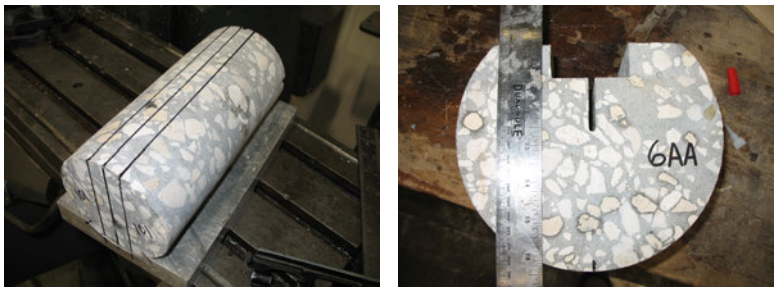

(a) Cutting

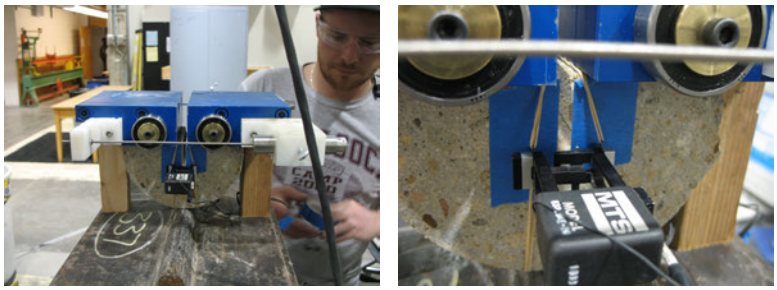

(b) Instrumentation

Figure A.4: Specimen preparation

(a) Under COD control in a closed loop, servo-controlled test system, at a COD rate of 0.1 mm/min.

(b) Under stroke control, at a stroke (cross-head) displacement rate of δ_v equals to 0.2 mm/min.

7. Fig. A.1 illustrates the test set-up with a (prismatic) specimen with the forces induced by the imposed COD or crosshead displacement. The resultant splitting force acts at 10 mm below the top side of the specimen.
8. For fracture toughness test, perform an unload/reload at the same rate as loading, Fig. A.5:

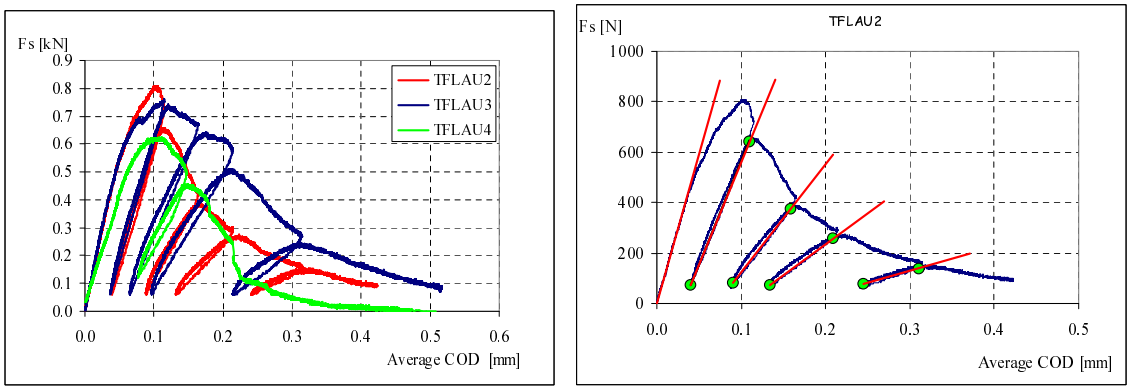

Figure A.5: Representative Experimental Load-COD Curve

(a) Close to the peak load.

(b) At least 4 times in the post-peak zone.

A.3.1 Measured Values

Measured values should include as a minimum:

1. Vertical force F_v as a function of time.
2. Crack Opening Displacements COD_1 and COD_2 on both sides of the specimen, as a function of time.

Additional (optional) instrumentation includes acoustic emission sensors to correlate (micro)crack formation with AE noise.

A.3.2 Calculation

A.3.2.1 Fracture Energy G_F

Evaluation of fracture energy G_F is relatively straightforward:

1. Determine the (horizontal) splitting force acting on the roller bearing, F_S from:

$$F_S = \frac{1}{2\tan\alpha} \tag{A.1}$$

$$F_V = \frac{1}{2\tan 15^o} F_V = 1.866 F_V \tag{A.2}$$

2. Determine the average of the two displacements measured:

$$COD = \frac{COD_1 + COD_2}{2} \tag{A.3}$$

3. Plot F_S in terms of average COD and, if necessary, extrapolate curve to zero F_S.
4. Determine the ligament area A_{Lig} corresponding to the projected area of the crack on the ligament.
5. Determine the work of fracture W_F as the area under the $F_S - COD$ curve (Fig. A.6).

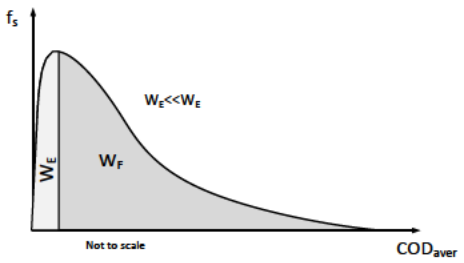

Figure A.6: Definition of the work of fracture and specific fracture energy

6. Determine the specific fracture energy G_F:

$$G_F = \frac{W_F}{A_{Lig}} \tag{A.4}$$

A.3.2.2 Tensile Softening Diagram

Whereas this standard focuses on the determination of G_f, application of G_F in advanced numerical simulations of structural concrete requires the tensile softening diagram in terms of the concrete uniaxial tensile strength f_t, and G_F. The uniaxial tensile strength, f_t, shall be preferably determined independently, by means of a uniaxial tensile test. Alternatively, f_t can be estimated either by means of a tensile splitting test in accordance with ASTM C496 (2016). From the knowledge of G_F and f_t, the uniaxial tensile softening diagram can be represented as a first approximation by the following bilinear curve, valid for concretes with a D_{max} between 8 and 32 mm Fig. A.7(a). Brühwiler and Whitman (1990) found that for 1" maximum size aggregate"

$$s_1 = 0.4 f_t' \tag{A.5}$$

$$w_1 = 0.8 \frac{G_F}{f_t'} \tag{A.6}$$

$$w_2 = 3 \frac{G_F}{f_t'} \tag{A.7}$$

For structural concrete, Whitman et al. (1988) determined

$$s_1 = \frac{f_t'}{4} \tag{A.8}$$

$$w_1 = 0.75 \frac{G_F}{f_t'} \tag{A.9}$$

$$w_2 = 5 \frac{G_F}{f_t'} \tag{A.10}$$

where f_t' is the uniaxial tensile strength.

A.3.2.3 Fracture Energy G_f

The maximum loads of structures depend mainly on the initial tangent of the softening stress-separation curve, which is fully characterized by G_f. They are almost independent of the tail of this curve, which depends mainly of G_F.

The prediction of the entire postpeak softening load-deflection curve of a structure, which is often of secondary interest for design, depends mainly on the tail of the stress- separation curve of the cohesive crack model, and thus on G_F.

Bažant and Becq-Giraudon (2001) obtained two simple approximate formulae for the means of G_f and G_F as functions of the compressive strength f_c', maximum aggregate size d_a, water-cement

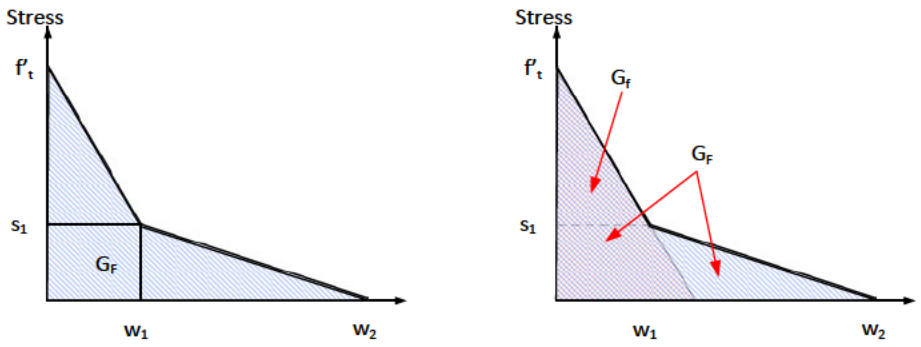

(a) Bilinear softening diagram

(b) G_F *vs* G_f

Figure A.7: Concrete Fracture Energy

ratio w/c, and shape of aggregate (crushed or river);

$$\begin{aligned} G_f &= \alpha_0 \left(\frac{f'_c}{0.051}\right)^{0.46} \left(1+\frac{d_a}{11.27}\right)^{0.22} \left(\frac{w}{c}\right)^{-0.30} && \omega_{G_f} = 17.8\% \\ G_F &= 2.5\alpha_0 \left(\frac{f'_c}{0.051}\right)^{0.46} \left(1+\frac{d_a}{11.27}\right)^{0.22} \left(\frac{w}{c}\right)^{-0.30} && \omega_{G_F} = 29.9\% \\ c_f &= \exp\left[\gamma_0 \left(\frac{f'_c}{0.022}\right)^{-0.019} \left(1+\frac{d_a}{15.05}\right)^{0.72} \left(\frac{w}{c}\right)^{0.2}\right] && \omega_{c_f} = 47.6\% \end{aligned} \tag{A.11}$$

Here $\alpha_0 = \gamma_0 = 1$ for rounded aggregates, while $\alpha_0 = 1.44$ and $\gamma_0 = 1.12$ for crushed or angular aggregates; ω_{G_f} and ω_{G_F} are the coefficients of variation of the ratios G_f^{test}/G_f and G_F^{test}/G_F, for which a normal distribution may be assumed, and ω_{c_f} is the coefficient of variation of c_f^{test}/c_f, for which a lognormal distribution should be assumed (ω_{c_f} is approximately equal to the standard deviation of $\ln c_f$).

A.4 Report

Report the following information:

1. Identification number.
2. Specifications of the material.
3. Specimen age.
4. Specimen dimensions, Fig. A.8(b).
5. Whether the notch was cast or cut-in.
6. Test control method (stroke displacement or COD control, and displacement rate).
7. Description of the fracture surface, especially any unusual appearance or significant deviation from a vertical plane centered on the pre-notch tip.
8. Splitting force - average COD curve.
9. Work of Fracture W_F and Specific Fracture Energy G_F.

Figure A.8: Measuring specimen dimensions

A.5 Additional Illustrations

A.5.1 Apparatus Fabrication Drawings

Technical drawings for the WST apparatus are shown in Fig. A.9.

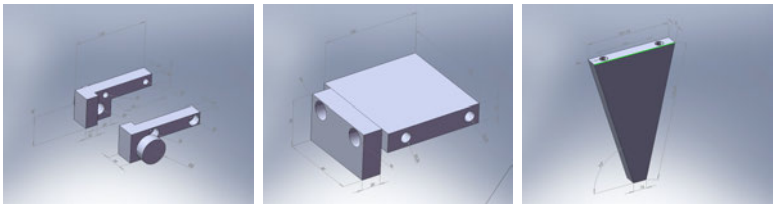

Figure A.9: Wedge Splitting Test Parts dimensions

A.5.1.1 WST from Cores

Though the test method lends itself for core based specimens, should it be desirable to have a prismatic test one (due to possible anisotropy), Fig. A.10 illustrates the process.

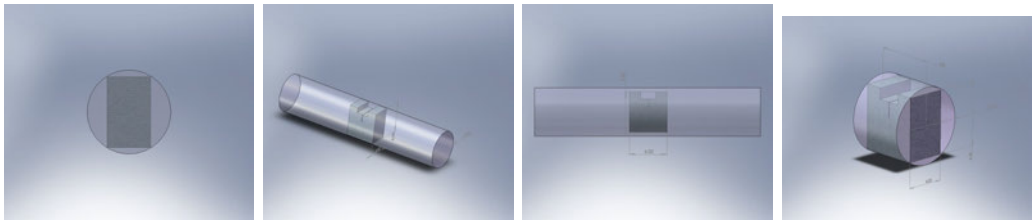

Figure A.10: From cores to small prismatic specimens

A.5.1.2 Scaling

The wedge splitting test has been, in great part, developed through an EPRI report where specimens up to five by five feet and MSA ranging from 0.75" to 3.0" (Saouma et al., 1991), Fig.

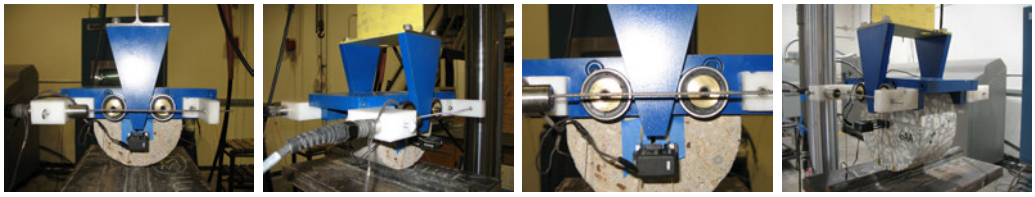

Figure A.11: Details of the specimens

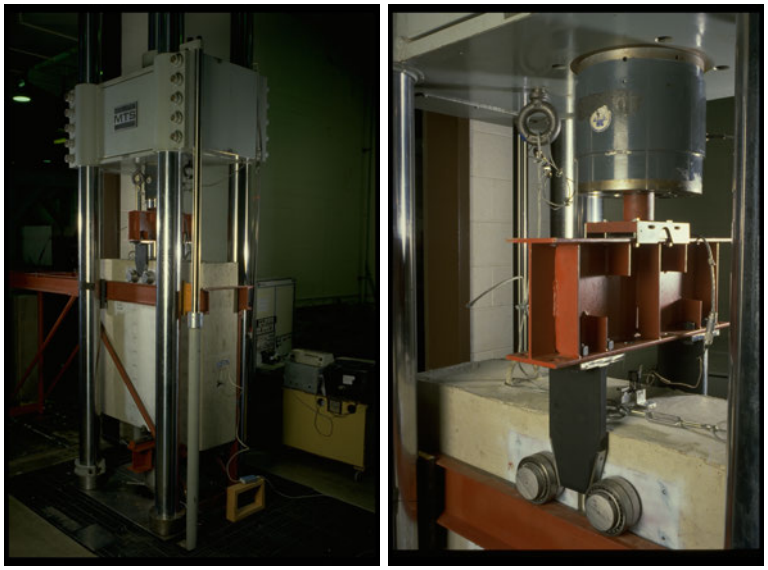

(a) Test setup (b) Detail of the load application

(c) 1.5', 3' and 5' specimens with up to 3" MSA

Figure A.12: Scaled up wedge splitting test (Saouma et al., 1991)

B Benchmark Problems for AAR FEA Code Validation

The finite element analysis of AAR affected dams advocated in this report (§6.2.2) seeks to capture the kinetics of the reaction. Given the limited availability of finite element codes capable of such an undertaking, it is highly desirable that any (possibly modified) code be first validated.

Hence, this chapter (adapted from (Saouma, 2020) will provide the analyst with a battery of test problems (ranging from the simplest to the most complex) for such a validation.

B.1 Introduction

There are three components to the investigation of structures suffering from such an internal deterioration: a) Chemo-physical characterization focusing primarily on the material; b) Computational modeling of the evolution of damage and assessing the structural response of the structure; and c) managing the structure, (Fasseu, 1997).

When focusing on the second aspect, the ultimate objective is to make a predictive assessment of the structural condition and its significance under accidental or extreme scenarios, raising numerous considerations: a) Would future operation and serviceability be affected?, b) Would safety be compromised at some point in time?, and c) How will degradation and structural significance evolved over time. Answering those questions require predictive capabilities that are best addressed through numerical simulation (usually finite element analysis) accounting for the structure's inherent complexities. Assessing the capabilities of current finite element models to perform reliable are predictive structural assessment of ASR-affected concrete structure is the subject of the benchmark proposed in this chapter.

The assessment of finite element codes has been partially performed within the ICOLD International Benchmark Workshops on Numerical Analysis of Dams, and only limited discussion about AAR within the European project Integrity Assessment of Large Concrete Dams[1], NW-IALAD

[1]The sixth (Salzburg) and the eighth (Wuhan) benchmarks invited participants to analyze Pian Telessio and Poglia dams respectively. There was no submission to the former, and only two for the second.

were conducted. Nevertheless a rigorous and rational assessment of existing codes capabilities remain to be conducted. This observation was recently strengthened by a benchmark study about shear walls subjected to AAR before being tested under reverse cyclic loading. For the sake of practice, models calibration of large structures should ideally be based on the inherently limited past inspection data, including permanent deformations of a dam's top of the spillway, or surface cracking maps for reinforced concrete. In the field of science and engineering, sound extrapolation and prediction of future degraded states rely on the validation of sophisticated numerical tools and softwares.

To date, finite element models of ASR-affected concrete structures are yet to be validated within a formal and rather systematic framework. The objective of this benchmark is perceived to be the initial step toward developing a formal approach recognized by the profession.

The proposed benchmark includes two sets of problems, the first on material-scale concrete specimens, and the second, at the structural scale.

The material-scale problems have been conceived to test the specific capabilities (strengths and deficiencies) of the benchmarked models to capture the effects of environmental factors and loading, individually or concurrently.

Test problems are presented with increasing complexity and difficulty with only a limited number of output parameters (generally only one). It is believed such a gradual validation of the constitutive models is needed and provides adequate validation to complex simulation of large-scale aging structures such as hydro-electric concrete dams subjected to either static and dynamic loading.

B.2 Objectives

The study includes two parts, the first addresses material modeling, and the second structure modeling. For the material modeling each study is split in two parts: a) parameter identification for the constitutive model (through calibration of the model with provided laboratory test results); and b) predictive capabilities.

B.3 Important Factors in Reactive Concrete

Assuming that the final residual swelling of the reactive concrete is known, and based on experimental and field observations, indications are that the following factors[2] should be considered in the finite element analysis of a structure:

1. Environmental Conditions of the concrete
   (a) Temperature
   (b) Humidity

[2]There is no general agreement on the importance of all these parameters, the list is intended to be inclusive of all those perceived by researchers to be worth examining.

2. Constitutive models
   (a) Solid concrete (tension, compression, creep, shrinkage)
   (b) Cracks/joints/interfaces.
3. Load history
4. Mechanical Boundary Conditions
   (a) Structural Arrangement
   (b) Reinforcement
   (c) Anchorage

B.4 Test Problems

Table B.1 describes the 10 problems.

Table B.1: List of Benchmark Problems

No.	Description
P0	Textual description of finite element code/models
	Material Response
P1	Constitutive model
P2	Capturing drying and shrinkage
P3	Capturing creep
P4	Effect of Temperature
P5	Effect of RH
P6	Effect of confinement
	Structural Response
P7	Internal reinforcement
P8	Reinforced concrete beam
P9	Dam (simplified)
P10	Dam followed by an earthquake

B.4.1 Units

For all problems use: m, sec., MN, and MPa.

B.4.2 P0: Finite Element Model Description

This very first section should include up to five pages of description of the model adopted in this particular order:

Constitutive Model

1. Basic principles of the model and its implementation.
2. Nonlinear constitutive model of sound or damaged concrete (clarify)
   (a) Instantaneous response (elasticity, damage, plasticity, fracture and others)

(b) Delayed response (creep and shrinkage)

3. Effect on the chemically induced expansion by
   (a) Moisture
   (b) Temperature
   (c) Stress confinement
4. Effect on the mechanical properties of concrete by
   (a) Expansion
   (b) Shrinkage and creep

Finite Element Code Features

1. Gap Element
2. Coupled hydro-thermo-mechanical
3. Others

B.4.3 Materials

In light of the preceding list of factors influencing AAR, the following test problems are proposed.

B.4.3.1 P1: Constitutive Models

At the heart of each code is the constitutive model of concrete. This problem will assess the code capabilities to capture the nonlinear response in both tension and compression.

It should be noted that in some codes, (Sellier et al., 2009b) the constitutive model is tightly coupled (in parallel) with the AAR expansion one (modeled as an internal pressure), in other, (Saouma and Perotti, 2006) it is more loosely coupled (in series) with the AAR (modeled as an additional strain).

B.4.3.1.1 Constitutive Model Calibration Perform a finite element analysis of a 16 by 32 cm concrete cylinder with f'_c, f'_t and E equal to 38.4 MPa, 3.5 MPa and 37.3 GPa respectively[3]. Traction is applied on the top surface, and a frictionless base is assumed. Make and state any appropriate assumption necessary, use the following imposed strain histogram:

$$0 \rightarrow 1.5\frac{f'_t}{E} \rightarrow 0 \rightarrow 3\frac{f'_t}{E} \rightarrow 1.5\varepsilon_c \rightarrow 0 \rightarrow 3\varepsilon_c \tag{B.1}$$

where $\varepsilon_c = -0.002$. If needed, the fracture energy G_F in tension and compression are equal to 100Nm/m^2 and 10,000 Nm/m^2 respectively.

B.4.3.1.2 Prediction Repeat the previous analysis following an AAR induced expansion of 0.5%, you may use the experimentally obtained degradation curve, by (Institution of Structural Engineers, 1992) and published by Capra and Sellier (2003), Fig. B.1

[3]These parameters should be used in all subsequent test problems.

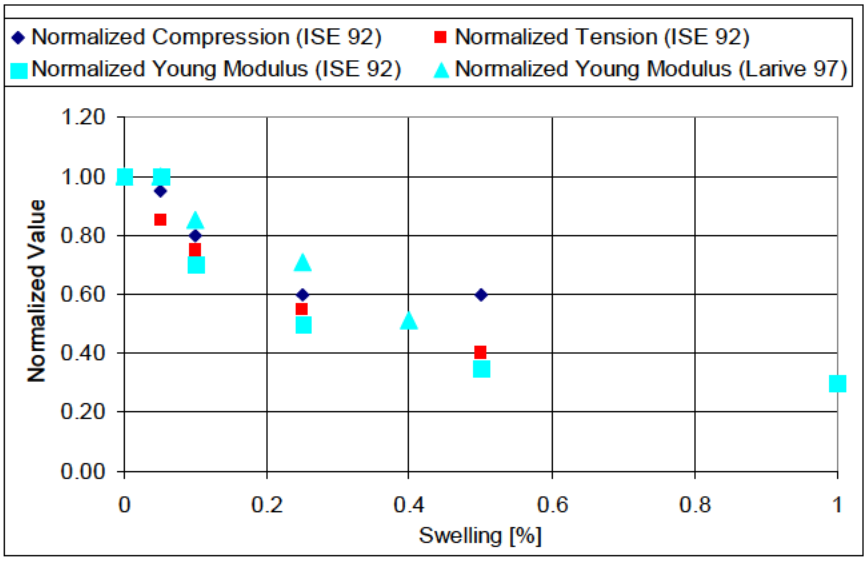

Figure B.1: Deterioration of AAR affected concrete (Capra and Sellier, 2003)

Prediction should highlight concrete mechanical properties degradation in terms of ASR evolution; in particular: Young modulus, tensile and compressive strengths.

B.4.3.2 P2: Drying and Shrinkage

For some structures not necessarily under water (such as bridges or certain hydraulic structures), drying shrinkage strains may be of similar order of magnitude as the AAR induced ones. As shown in Fig. B.2 one must consider various cases of drying and shrinkage, reactive and non reactive concrete, and at relative humidities ranging from a low 30% to a fully saturated environment, and sealed or not. There are a total of 6 potential cases of interest:

a. Non reactive concrete at 30% RH
b. Reactive concrete at 30% humidity
c. Non Reactive concrete sealed specimen
d. Non Reactive concrete under water.
e. Reactive Concrete, sealed cylinder.
f. Reactive concrete under water. Note that this is not identical to a 100% RH if leaching is to be accounted for.

which will be analyzed in P2 and P5

B.4.3.2.1 Constitutive Model Calibration For calibration purposes, the parameters can be fitted using a 16 by 32 cm cylinder to perform the following analyses: a, c, and d with respect to the temporal variation of mass (Fig. B.3(a)) and longitudinal strain (Fig. B.3(b)). For initial condition, assume an initial saturation of 0.85, and $T(t = 0) = 38°C$

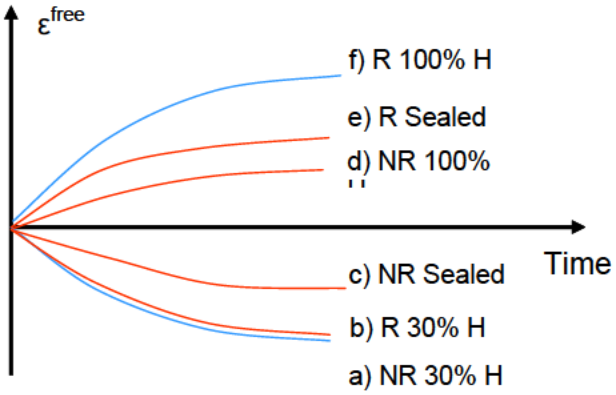

Figure B.2: Drying and Shrinkage test Cases

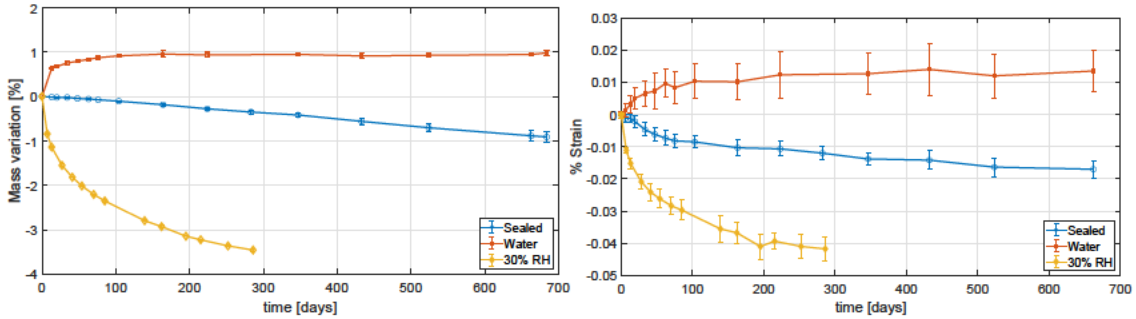

(a) Mass variations

(b) Strain Variation

Figure B.3: Non reactive concrete under various RH conditions; (Multon and Toutlemonde, 2006)

B.4.3.2.2 Prediction Using the parameter determined from the previous section, repeat the same analysis with the temporal annual variation of external RH for the cylinder shown in Fig. B.4.

$$RH(\text{week}) = \frac{RH_{\max} - RH_{\min}}{2} \sin\left(2\pi \frac{t-16}{52}\right) + \frac{RH_{\max} + RH_{\min}}{2} \tag{B.2}$$

where $RH_{\max}$ and $RH_{\min}$ are equal to 95% and 60% respectively, and $T(t=0) = 20°\text{C}$. The model response should first exhibit a negative strain due to shrinkage and then a positive strain due to water absorption until 30 weeks and finally new shrinkage until 52 weeks.

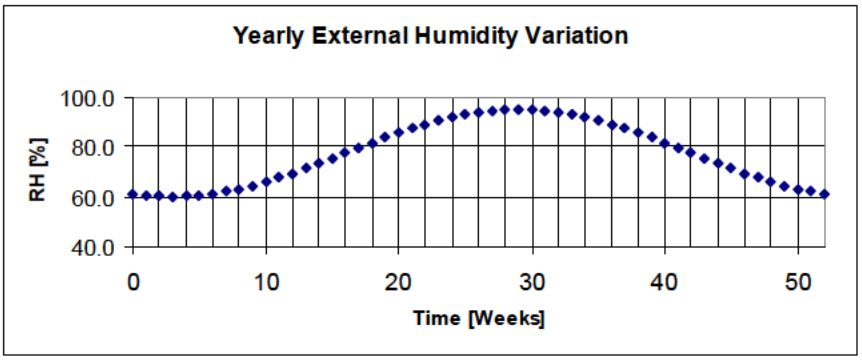

Figure B.4: Humidity variation

B.4.3.3 P3: Basic Creep

There is strong experimental and field indications that creep plays a dominant role in the irreversible long term deformation concrete subjected to constant load. Its effect must be accounted for to properly extract the AAR expansion. This may be explained through biaxially or triaxially loaded elements where swelling is restricted in one direction while free to occur on the other(s). Therefore, in the AAR constrained direction creep deformation will be predominant. This is more likely to occur in arch dams.

B.4.3.3.1 Constitutive Model Calibration For a 13 by 24 cm cylinder subjected to 10 and 20 MPa axial compression, plot the longitudinal and radial displacements. You may calibrate your model on the experimental curve shown in Fig. B.5.

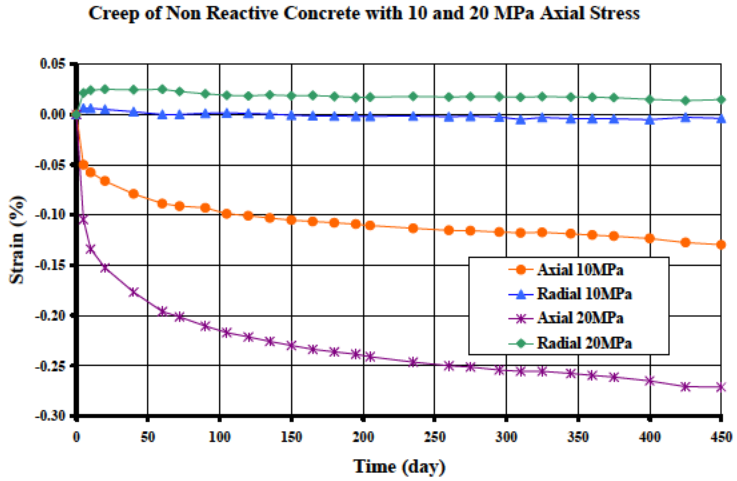

Figure B.5: Creep in non-reactive concrete under sealed condition for different axial stress; (Multon and Toutlemonde, 2006)

B.4.3.3.2 Prediction Using the previously determined parameters, repeat the same analysis for the axial load history shown in Fig. B.6. During the first 16 first weeks, the model should exhibit

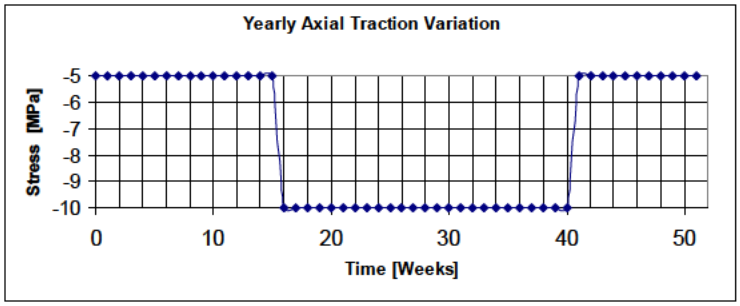

Figure B.6: Stress variation

negative strain due to creep. The load increase at the 16th week should imply an instantaneous strain followed by creep until the 40th week. Then, partial creep recovery should be observed during the first days following unloading.

B.4.3.4 P4: AAR Expansion; Temperature Effect

All chemical reactions are thermodynamically driven. Reactive concrete expansion varies widely with temperature ranges usually encountered in the field or laboratories. Hence, it is of paramount importance that the kinetics of the reaction captures this dependency.

B.4.3.4.1 Constitutive Model Calibration Perform the finite element analysis of a 13 by 24 cm cylinder under water, free to deform at the base and undergoing a free expansion, and for $T = 23^o$C and 38°C. Fit the appropriate parameters of your model with Fig. B.7 obtained by Larive (1998a).

B.4.3.4.2 Prediction Repeat the previous analysis using the variable internal annual temperature variation

$$T(\text{week}) = \frac{T_{\max} - T_{\min}}{2} \sin\left(2\pi \frac{t-16}{52}\right) + \frac{T_{\max} + T_{\min}}{2} \tag{B.3}$$

where $T_{\max}$ and $T_{\min}$ are equal to 25°C and 0°C respectively, as shown in Fig. B.8. Use $RH(t = 0) = 100\%$ and $T(t = 0) = 10$°C.

As the dependence of ASR characteristic times to temperature is exponential, the predictions should be highly non linear. ASR rate should be very slow down during cold period and accelerate during hot period without in a nonlinear response.

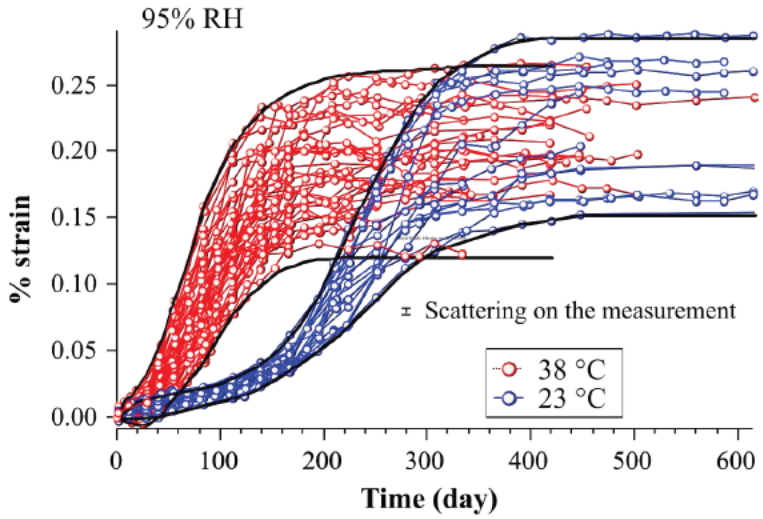

Figure B.7: Free expansion from Larive's tests;(Larive, 1998a)

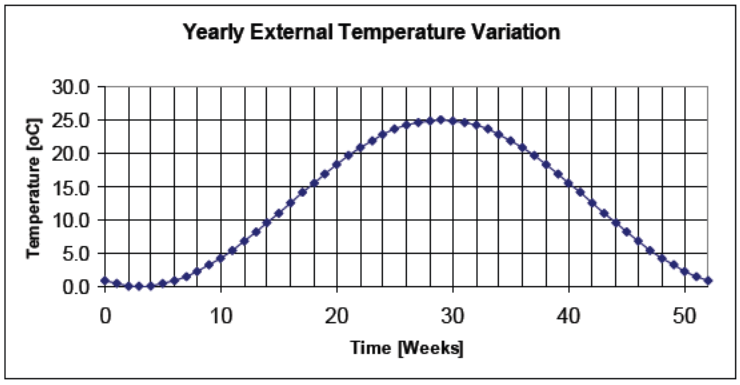

Figure B.8: Temperature variation

B.4.3.5 P5: Free AAR Expansion; Effect of RH

Relative humidity plays a critical role in the expansion of AAR affected concrete. It is well established (Poole, 1992) that expansion will start for a RH at least equal to 80%, and will then increase with RH (RH^8 is a widely accepted formula). For external bridge structures and some dams this can be critical.

B.4.3.5.1 Constitutive Model Calibration Using a 16 by 32 cm cylinder, and assuming a temperature of 38°C, fit the appropriate parameters for mass and vertical strain variation of reactive concrete as shown in Fig. B.9(a) and B.9(b) respectively. Use $RH(t = 0) = 85\%$.

B.4.3.5.2 Prediction Repeat previous analysis using the RH variation shown in Fig. B.4. ASR rate should be increased during high saturation and decreased during dry periods.

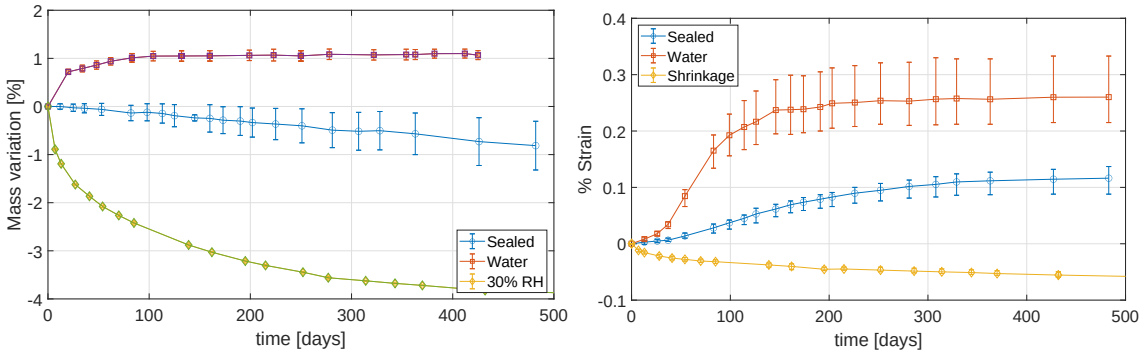

(a) Mass variation

(b) Strain Variation

Figure B.9: Reactive concrete under various RH conditions;(Multon, Seignol, and Toutlemonde, 2005)

B.4.3.6 P6: AAR Expansion; Effect of Confinement

It has long been recognized that confinement inhibits reactive concrete expansion, (Charlwood et al., 1992), (Léger, Côte, and Tinawi, 1996) and most recently (Multon and Toutlemonde, 2006). This test series seeks to ensure that this is properly captured by the numerical model.

B.4.3.6.1 Constitutive Model Calibration For a 13 by 24 cm cylinder, and assuming a temperature of 38°C, analyze the following test cases (all of which consist of sealed specimens):

P6-a. No vertical stress, no confinement (Free swelling), Fig. B.10(a).

P6-b. Vertical stress of 10 MPa, no confinement, Fig. B.10(b).

P6-c. No vertical stress, concrete cast in a 5 mm thick steel container, Fig. B.10(c).

P6-d. Vertical stress of 10 MPa and concrete cast in a 5 mm thick steel container, Fig. B.10(d).

In all cases, plot both the axial and radial strains.

B.4.3.6.2 Prediction Repeat the analysis with the vertically imposed stress histogram shown in Fig. B.6.

With such compressive loading, ASR expansion should not be observed in the axial direction. However, creep should be the main cause of negative strain. In radial direction, ASR expansion should be higher than for stress-free expansion.

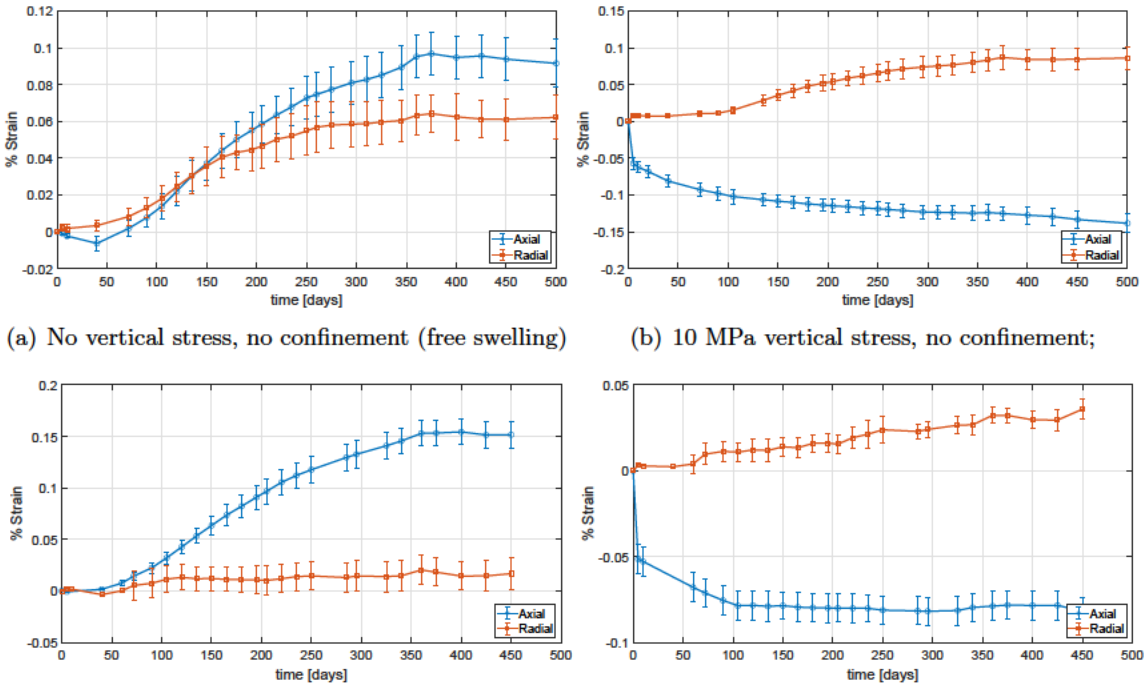

(a) No vertical stress, no confinement (free swelling)

(b) 10 MPa vertical stress, no confinement;

(c) Vertical stress of 10 MPa and concrete cast in a 5 mm thick steel container;

(d) Vertical stress of 10 MPa and concrete cast in a 5 mm steel container;

Figure B.10: Expansions in terms of confinements (Multon and Toutlemonde, 2006)

B.4.4 Structures

B.4.4.1 P7: Effect of Internal Reinforcement

B.4.4.1.1 Description Internal reinforcement inhibits expansion and AAR induced cracking would then align themselves with the direction of reinforcement as opposed to the traditional "map cracking". This test problem seeks to determine how the numerical model accounts for this, especially when cracking (thus a nonlinear analysis is needed) occurs.

Analyze the cylinder shown in Fig. B.11 under the same condition (free expansion, 38°C, 100% RH), for the same duration with a single internal reinforcing bar of diameter 12 mm in the center, and E=200,000 MPa and f_y =500 MPa.

B.4.4.1.2 Prediction Determine longitudinal strain in the rebar and the longitudinal and radial strains on the surface of the concrete cylinder. In both cases values are to be determined at mid-height.

Expansion should be reduced along the reinforcement and compressive stresses should develop orthogonally. Small modification of expansion should be observed in the directions perpendicular to steel bar. If evaluated, cracking should be parallel to the reinforcement.

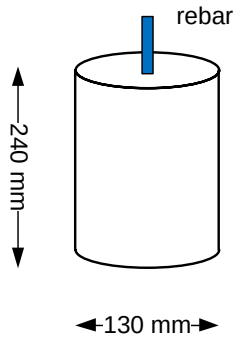

Figure B.11: Concrete prism with internal reinforcement

B.4.4.2 P8: Reinforced Concrete Beams

B.4.4.2.1 Description The mechanical behavior of two concrete beams, studied by S. Multon during his Ph.D. works at LCPC, is proposed. One beam is damaged by ASR during two years of exposure in a 38°C environment and differential water supply, leading to differential ASR expansion within the structures (Multon, 2004). The other made with non-reactive aggregates was stored in similar conditions. Namely, the effects of the ASR development have been quantified in a 4-points bending test of the beams, resulting in a lot of data among which the residual stiffness and the flexural strength of both reactive and non-reactive beams. The objective is to simulate the evolution of the two beams during the two years of tests, and to finish by a simulation of beam failure in four points bending, Fig. B.12.

Material characteristic are the same then in tests P1 to P6, therefore, the LCPC performed tests at several dates since the fabrication. Results are given in Table B.2. During the 2-years aging phase, beams were placed on simple bearings along the geometrical mid-height (span of 2.8 m): steel bars were embedded at mid-height of the structure. During the 4-point bending test, beams were simply supported on the lower face (span of 2.75 m).

In the present benchmark only beams P4 and P6, Fig. B.12, have to be simulated.

As AAR depends on humidity, a humidity profile must be fitted, in order to consider effect of saturation on the reaction. In order to fit the drying-humidification cycle, the mass evolutions of

Table B.2: Reinforced Concrete beam mechanical properties

	28 days	180 days	2 years	
	Reactive Concrete			
E	37,300	30,100	34,600	MPa
f_c	38.4	41.2	43	MPa
f_t	3.5	3.4	3.8	MPa
	Non-Reactive Concrete			
E	38,700	37,800	38,700	MPa
f_c	35.5	40.4	43	MPa
f_t	3.6	3.2	3.7	MPa

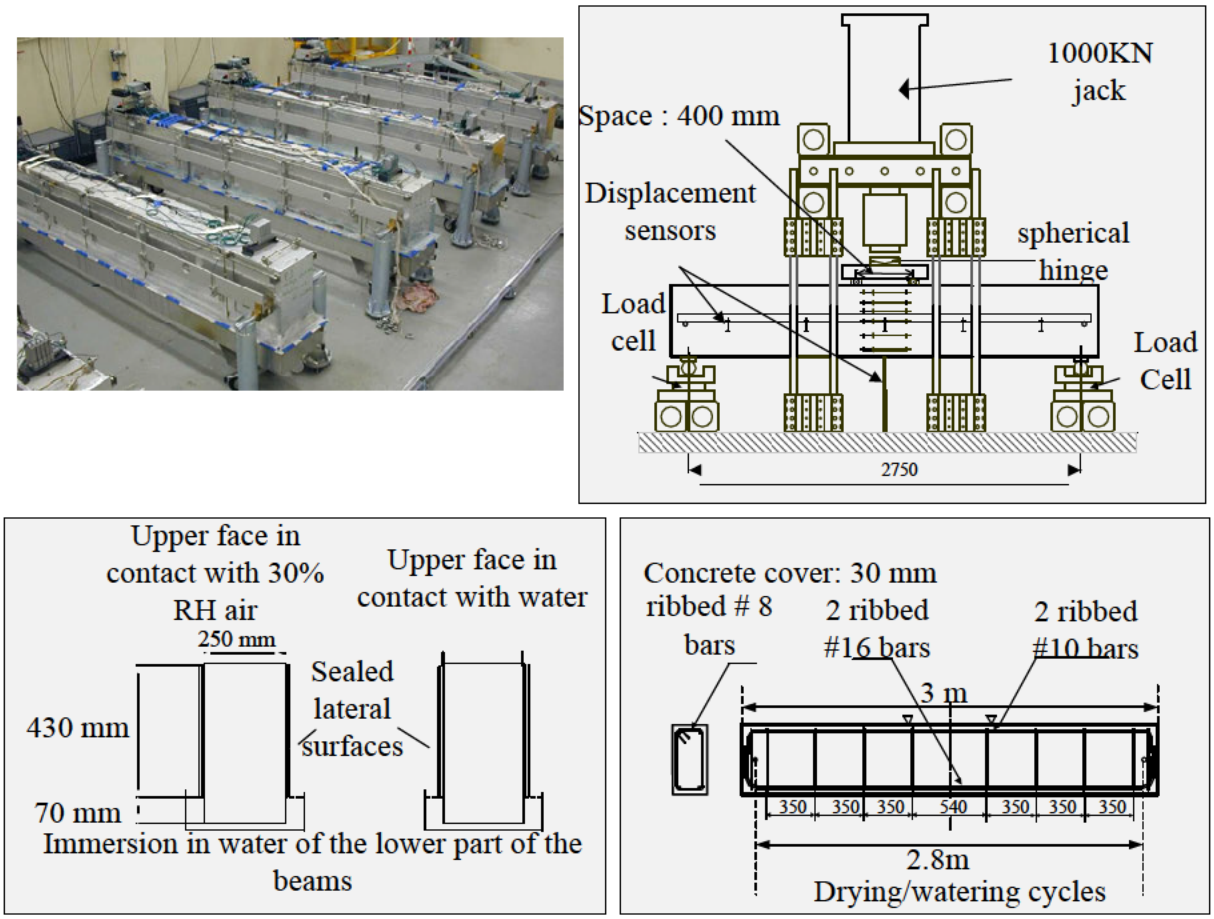

Figure B.12: Multon's Beams

the beams are given below.

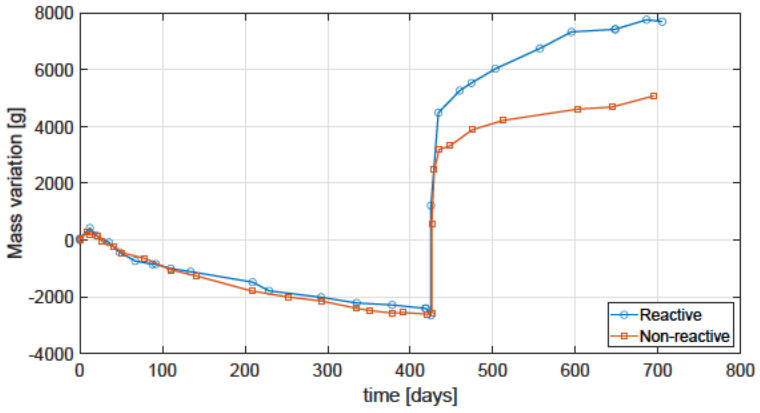

Figure B.13: Mass variation of the beams

Initial saturation of the beam is 0.85, temperature is constant and equal to 38°C. The concrete

porosity is around 16% (15% at the bottom and 17% at the top of the beam).

B.4.4.2.2 Prediction

- The first objective is to find a realistic humidity profile compatible with the mass variation history given in figure B.13.
- The second objective is to predict the deflection of each beam, at mid span, versus time
- The third objective is the evolution of stress versus time, in the bottom longitudinal reinforcement #16, at mid span.
- The last stage consists in simulating for the two beams a four point bending test schematized in Fig. B.12. The force-deflection curve until failure of each beam should be provided.

Numerical results can be compared to experimental results presented in (Multon, 2004) to assess precision of the model.

B.4.4.3 P9: AAR Expansion; Idealized Dam

B.4.4.3.1 Description This next test problem assesses the various coupling amongst various parameters as well as the finite element code and its ability to simulate closure of joint. A common remedy for AAR induced damage in dams is to cut a slot in the structure (Caron et al., 2003; Gilks and Curtis, 2003; Metalssi et al., 2014; Newell and Wagner, 1999). This will relieve the state of stress, and allow the concrete to expand freely. However, at some point concrete swelling will result in a contact between the two sides of the slot. Hence, this problem will test the model ability to capture this important simulation aspect as well.

Consider the reduced dam model shown in Fig. B.14 with the following conditions: a) lateral and bottom faces are all fully restrained; b) front back and top faces are free; c) slot cut at time zero, total thickness 10 mm; d) concrete on the right is reactive, and concrete block on the left is not reactive; e) hydrostatic pressure is applied only on the right block.

B.4.4.3.2 Prediction Using the fitting data of P6, and an friction angle of 50° for concrete against concrete, and zero cohesion, consider two cases:

- Homogeneous field of internal temperature (20°C), relative humidity (100%), and an empty reservoir.
- Transient field of external temperature Fig. B.8, relative external humidity Fig. B.4, and pool elevation variation Fig. B.15 given by where ELmax and ELmin are equal to 95 and 60 respectively.

For both analysis, the specified temperature and relative humidity is the one of the concrete surface. Zero flux condition between dam and foundation. Reference base temperature of the dam is 20^oC.

- x, y, z displacements of point A.
- Fx, Fy and Fz resultant forces on the fixed lateral face versus time (25 years). Assume the typical yearly variations of external air temperature and pool elevation shown in Fig. B.8

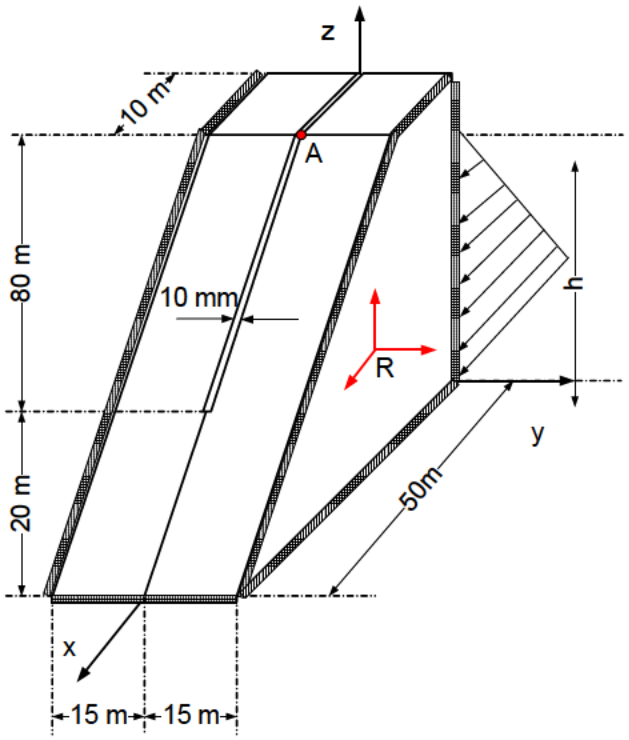

Figure B.14: Idealized dam

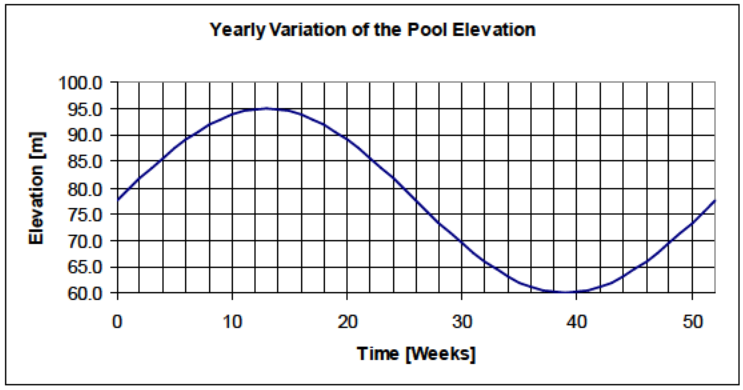

Figure B.15: Yearly variation of pool elevation

and B.15 respectively.

This model seeks to capture: a) general finite element program capabilities in modeling the joint response; b) ease (or difficulty in preparing the input data file for a realistic problem; and c) coupling of the various parameters.

$$EL(\text{week}) = \frac{EL_{\max} - EL_{\min}}{2} \sin\left(2\pi \frac{t}{52}\right) + \frac{EL_{\max} - EL_{\min}}{2} \tag{B.4}$$

where $EL_{\max}$ and $EL_{\min}$ are equal to 95 and 60 respectively.

The slot cutting and subsequent joint closure due to ASR expansion reflect the high nonlinearity of the FE calculation. In this case, modelling should capture stress release caused by cutting and subsequent contact of the surfaces without numerical convergence problems. Of primordial importance will be the stress redistribution in the dam through the various phases.

B.4.4.4 P10: AAR Expansion of a Dam by an Earthquake

B.4.4.4.1 Description In many instances, ultimately, codes should be able to analyze dams, having suffered from AAR, under dynamic excitation. This is the objective of this last verification problem.

The simplified dam previously used does not lend itself to such an analysis, hence, it is left to the user to select a dam. The objective will be to contrast the dynamic response without ASR with the one where ASR has been previously captured. Such an undertaking is reported in (Saouma and Hariri-Ardebili, 2019) albeit for a nuclear containment vessel.

B.5 Conclusion

Given that ASR is already a prevalent problem worldwide and that even more are likely to be identified in the near-distant future, it is of the utmost importance that proper numerical tools are available to offer a diagnosis and prognosis.

For a credible prediction, those tools ought to be first validated through the analysis of simple experimental tests to determine if separate and identifiable phenomena can indeed be captured.

Only, once these tools have been validated through material testing, then they ought to be assessed through the analysis of structural components where many separate phenomenon interplay.

Then, and only then, should those tools be deemed (to various degrees) capable of providing engineers with credible set of predictions.